



TATA INSTITUTE OF FUNDAMENTAL
RESEARCH-CAM, BANGALORE

M.PHIL THESIS

**Optical Flows -
Determination of 2-D velocities of
a moving fluid.**

Author:
Souvik Roy

Supervisors:
Prof.A.S.Vasudevamurthy
Dr.Praveen Chandrashekhar

November 16, 2011

A thesis submitted to the Tata Institute of Fundamental
Research, Centre For Applicable Mathematics, Bangalore,
for the partial fulfillment of the degree of Master of
Philosophy in Mathematics.

DECLARATION

This thesis is a presentation of my original research work. Wherever contributions of others are involved, every effort is made to indicate this clearly, with due reference to the literature, and acknowledgement of collaborative research and discussions.

The work was done under the guidance of Prof. A.S.Vasudevamurthy and Dr. Praveen Chandrashekhar at the Tata Institute of Fundamental Research, Centre For Applicable Mathematics , Bangalore.

SOUVIK ROY

In my capacity as supervisor of the candidate's thesis, I certify that the above statements are true to the best of my knowledge.

Prof. A.S.Vasudevamurthy

Dr. Praveen Chandrashekhar

Date: November 16, 2011

Abstract

Optical flow or optic flow is the pattern of apparent motion of objects, surfaces, and edges in a visual scene caused by the relative motion between an observer (an eye or a camera) and the scene. Optical Flow cannot be computed locally, since only one independent measurement is available from the image sequence at a point, while the flow velocity has two components. A second constraint is needed.

Two methods of finding the optical flow velocity are presented which assumes that the apparent velocity of the brightness pattern varies smoothly almost everywhere in the image. One is a finite difference iterative method based on the work of Horn and Schunck. In this method the image, we minimize a functional proposed by Horn and Schunck and try to find a solution to the problem by using discrete approximations of the image and its derivatives.

We then try to implement a new method - the finite element method. We again minimize the same functional as proposed by Horn and Schunck and then finite dimensional approximations of the underlying solution space is made and solution is computed on these spaces. Continuous and discrete images are taken and their optical flow velocities are calculated. Both the algorithms can handle image sequences that are quantized rather coarsely in space. Both the methods are then compared based on the results obtained.

Finally we will consider the main aim of the thesis- to investigate cloud motion. We will assume that our flow is potential and incompressible and we will to recover the optical flow velocity by minimizing a new functional. The numerical implementation is based on the better of the two methods which were tested in the previous cases.

Acknowledgements

My first, foremost and sincere thanks to my research guides - Prof. A.S. Vasudevamurthy and Dr. C. Praveen for their constant support and encouragement. They were a great source of inspiration for me. They were always there for me anytime I needed them. Without their guidance, this thesis would not have been as it is now. My collaboration with them has been highly productive and cherishable.

I would also like to extend my thanks to my institute TIFR-CAM, Bangalore for providing excellent research facilities and environment. I would also thank all the teachers of TIFR-CAM who helped me even in small matters.

My next thanks goes to my friends Ali Hyder, Deep Ray and Pranav Gujar from TIFR-CAM who helped me carry out the experiment for demonstrating the shading effect.

Last but not the least, whatever I am now as a human being or a student is because of my family. I express my gratitude to my loving father (who passed away recently). His constant words of encouragement was a great source of inspiration for me. Inspite of his absence, he still remains a strong motivating factor in pursuing my research. Next I express my gratitude to my mother who cared for me always. Finally I express my gratitude to my sister and brother-in-law.

Contents

1	Introduction	8
1.1	What is Optical Flow	8
1.2	Relationship To Object Motion	9
1.3	Discontinuities in optical flow	10
1.4	Problems In Computing The Optical Flow Pattern	11
1.5	Applications of optical flow	12
1.6	Application to Cloud Motion	13
1.7	Other Applications of Optical Flow	15
1.7.1	Computer vision	15
1.7.2	Visual Odometry	16
1.7.3	Video Compression	17
1.8	Overview of the thesis	18
2	Finite Difference Iterative Method	19
2.1	Introduction	19
2.2	Domain of the restricted problem	19
2.3	Constraints on the motion of an image	19
2.3.1	Data conservation	19
2.3.2	Smoothness constraints	22
2.4	Problem statement	24
2.5	Discretization	24
2.6	Estimating the partial derivatives of E	25
2.7	Estimating the Laplacian of flow velocities	25
2.8	Minimization	27
2.9	Discretized iterative scheme	29
2.10	Introduction of Courant-Friedrich-Lewey(CFL) condition . .	29
2.11	The case we consider	30
2.12	The modified discretized iterative formula	31
2.13	Convergence of Horn and Schunck Optical Flow estimation method	31
2.14	Programming implementation	32
2.15	Programming data	32

2.16	Results obtained	33
2.16.1	With discrete image derivatives	34
2.16.2	With continuous image derivatives	36
2.17	Conclusions	37
3	Existence Of Minimizer	40
3.1	Introduction	40
3.2	Formulation Of The Problem	40
3.3	Existence and Uniqueness Of Solution Of $J'(U) = 0$	44
3.3.1	Zero Dirichlet boundary condition for velocity	44
3.3.2	Zero Neumann boundary condition for velocity	45
3.4	Estimates For The Minimizer	50
3.4.1	Dirichlet Case	50
3.4.2	Neumann Case	52
4	Finite Element Method for the optical flow problem	54
4.1	Introduction	54
4.2	Approximation via the Galerkin method	54
4.3	Analysis of the Galerkin method	56
4.3.1	Existence and uniqueness	57
4.3.2	Stability	57
4.3.3	Convergence	57
4.4	The finite element method	59
4.4.1	Examples of finite elements	60
4.4.2	Finite element spaces	64
4.5	Interpolation Theory	65
4.6	Finite element method for the Optical flow problem (2.2)	67
4.6.1	Data	68
4.6.2	Programming procedure	68
4.6.3	Results	68
4.6.4	Conclusion	69
5	Finite Element method for the Potential flow problem	72
5.1	Introduction	72
5.2	Constraints	72
5.3	Problem Statement	73
5.4	Minimization equations	73
5.4.1	Equation for Φ given from $\frac{\partial \tilde{J}}{\partial \psi} = 0$	74
5.4.2	Equation for ψ given from $\frac{\partial \tilde{J}}{\partial \Phi} = 0$	74
5.4.3	Equation for g given from $\frac{\partial \tilde{J}}{\partial \lambda} = 0$	74
5.4.4	Minimization equation obtained from $\frac{\partial \tilde{J}}{\partial g} = 0$	74
5.5	Solving the problem	75
5.6	Data for constant flow	75

5.7	Programming procedure	76
5.8	Results	76
5.9	Flow due to point vortex	82
5.10	Results	82
5.11	Conclusions	88
6	Conclusion	90
6.1	Contributions	90
6.1.1	Methodology	90
6.1.2	Results	91
6.1.3	Inference	91
6.2	Future work	91
A	Rate of change of image brightness	93
B	Existence Of An Unique Global Minimizer	94
B.1	Existence Of Gateaux Derivative Of J	96
B.2	Equivalence of $J'(U)=0$ and existence of a minimizer for J	98
C	Conjugate Gradient method	100
C.1	Introduction	100
C.2	Conjugate gradient	100
	Bibliography	103

List of Figures

1.1	Shading effect: Courtesy TIFR-CAM, Bangalore	9
1.2	Motion of a camera	10
1.3	Uses of optical flows	11
1.4	Demonstration of optical flow	13
1.5	Images from different channels of the MSG satellite	14
1.6	Classification of cloud layer	15
2.1	Data conservation assumption	20
2.2	The aperture problem	21
2.3	Constraint on optical flow velocity	22
2.4	Illustration of the aperture problem.	23
2.5	Another illustration of the aperture problem	23
2.6	Estimation of the partial derivatives	26
2.7	Estimation of the Laplacian of the flow	27
2.8	Line of action of the flow velocity	28
2.9	Image at initial time for an example	33
2.10	The magnified figure of the given initial image.	33
2.11	Image at time Δt	34
2.12	The magnified figure of the image at time Δt	34
2.13	The velocities obtained at time Δt	35
2.14	The image obtained at time Δt by moving the initial image with the obtained velocities	35
2.15	Magnification of the image obtained by moving the initial image with the obtained velocities	36
2.16	The velocities obtained at time $\frac{\Delta t}{2}$	36
2.17	Image obtained at time $\frac{\Delta t}{2}$ by moving the initial image with the obtained velocities.	37
2.18	Magnification of the image obtained by moving the initial image with the obtained velocities.	37
4.1	n -simplex of Type 2	61
4.2	Rectangle of Type 1	61
4.3	Rectangle of Type 2	62
4.4	The orientations of the normals in adjacent finite elements . .	64

4.5	The map F_K between the reference triangle \hat{K} and the generic triangle K	66
4.6	Image along with the velocity vectors for $K = 0.9$	69
4.7	Image along with the velocity vectors for $K = 1.5$	69
4.8	Graph of L^2 error vs K	70
4.9	Graph of L^2 error vs K	71
5.1	Ω divided into triangles	77
5.2	Image E	77
5.3	Velocity vectors for $K = 1$	78
5.4	Velocity vectors for $K = 1.1$	79
5.5	Velocity vectors for $K = 1.5$	79
5.6	Velocity vectors for $K = 1.75$	80
5.7	Velocity vectors for $K = 2$	80
5.8	Graph of Relative L2 error vs K showing existence of an optimal K	82
5.9	Vortex velocity vectors for $K = 0.8$	83
5.10	Vortex velocity vectors for $K = 1$	83
5.11	Vortex velocity vectors for $K = 1.04$	84
5.12	Vortex velocity vectors for $K = 1.1$	84
5.13	Vortex velocity vectors for $K = 1.2$	85
5.14	Vortex velocity vectors for $K = 1.4$	85
5.15	Vortex velocity vectors for $K = 1.8$	86
5.16	Vortex velocity vectors for $K = 2$	86
5.17	Vortex velocity vectors for $K = 2.5$	87
5.18	Vortex velocity vectors for $K = 3$	87
5.19	Graph of Relative L2 error vs K showing existence of an optimal K for vortex flow.	89

List of Tables

2.1	Variation of relative L^2 error with the smoothing parameter α	38
4.1	Variation of relative L^2 error and Advection error with the smoothing parameter K	70
5.1	Variation of relative L^2 error and advection error with the smoothing parameter K	81
5.2	Variation of relative L^2 error with the smoothing parameter K for vortex flow.	88

Chapter 1

Introduction

Clouds are an important part of our daily life. Our food depends on the harvest a farmer does which in turn depends on the amount of rain. Movement of clouds and their growth rate will suggest the rate of rainfall in a particular region. Hence study of cloud motion is of great significance to meteorologists. Also such a study can help in preventing natural calamities to some extent. The aim of this thesis is precisely to study fluid motion and try to apply it to cloud motion. In this thesis, we use the technique of optical flow estimation to analyze moving objects.

To derive the velocity of an object in three dimensional space from a sequence of two dimensional images or optical flow, Horn and Schunck [HS81] introduced the fluid dynamics constraint reducing the ambiguity of the velocity field, enabling the recovery of an object's motion. The idea is also relevant to cloud motion, which is a special case of fluid motion and consists of very complex motion dynamics [LZ]. Furthermore, its probability distribution allows representation of the uncertainties in the optical flow computation [ES91]. We then use first a modified version of the finite difference iterative scheme proposed by HS and test with a smooth image. Then we use the finite element technique to recover the optical flow velocity for the same image. We compare the two methods and finally the original model of the optical flow is adjusted to cater to capturing the cloud motion satisfying potential and incompressible flow.

1.1 What is Optical Flow

In our daily life we see motion of different sorts. Motions occur from micro to macro scale level. For example motion of atoms in our body occurs at a micro scale level whereas our planet Earth moves around the sun at a macro scale level. Eating, drinking, sleeping, dancing, singing etc. all of the activities induces motion. Such is human nature that we cannot do without motion. But all of these are so so natural that we take it for granted. We

need to understand the transformations our world is undergoing else we would not be able to survive. The main difference between us and robots is the concept of perception of changing objects. If robots were to exist in our world, along with us, then they should also have this sense of perception. What is required is a general and flexible representation of visual motion that can be used for many purposes and can be computed efficiently [TB91].

Optical Flow is the distribution of movement of brightness pattern in an image. It can arise from relative motion of objects and viewer. Thus, a good bit of information can be obtained from the optical flow about the spatial arrangement of the objects viewed and the rate of change of this arrangement.

1.2 Relationship To Object Motion

The relationship between optical flow in the image plane and velocities of objects in the 3-D world is not an easy proportion. For example, when a changing picture is projected onto stationary screen we sense motion.

Conversely, a moving object may give rise to constant brightness pattern. For example, an uniform sphere exhibits shading because its surface elements are oriented in many directions. Yet when it is rotated, there is no optical flow at any point of the image, as shading does not move with the surface. (Fig 1.1).



(a) Original Image (b) Image after object was rotated

Figure 1.1: Shading effect: The shading at the bottom of the object looks same even though the object has been rotated. These images were taken at TIFR-CAM, Bangalore

More specifically, consider the diagram in Figure 1.2 which illustrates how the translation and rotation of the camera cause the projected location p in the scene to move.

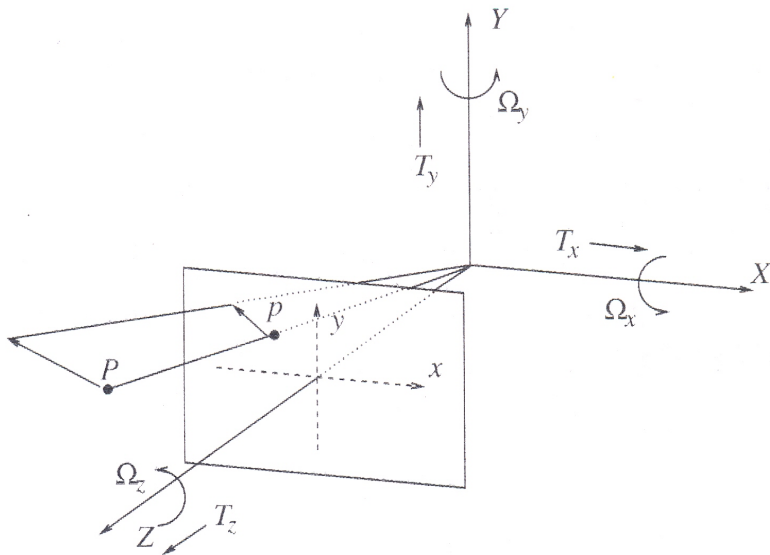


Figure 1.2: A point P in the scene projects to a point in the $[x, y]$ coordinate system of the image plane of a camera centered at the origin of the camera coordinate system $[X, Y, Z]$, with its optical axis pointing in the direction Z . The motion of the camera is described by its translation $[T_X, T_Y, T_Z]$ and rotation $[\Omega_X, \Omega_Y, \Omega_Z]$: Courtesy ([MB92]).

Likewise, if point of a point P is moving independently, its projection on the image plane will change, even when the camera is stationary. It is this vector field, $U(x, y) = [u(x, y), v(x, y)]$, describing the horizontal and vertical image motion, that is to be recovered at every point in the image.

1.3 Discontinuities in optical flow

Discontinuities in optical flow pattern can help us to distinguish the movement. Consider the image sequence in Figure 1.3 where a camera is translating parallel to the image plane.

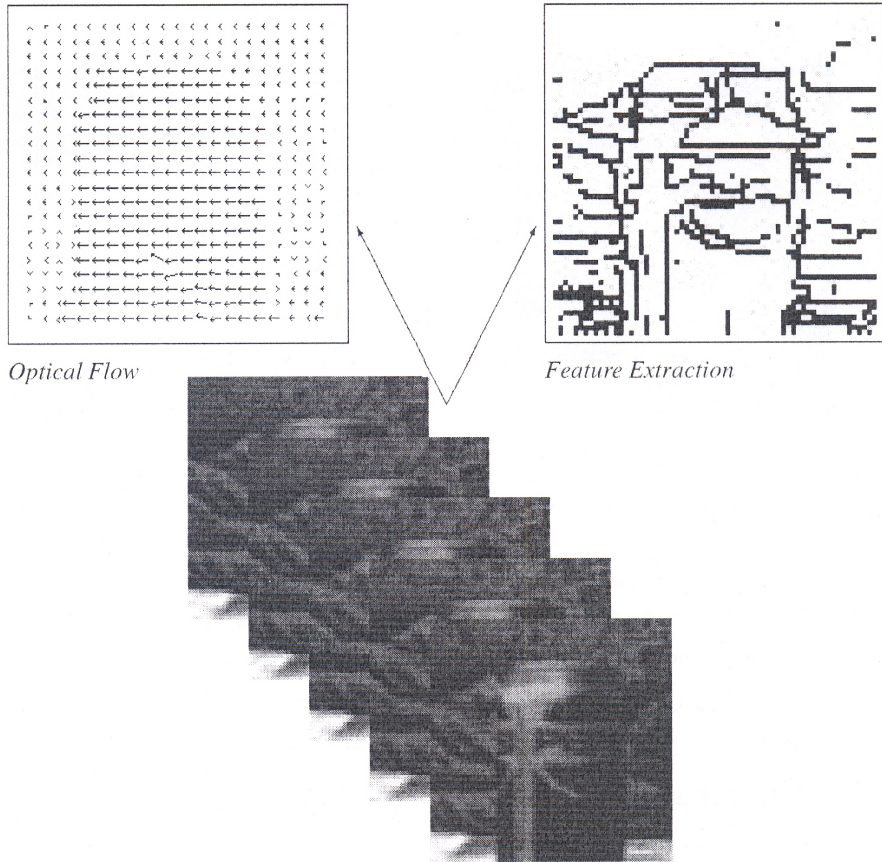


Figure 1.3: Discontinuities in optical flow helps in spotting motion of an object efficiently: Courtesy ([MB92])

The flow field, in the top left of the figure, contains two distinct motions. It suggests us that the soda can is moving more rapidly than the background. So in the above case, discontinuities helped us to distinguish the movement of the can from the background. So discontinuities help in segmentation of images into regions that correspond to different objects [BA90a]; [SU87]; [TH85]; [TH82] or segment the scene into distinct objects [BR87]; [HB90]; [MB87];[PR90]; [PO80];[SC89a].

1.4 Problems In Computing The Optical Flow Pattern

Optical flow cannot be computed at a point in the image independently of neighbouring points without introducing additional constraints, because the velocity field at each image point has two components while the change in

image brightness at a point in the image plane due to motion yields only one constraint.

Consider for example a patch of a pattern where brightness varies as a function of one image coordinate but not the other. Movement of the pattern in one direction alters the brightness at a particular point, but motion in the other coordinate yields no change. So components of movement in the latter direction cannot be computed locally. So additional constraints must be introduced to determine the flow fully.

1.5 Applications of optical flow

The application of optical flow includes the problem of inferring not only the motion of the observer and objects in the scene, but also the structure of objects and the environment. Since awareness of motion and the generation of mental maps of the structure of our environment are critical components of animal (and human) vision, the conversion of this innate ability to a computer capability is similarly crucial in the field of machine vision.

Consider a five-frame clip of a ball moving from the bottom left of a field of vision, to the top right. Motion estimation techniques can determine that on a two dimensional plane the ball is moving up and to the right and vectors describing this motion can be extracted from the sequence of frames. For the purposes of video compression (e.g., MPEG), the sequence is now described as well as it needs to be. However, in the field of machine vision, the question of whether the ball is moving to the right or if the observer is moving to the left is unknowable yet critical information. Not even if a static, patterned background were present in the five frames, could we confidently state that the ball was moving to the right, because the pattern might have an infinite distance to the observer.

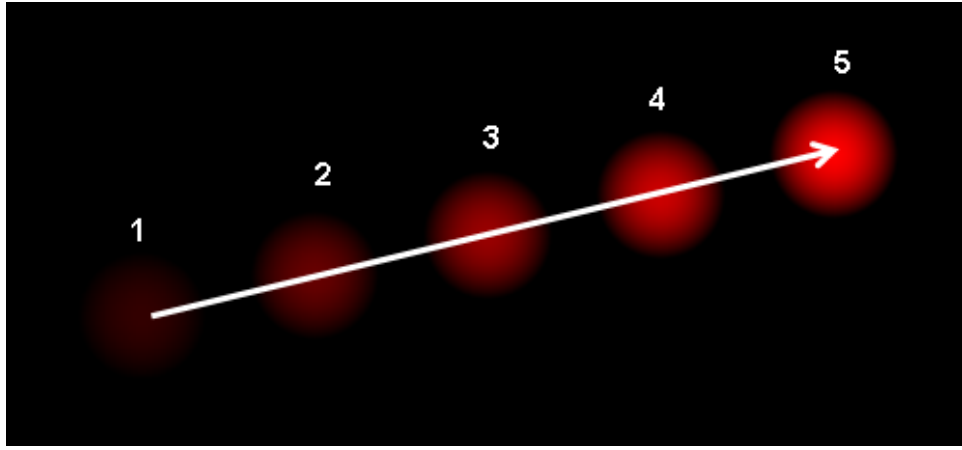


Figure 1.4: Image demonstrating the principle of optical flow. Generated by Doug Hatfield.

In this thesis our main aim is to apply optical flow techniques to one of the most important and interesting research area: the area of cloud motion.

1.6 Application to Cloud Motion

Geostationary satellites are a valuable source of rainfall information due to the availability of a global view of clouds at an acceptable spatial and temporal resolution. However to retrieve the information from the satellite images is a significant challenge. For example, precipitation peaks while the cloud area is rapidly growing and reduces at the time of maximum cloud area [SMS79], Visible (VIS) and Infrared (IR) channels of the satellites can see only the top-of-the-clouds, not rain at the surface of the earth. Moreover, how a cloud changes with time reflects atmospheric instabilities that occur and most instabilities lead to precipitation. As a consequence, we need some descriptions of cloud motion and pattern changes as an explicit link to rain rate.

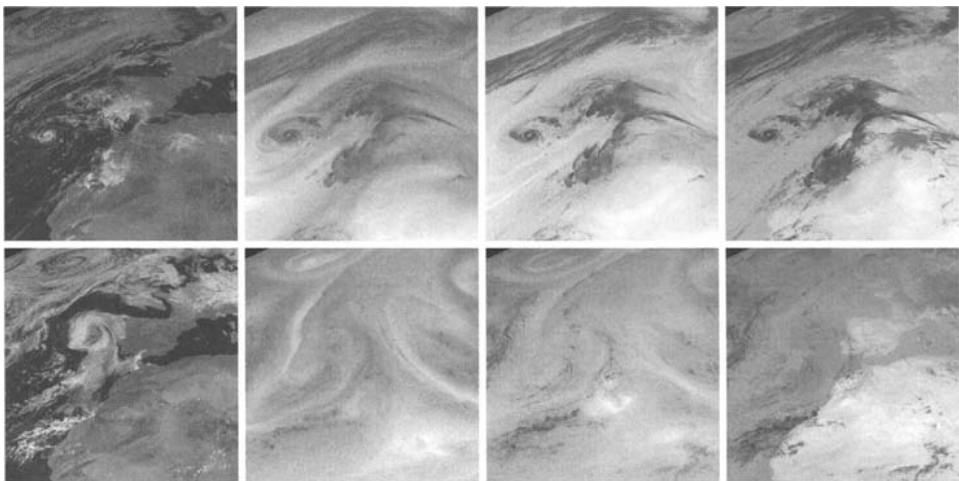


Figure 1.5: Images from different channels of the MSG satellite. From left to right, respectively, the VIS 0.8, WV 6.2, WV 7.3 and IR 10.8. Top row: Images from the Vince hurricane. Bottom row: Images from the sequence on June 5, 2004. Both sequences are from the North Atlantic area.

Meteosat Second Generation satellites replaced in 2002 the former Meteosat, providing a significantly increased amount of information as compared to the previous version in order to continuously observe the whole Earth. In this sense, MSG generates images every 15 min with a 10-bit quantization, a spatial sampling distance of 3 km at subsatellite point in 11 channels, from the visible to the infrared channel, and 1 km in the high resolution visible channel.

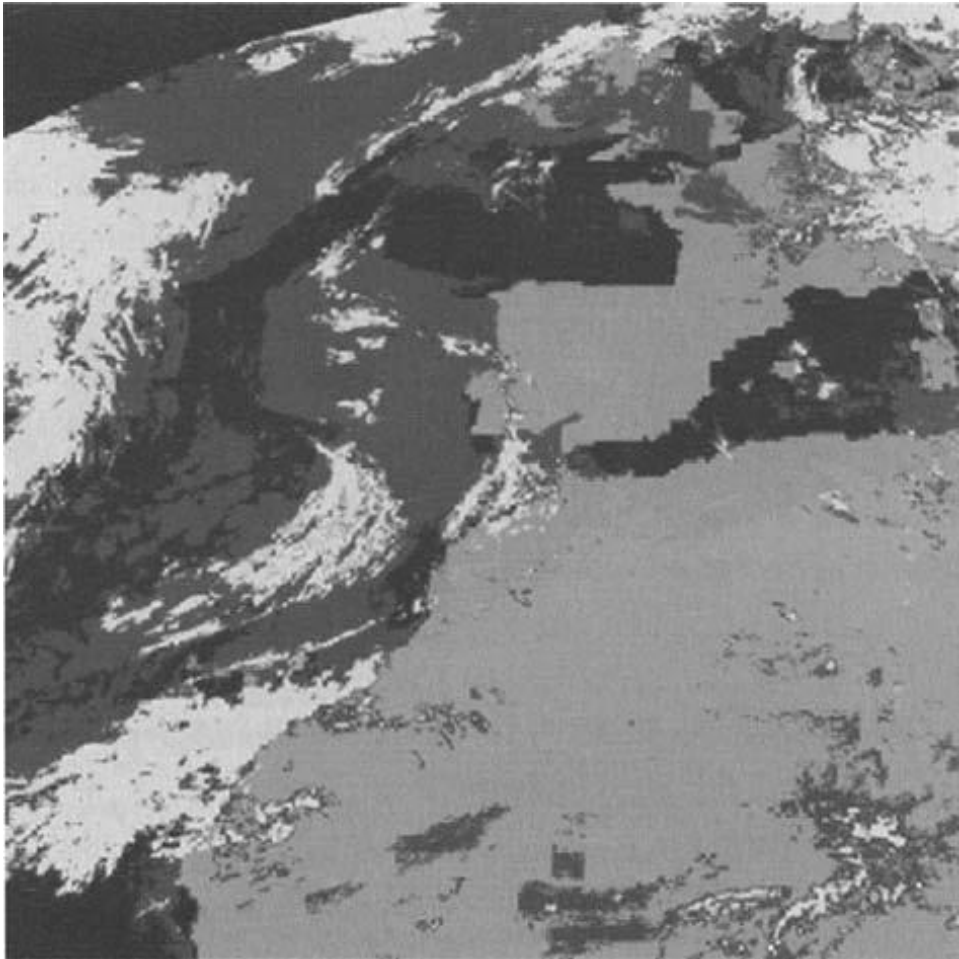


Figure 1.6: In this image, we illustrate, using different greyscale values, the original cloud structure layer classification estimated from the meteorological satellite channels.

Among the most important applications, numerical weather prediction combines the information from different channels, mainly from the VIS 0.8, WV 6.2, WV 7.3 and IR 10.8 channels, to compute the displacement of the clouds between two time instants, that constitute the most important source of information for this application.

1.7 Other Applications of Optical Flow

1.7.1 Computer vision

In computer vision, one is often interested in other properties of the scene that are unrelated to motion; for example, in the case of object recognition, it may be necessary to detect perceptually significant image properties like

intensity edges (upper right of Figure 1.3). Motion and intensity information can be combined to improve the accuracy of motion segmentation [B92a]; [GP87];[HB90]; [TH80], and to distinguish between perceptual features that represent structural properties of the scene and those that are purely surface markings [B92a]. Additionally, if the optical flow is known, then traditionally static computation of image properties, like intensity edges, can be made dynamic and extended over an image sequence. The general problem of motion understanding, and in particular the computation of optical flow, has been one of the most intensely studied areas of computer vision. Despite rich mathematical foundations and steady progress, the results from years of computing and using optical flow have resulted in few practical applications.

1.7.2 Visual Odometry

In robotics, visual odometry is the process of determining the position and orientation of a robot by analyzing the associated camera images. It has been used in a wide variety of robotic applications, such as on the Mars Exploration Rovers. In navigation, odometry is the use of data from the movement of actuators to estimate change in position over time through devices such as rotary encoders to measure wheel rotations. While useful for many wheeled or tracked vehicles, traditional odometry techniques cannot be applied to robots with non-standard locomotion methods, such as legged robots.

In addition, odometry universally suffers from precision problems, since wheels tend to slip and slide on the floor creating a non-uniform distance traveled as compared to the wheel rotations. The error is compounded when the vehicle operates on non-smooth surfaces. Odometry reading become increasingly unreliable over time as these errors accumulate and compound over time. Most existing approaches to visual odometry are based on the following stages.

- Acquire input images: using either single cameras, stereo cameras, or omnidirectional cameras.
- Image correction: apply image processing techniques for lens distortion removal, etc.
- Feature detection: define interest operators, and match features across frames and construct optical flow field.
 - Use correlation to establish correspondence of two images, and no long term feature tracking.
 - Feature extraction and correlation (Lucas–Kanade method).
 - Construct optical flow field.

- Check flow field vectors for potential tracking errors and remove outliers.
- Estimation of the camera motion from the optical flow.
 - Choice 1: Kalman filter for state estimate distribution maintenance.
 - Choice 2: find the geometric and 3D properties of the features that minimize a cost function based on the re-projection error between two adjacent images. This can be done by mathematical minimization or random sampling.
- Periodic repopulation of trackpoints to maintain coverage across the image.

An alternative to feature-based methods is the "direct" or appearance-based visual odometry technique which minimizes an error directly in sensor space and subsequently avoids feature matching and extraction. Another method, coined 'visiodometry' estimates the planar roto-translations between images using Phase correlation instead of extracting features.

1.7.3 Video Compression

Video compression refers to reducing the amount of data used to represent digital video images, and is a combination of spatial image compression and temporal motion compensation. Video compression is an example of the concept of source coding in Information theory.

Video compression typically operates on square-shaped groups of neighboring pixels, often called macroblocks. These pixel groups or blocks of pixels are compared from one frame to the next and the video compression codec sends only the differences within those blocks. This works extremely well if the video has no motion. A still frame of text, for example, can be repeated with very little transmitted data. In areas of video with more motion, more pixels change from one frame to the next. When more pixels change, the video compression scheme must send more data to keep up with the larger number of pixels that are changing. If the video content includes an explosion, flames, a flock of thousands of birds, or any other image with a great deal of high-frequency detail, the quality will decrease, or the variable bitrate must be increased to render this added information with the same level of detail.

Video is basically a three-dimensional array of color pixels. Two dimensions serve as spatial (horizontal and vertical) directions of the moving pictures, and one dimension represents the time domain. A data frame is a set of all pixels that correspond to a single time moment. Basically, a frame is the same as a still picture. Video data contains spatial and temporal redundancy. Similarities can thus be encoded by merely registering

differences within a frame (spatial), or between frames (temporal). Spatial encoding is performed by taking advantage of the fact that the human eye is unable to distinguish small differences in color as easily as it can perceive changes in brightness, so that very similar areas of color can be averaged out in a similar way to jpeg images. With temporal compression only the changes from one frame to the next are encoded as often a large number of the pixels will be the same on a series of frames.

1.8 Overview of the thesis

Chapter 2. The Horn-Schunck optical flow estimation method is reviewed and applied on a simple example to test the method. The image taken as an example is a compact distribution in the unit square in \mathbb{R}^2 and moved with a constant velocity. Two cases are considered: in the first case, discrete image derivatives are taken and in the second case, continuous image derivatives are taken. Then the finite difference iterative method is applied to calculate the optical flow velocities and the results are analyzed.

Chapter 3. In this chapter, the mathematical theory of the Horn-Schunck method is developed, with Dirichlet and Neumann boundary conditions on the optical flow velocities, and existence and uniqueness of the solution to the optical flow problem is proved.

Chapter 4. The finite difference method in Chapter 2 did not give very good results and so another method was tried out using finite elements and the same example was tested and the results were analyzed.

Chapter 5. Finally, our main aim was to apply optical flow estimation method to cloud motion. So we conclude by considering a special case of cloud motion: we considered the flow to be potential and incompressible and then modified the HS method to apply it to two examples:- the first one is an object given by a compact distribution moving in the unit square in \mathbb{R}^2 and the second one as flow of a fluid due to a vortex field situated outside the domain i.e the unit square.

Chapter 2

Finite Difference Iterative Method

2.1 Introduction

In this chapter we want to determine the optical flow velocity of a given brightness pattern using the finite difference method. The corresponding method was developed by Horn and Schunck[HS81]. Here gradient-based approaches are used.

2.2 Domain of the restricted problem

We consider a relatively simple world where apparent velocity of brightness patterns can be directly identified with the movement of surfaces in the scene. To avoid variations in brightness due to shading effects we assume the surface is flat. We also assume that incident illumination is uniform across the surface. Then the brightness at a point of the image is proportional to the reflectance of surface at the given point. Also we assume initially that reflectance varies smoothly and has no spatial discontinuities which would imply that the image brightness is differentiable.

Due to all these restrictions, the motion of brightness patterns in the image is determined directly by motion of corresponding points on surface of the object.

2.3 Constraints on the motion of an image

2.3.1 Data conservation

The approach of [HS81] exploits the assumption of data conservation (See Fig 2.1) i.e. image intensity corresponding to a small image region remains the same, although the location of the region may change.

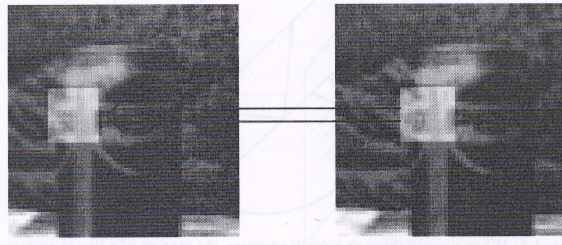


Figure 2.1: Data Conservation assumption. The highlighted region in the right image looks roughly the same as the region in the left image, despite the fact that it has moved: Courtesy ([MB92]).

Our given data is a sequence of brightness patterns $E(x, y, t)$ where (x, y) represents the spatial coordinates and t is the time coordinate. As brightness of a particular point in the pattern is constant, so

$$\frac{dE}{dt} = 0$$

By the chain rule for derivatives (See Appendix A) we have,

$$\frac{\partial E}{\partial x} \cdot \frac{dx}{dt} + \frac{\partial E}{\partial y} \cdot \frac{dy}{dt} + \frac{\partial E}{\partial t} = 0$$

So we have the data conservation constraint,

$$E_x u + E_y v + E_t = 0 \quad (2.1)$$

where

$$u = \frac{dx}{dt}, v = \frac{dy}{dt}.$$

The equation (2.1) can also be written as $(E_x, E_y) \cdot (u, v) = -E_t$.

or

$$E_t + \nabla E \cdot U = 0 \text{ where } U = \begin{pmatrix} u \\ v \end{pmatrix}$$

This means the solution set of (2.1) defines a line in the $u-v$ space which is perpendicular to the intensity spatial gradient ∇E . The component of the optical flow in the direction of the brightness gradient (E_x, E_y) equals

$$\frac{-E_t}{\sqrt{E_x^2 + E_y^2}}$$

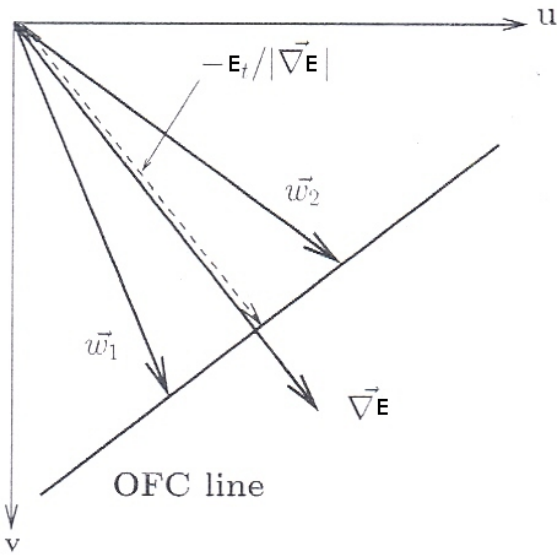


Figure 2.2: The aperture problem: the solutions of (2.1) define a line in the (u, v) -space. The vectors w_1 and w_2 are possible solutions: Courtesy ([MB92])

The problem is ill-posed as we cannot determine the component of movement in the direction of iso-brightness contours, at right angles to brightness gradient (one equation and two unknowns). This is commonly referred to as the aperture problem. So the flow velocity (u, v) cannot be computed locally without additional constraints

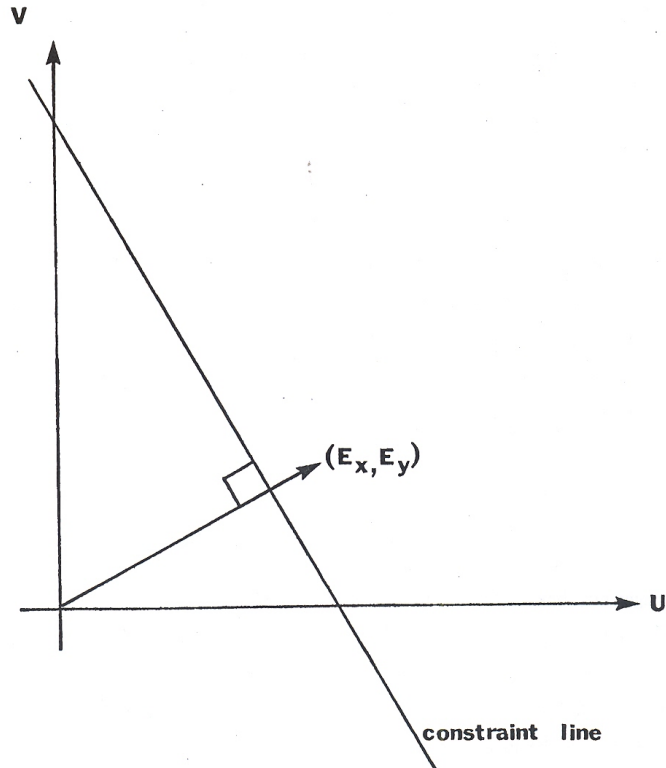


Figure 2.3: The basic rate of change of image brightness equation constrains the optical flow velocity. The velocity (u, v) has to lie along a certain line perpendicular to the brightness gradient vector (E_x, E_y) in the velocity space: Courtesy ([HS81]).

2.3.2 Smoothness constraints

The data conservation constraint (2.1) alone is not sufficient to accurately recover optical flow. First, local motion estimates, based on data conservation, may only partially constrain the solution. Consider a motion of a line in Figure 2.3. Within a small region, the data conservation constraint cannot uniquely determine the motion of the line; an infinite number of interpretations are consistent with the constraint. This is commonly referred to as the aperture problem [H86]. This can be seen in Fig 2.4. In the first picture the original image pattern is viewed through an aperture. In the second picture the image is moved up and then viewed through the aperture. In the third picture the image is moved to the left and viewed through the aperture. In all the three cases we see that through the aperture the image pattern is the same. Another illustration is shown in Fig 2.5 with the interpretations of the movement of the brightness pattern. Hence we cannot predict the motion of the image pattern when viewed through a small aperture.

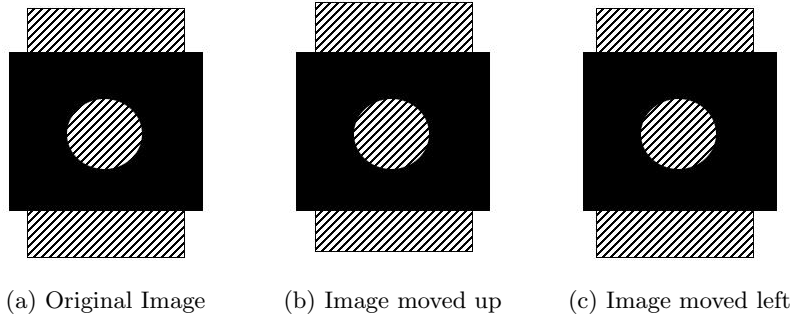


Figure 2.4: Illustration of the aperture problem.

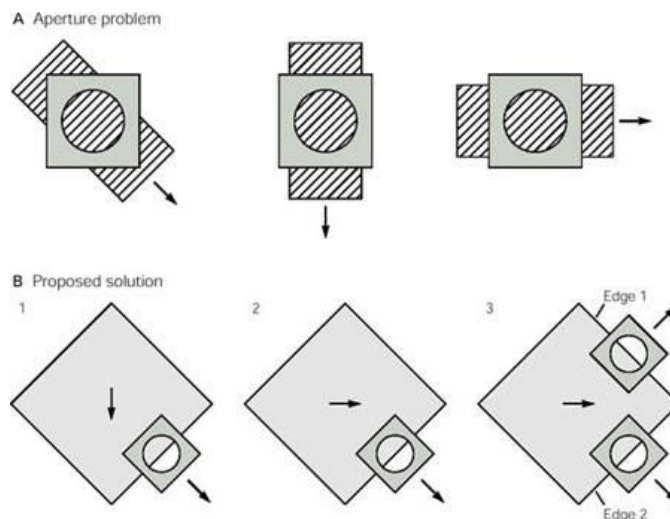


Figure 2.5: Another illustration of the aperture problem

Second and more importantly, motion estimates based on data conservation constraint are very sensitive to noise in the images, particularly in regions where there is very little spatial variation.

To overcome these problems, many approaches have exploited a spatial coherence assumption:

Neighbouring points in the scene typically belong to the same surface and hence have similar velocities. Since neighbouring points in the scene project to neighbouring points in the image plane, we expect optical flow to vary smoothly. This assumption is typically implemented as the smoothness constraint.

So here we try to limit the difference between the flow velocity at a point and the average velocity over a small neighbourhood, containing the point. Equivalently, we can minimize the sum of the squares of the Laplacians of

x and y components of the flow. We use this fact while calculating the minimization equations.

2.4 Problem statement

So with all the constraints taken care of, finally we can formulate the problem statement.

Let $E : \Omega \times \mathbb{R}^+ \rightarrow \mathbb{R}$, be an image sequence, where $\Omega \subseteq \mathbb{R}^2$ is a bounded domain of the spatial coordinates and \mathbb{R}^+ is the domain of the time coordinate.

HS estimated the optical flow, the field U of optical velocities over Ω , by minimizing the functional,

$$J(U) = \frac{1}{2} \int_{\Omega} (\nabla E \cdot U + E_t)^2 dx dy + \frac{K}{2} \int_{\Omega} \|\nabla U\|^2 \quad (2.2)$$

where $U = (u, v)$.

The first term in the functional is the data conservation constraint and the second term in the functional is the smoothness constraint. $K > 0$ is a parameter, called Smoothing Parameter, which is used to make the order of both the terms same so that each of them has a significant contribution in calculation of the flow velocities.

The boundary conditions on the flow velocity could be either Dirichlet or Neumann. Neumann boundary conditions will be the preferred choice as we usually do not expect the flow velocity to attain a particular value on the boundary. We only expect the change of the flow velocity across the boundary to be constant. But we will also deal with Dirichlet boundary conditions where we assume that there is no flow across the boundary.

The Euler-Lagrange equations obtained by the minimization of J are

$$\begin{aligned} (E_t + \nabla E \cdot U) E_x - K \Delta u &= 0 \\ (E_t + \nabla E \cdot U) E_y - K \Delta v &= 0 \end{aligned} \quad (2.3)$$

(See Section 3.2).

2.5 Discretization

Let Ω be discretized by the unit spacing grid and the grid points be indexed by (x_i, y_j) where $1 \leq i, j \leq N$. Let the time axis be discretized by the unit spacing grid and indexed by t_k , $1 \leq k \leq M$.

2.6 Estimating the partial derivatives of E

Horn-Schunck proposed the idea of replacing the derivatives of the image E with their finite difference approximations. The following estimates are used. Let $E_x(x_i, y_j, t_k) = E_x^{i,j,k}$, $E_y(x_i, y_j, t_k) = E_y^{i,j,k}$, $E_t(x_i, y_j, t_k) = E_t^{i,j,k}$. Each of the estimates is the average of the first four differences taken over adjacent measurements in the cube as shown in (Fig 2.6).

$$\begin{aligned} E_x^{i,j,k} &\approx \frac{1}{4} \{E_{i,j+1,k} - E_{i,j,k} + E_{i+1,j+1,k} - E_{i+1,j,k} + E_{i,j+1,k+1} \\ &\quad - E_{i,j,k+1} + E_{i+1,j+1,k+1} - E_{i+1,j,k+1}\} \\ E_y^{i,j,k} &\approx \frac{1}{4} \{E_{i+1,j,k} - E_{i,j,k} + E_{i+1,j+1,k} - E_{i,j+1,k} + E_{i+1,j,k+1} \\ &\quad - E_{i,j,k+1} + E_{i+1,j+1,k+1} - E_{i,j+1,k+1}\} \\ E_t^{i,j,k} &\approx \frac{1}{4} \{E_{i,j,k+1} - E_{i,j,k} + E_{i+1,j,k+1} - E_{i+1,j,k} + E_{i,j+1,k+1} \\ &\quad - E_{i,j+1,k} + E_{i+1,j+1,k+1} - E_{i+1,j+1,k}\} \end{aligned} \quad (2.4)$$

where i corresponds to the x -axis direction, j corresponds to the y -axis direction and k corresponds to the time axis and $E_{i,j,k}$ represents the value of the image intensity at the (i, j) position and at the k th stage i.e. $E_{i,j,k} = E(x_i, y_j, t_k)$.

2.7 Estimating the Laplacian of flow velocities

Δu and Δv can be approximated using

$$\begin{aligned} \Delta u(x_i, y_j, t_k) &\approx \kappa(\bar{u}_{i,j,k} - u_{i,j,k}) \\ \Delta v(x_i, y_j, t_k) &\approx \kappa(\bar{v}_{i,j,k} - v_{i,j,k}) \end{aligned}$$

where

$$\begin{aligned} \bar{u}_{i,j,k} &= \frac{1}{6} \{u_{i-1,j,k} + u_{i,j+1,k} + u_{i+1,j,k} + u_{i,j-1,k}\} \\ &\quad + \frac{1}{12} \{u_{i-1,j-1,k} + u_{i-1,j+1,k} + u_{i+1,j+1,k} + u_{i+1,j-1,k}\}. \\ \bar{v}_{i,j,k} &= \frac{1}{6} \{v_{i-1,j,k} + v_{i,j+1,k} + v_{i+1,j,k} + v_{i,j-1,k}\} \\ &\quad + \frac{1}{12} \{v_{i-1,j-1,k} + v_{i-1,j+1,k} + v_{i+1,j+1,k} + v_{i+1,j-1,k}\}. \end{aligned} \quad (2.5)$$

The proportionality factor $\kappa = 3$ if the averages are computed as above and if the grid spacing interval is of unit length. (Fig 2.7) illustrates the assignment of weights to neighbouring points.

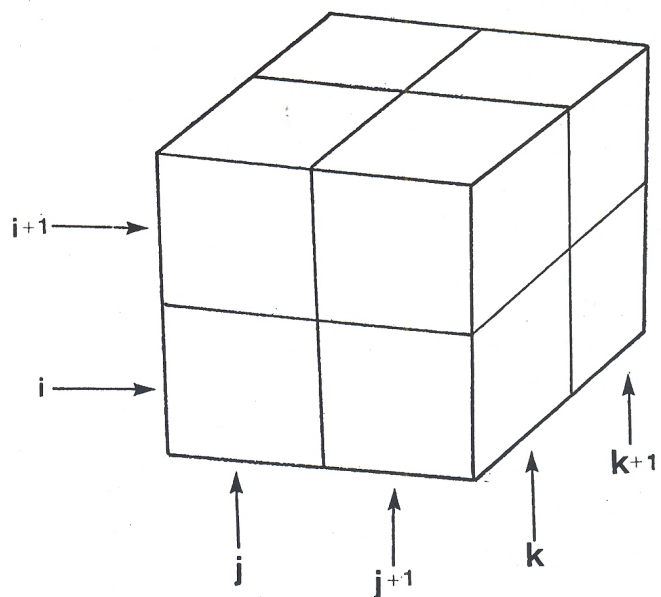


Figure 2.6: The 3 partial derivatives of image brightness at the center of the cube are each estimated from the average of first differences along 4 parallel edges of the cube. Here the column index j corresponds to the x-direction in the image, the row index i to the y-direction, while k lies in the time direction: Courtesy ([HS81]).

$\frac{1}{12}$	$\frac{1}{6}$	$\frac{1}{12}$
$\frac{1}{6}$	-1	$\frac{1}{6}$
$\frac{1}{12}$	$\frac{1}{6}$	$\frac{1}{12}$

Figure 2.7: The Laplacian is estimated by subtracting the value at a point(represented in the figure by the central square with weight -1) from a weighted average of the values at neighbouring points. Shown here are suitable weights by which values can be multiplied: Courtesy ([HS81]).

2.8 Minimization

With all the approximations as shown in Sec 2.6 and Sec 2.7, the Euler-Lagrange Equations in (2.3) can be written as

$$\begin{aligned} (K + E_x^2)u + E_x E_y v &= (K\bar{u} - E_x E_t) \\ E_x E_y u + (K + E_y^2)v &= (K\bar{v} - E_y E_t) \end{aligned} \quad (2.6)$$

or

$$\begin{aligned} (K + E_x^2 + E_y^2)(u - \bar{u}) &= -E_x(E_x \bar{u} + E_y \bar{v} + E_t) \\ (K + E_x^2 + E_y^2)(v - \bar{v}) &= -E_y(E_x \bar{u} + E_y \bar{v} + E_t) \end{aligned} \quad (2.7)$$

The discretized Euler Lagrange equations are as follows

$$\begin{aligned} (K + (E_x^{i,j,k})^2 + (E_y^{i,j,k})^2)(u_{i,j,k} - \bar{u}_{i,j,k}) &= -E_x^{i,j,k}(E_x^{i,j,k}\bar{u}_{i,j,k} + E_y^{i,j,k}\bar{v}_{i,j,k} + E_t^{i,j,k}) \\ (K + (E_x^{i,j,k})^2 + (E_y^{i,j,k})^2)(v_{i,j,k} - \bar{v}_{i,j,k}) &= -E_y^{i,j,k}(E_x^{i,j,k}\bar{u}_{i,j,k} + E_y^{i,j,k}\bar{v}_{i,j,k} + E_t^{i,j,k}) \end{aligned} \quad (2.8)$$

This shows that the value of the flow velocity (u, v) which minimizes the error ε^2 lies in the direction towards the constraint line along a line that

intersects the constraint line at right angles. This relationship is illustrated geometrically in Fig. 2.8. The distance from the local average is proportional to the error in the basic formula for rate of change of brightness when \bar{u}, \bar{v} are substituted for u and v . Finally we see that K plays a significant role only for the areas where the brightness gradient is small, preventing haphazard adjustments to the estimated flow velocity occasioned by noise in the estimated derivatives.

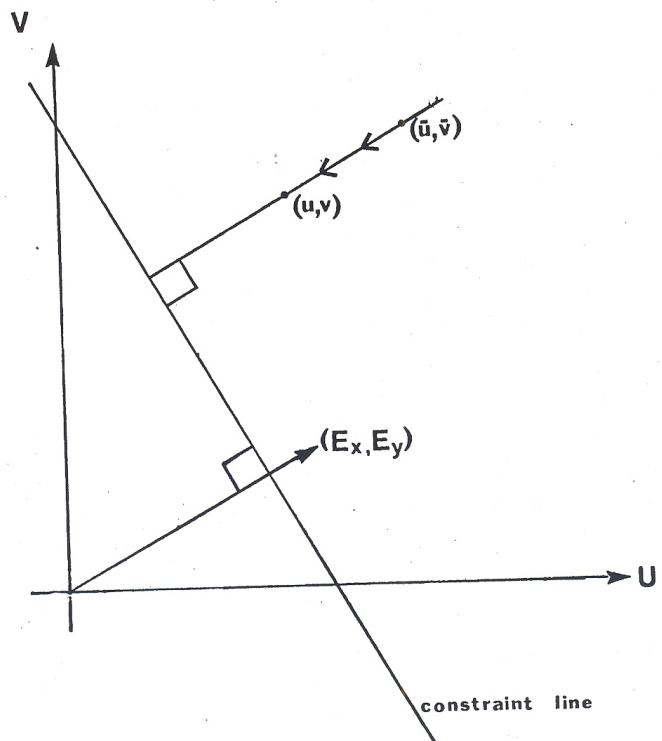


Figure 2.8: The value of the flow velocity which minimizes the error lies on a line drawn from the local average of the flow velocity perpendicular to the constraint line: Courtesy ([HS81]).

2.9 Discretized iterative scheme

The discretized Euler-Lagrange equations (2.8) lead to the following scheme for solving the optical flow problem

$$\begin{aligned} u_{i,j,k}^{n+1} &= \bar{u}_{i,j,k}^n - \frac{E_x^{i,j,k}(E_x^{i,j,k}\bar{u}_{i,j,k}^n + E_y^{i,j,k}\bar{v}_{i,j,k}^n + E_t^{i,j,k})}{K + (E_x^{i,j,k})^2 + (E_y^{i,j,k})^2} \\ v_{i,j,k}^{n+1} &= \bar{v}_{i,j,k}^n - \frac{E_y^{i,j,k}(E_x^{i,j,k}\bar{u}_{i,j,k}^n + E_y^{i,j,k}\bar{v}_{i,j,k}^n + E_t^{i,j,k})}{K + (E_x^{i,j,k})^2 + (E_y^{i,j,k})^2} \end{aligned} \quad (2.9)$$

where $E_x^{i,j,k}, E_y^{i,j,k}, E_t^{i,j,k}$ are given by (2.4) and $\bar{u}_{i,j,k}^n, \bar{v}_{i,j,k}^n$ are given by (2.5).

This type of scheme is an iterative scheme as we update the old value of the optical flow velocity with the new one using the above scheme depending on the accuracy limit we want the scheme to satisfy.

2.10 Introduction of Courant-Friedrich-Lewey(CFL) condition

Whatever we have done upto now was with unit spacing grid. We would now want to discretize our grid arbitrarily with x -spacing as Δx , y -spacing as Δy . To choose Δt , we now introduce some conditions which will depend on Δx and Δy . This has to be done so that the images we enter in our code should be such that they remain close to each other depending on the grid size. These conditions are called CFL conditions as they were invented by the trio- Courant, Friedrich and Lewey. The natural choice for CFL condition is that the distance covered by the image in time Δt will be less than the Δx and Δy so that two consecutive images remain in the same grid element.

So,

$$\begin{aligned} |u\Delta t| &\leq \Delta x = h \\ |v\Delta t| &\leq \Delta y = h \end{aligned}$$

This implies,

$$|\Delta t| \leq h \min \left\{ \frac{1}{|u|}, \frac{1}{|v|} \right\}$$

Since we do not know anything apriori about $\min \left\{ \frac{1}{|u|}, \frac{1}{|v|} \right\}$ so we will substitute $\min \left\{ \frac{1}{|u|}, \frac{1}{|v|} \right\}$ by some CFL Number so that $\Delta t (\leq h * \text{CFL Number})$ is sufficiently small.

2.11 The case we consider

The iterative formula (2.9) holds for $\Delta x = \Delta y = \Delta t = 1$.

For our case we choose $\Delta x = \Delta y = h$ and our Δt will be chosen such that it satisfies some CFL condition.

Then we have:-

$$u\left(\frac{K}{(\Delta x)^2} + E_x^2\right) + E_x E_y v = \left(\frac{K\bar{u}}{(\Delta x)^2} - E_x E_t\right).$$

$$v\left(\frac{K}{(\Delta y)^2} + E_y^2\right) + E_x E_y u = \left(\frac{K\bar{v}}{(\Delta y)^2} - E_y E_t\right).$$

So we can write the equation in matrix notations as follows:-

$$\begin{pmatrix} \frac{K}{(\Delta x)^2} + E_x^2 & E_x E_y \\ E_x E_y & \frac{K}{(\Delta y)^2} + E_y^2 \end{pmatrix} \begin{pmatrix} u \\ v \end{pmatrix} = \begin{pmatrix} \frac{K\bar{u}}{(\Delta x)^2} - E_x E_t \\ \frac{K\bar{v}}{(\Delta y)^2} - E_y E_t \end{pmatrix}$$

$$\text{Let } A = \begin{pmatrix} \frac{K}{(\Delta x)^2} + E_x^2 & E_x E_y \\ E_x E_y & \frac{K}{(\Delta y)^2} + E_y^2 \end{pmatrix}$$

$$\text{Then } \text{Det}(A) = \frac{\alpha^4}{(\Delta x \Delta y)^2} + K \left[\frac{E_x^2}{(\Delta y)^2} + \frac{E_y^2}{(\Delta x)^2} \right]$$

So,

$$\begin{pmatrix} u \\ v \end{pmatrix} = \frac{1}{\text{Det}(A)} \begin{pmatrix} \frac{K}{(\Delta y)^2} + E_y^2 & -E_x E_y \\ -E_x E_y & \frac{K}{(\Delta x)^2} + E_x^2 \end{pmatrix} \begin{pmatrix} \frac{K\bar{u}}{(\Delta x)^2} - E_x E_t \\ \frac{K\bar{v}}{(\Delta y)^2} - E_y E_t \end{pmatrix}$$

This gives,

$$u = \frac{1}{\frac{K}{(\Delta x \Delta y)^2} + \left[\frac{E_x^2}{(\Delta y)^2} + \frac{E_y^2}{(\Delta x)^2} \right]} \left[\frac{\bar{u}}{(\Delta x)^2} \left(\frac{K}{(\Delta y)^2} + E_y^2 \right) - \frac{E_x}{(\Delta y)^2} (\bar{v} E_y + E_t) \right]$$

$$v = \frac{1}{\frac{K}{(\Delta x \Delta y)^2} + \left[\frac{E_x^2}{(\Delta y)^2} + \frac{E_y^2}{(\Delta x)^2} \right]} \left[\frac{\bar{v}}{(\Delta y)^2} \left(\frac{K}{(\Delta x)^2} + E_x^2 \right) - \frac{E_y}{(\Delta x)^2} (\bar{u} E_x + E_t) \right]$$

Now let $\Delta x = \Delta y = h$ and let $\bar{E}_x = E_x \cdot \Delta x$, $\bar{E}_y = E_y \cdot \Delta y$, $\bar{E}_t = E_t \cdot \Delta t$

Then

$$\begin{pmatrix} u \\ v \end{pmatrix} = \frac{1}{\text{Det}(A)} \begin{pmatrix} \alpha^4 \bar{u} - K \lambda \bar{E}_x \bar{E}_t + K \bar{u} \bar{E}_y^2 - \bar{E}_x \bar{E}_y K \bar{v} \\ \alpha^4 \bar{v} - K \lambda \bar{E}_y \bar{E}_t + K \bar{v} \bar{E}_x^2 - \bar{E}_x \bar{E}_y K \bar{u} \end{pmatrix}$$

$$\text{where } A = \begin{pmatrix} K + \bar{E}_x^2 & \bar{E}_x \bar{E}_y \\ \bar{E}_x \bar{E}_y & K + \bar{E}_y^2 \end{pmatrix}, \text{ Det}(A) = \alpha^4 + K (\bar{E}_x^2 + \bar{E}_y^2) \text{ and } \lambda = \frac{h}{\Delta t}.$$

So we have,

$$\begin{aligned} u &= \frac{1}{K + \bar{E}_x^2 + \bar{E}_y^2} [(K + \bar{E}_x^2 + \bar{E}_y^2) \bar{u} - \bar{E}_x (\bar{E}_x \bar{u} + \bar{E}_y \bar{v} + \lambda \bar{E}_t)] \\ v &= \frac{1}{K + \bar{E}_x^2 + \bar{E}_y^2} [(K + \bar{E}_x^2 + \bar{E}_y^2) \bar{v} - \bar{E}_y (\bar{E}_x \bar{u} + \bar{E}_y \bar{v} + \lambda \bar{E}_t)] \end{aligned} \quad (2.10)$$

2.12 The modified discretized iterative formula

The modified discretized iterative solution is given by:-

$$\begin{aligned} u_{i,j,k}^{n+1} &= \bar{u}_{i,j,k} - \frac{\bar{E}_x^{i,j,k} (\bar{E}_x^{i,j,k} \bar{u}_{i,j,k}^n + \bar{E}_y^{i,j,k} \bar{v}_{i,j,k}^n + \lambda \bar{E}_t^{i,j,k})}{K + (\bar{E}_x^{i,j,k})^2 + (\bar{E}_y^{i,j,k})^2} \\ v_{i,j,k}^{n+1} &= \bar{v}_{i,j,k} - \frac{\bar{E}_y^{i,j,k} (\bar{E}_x^{i,j,k} \bar{u}_{i,j,k}^n + \bar{E}_y^{i,j,k} \bar{v}_{i,j,k}^n + \lambda \bar{E}_t^{i,j,k})}{K + (\bar{E}_x^{i,j,k})^2 + (\bar{E}_y^{i,j,k})^2} \end{aligned} \quad (2.11)$$

where $\bar{E}_x^{i,j,k} = E_x^{i,j,k} \cdot \Delta x$, $\bar{E}_y^{i,j,k} = E_y^{i,j,k} \cdot \Delta y$, $\bar{E}_t^{i,j,k} = E_t^{i,j,k} \cdot \Delta t$ and $E_x^{i,j,k}, E_y^{i,j,k}, E_t^{i,j,k}$ are given by (2.4), $\bar{u}_{i,j,k}^n, \bar{v}_{i,j,k}^n$ are given by (2.5), $\lambda = \frac{h}{\Delta t}$.

2.13 Convergence of Horn and Schunck Optical Flow estimation method

We have obtained an iterative formula for finding out the solution to the optical flow problem. The next important thing is whether this method converges or not. It is directly proved in [MM04] that the iterative equations (2.9) (commonly referred to as the Jacobi iterations) converge. Modifying

the proof we can find that (2.11) also converges. So we can proceed to implement this method using C program.

2.14 Programming implementation

We have already obtained the iterative formula. We have chosen our CFL Number as 1.0 and so Δt should be chosen s.t. $\Delta t \leq h$.

Our domain is the unit square in \mathbb{R}^2 i.e. $[0, 1] \times [0, 1]$.

We have taken our image at time t_0 to be E_0 defined as:-

$$E_0(x, y) = E(x, y, 0) = e^{[-50 * \{(x - 0.5)^2 + (y - 0.5)^2\}]}$$

and for testing the accuracy of the method we move the image with a pre-defined constant velocity of $u = 1.0$ and $v = 1.0$

So at time t , the image will be given by,

$$E(x, y, t) = E(x - ut, y - vt, 0) = E_0(x - ut, y - vt)$$

using the characteristic method

So for implementing the above iterative method, we take 2 successive images $E(x, y, 0)$ and $E(x, y, \Delta t)$ at times 0 and Δt respectively and try to recover the constant velocities as we expect.

We implement this method numerically using the C programming language in Ubuntu and compile it using the gcc compiler.

2.15 Programming data

DOMAIN:- Unit Square in \mathbb{R}^2 i.e. $[0, 1] \times [0, 1]$.

IMAGE:-

$$E(x, y, t) = e^{[-50 * \{(x - 1.0 * t - 0.5)^2 + (y - 1.0 * t - 0.5)^2\}]},$$

$$(x, y) \in [0, 1] \times [0, 1], t \in \mathbb{R}^+$$

h :- .01010101

CFL NUMBER:- 1.0

Time step Δt :- 0.01

SMOOTHING PARAMETER K:- 1.0

2.16 Results obtained

The following are the given images at time $t = 0$

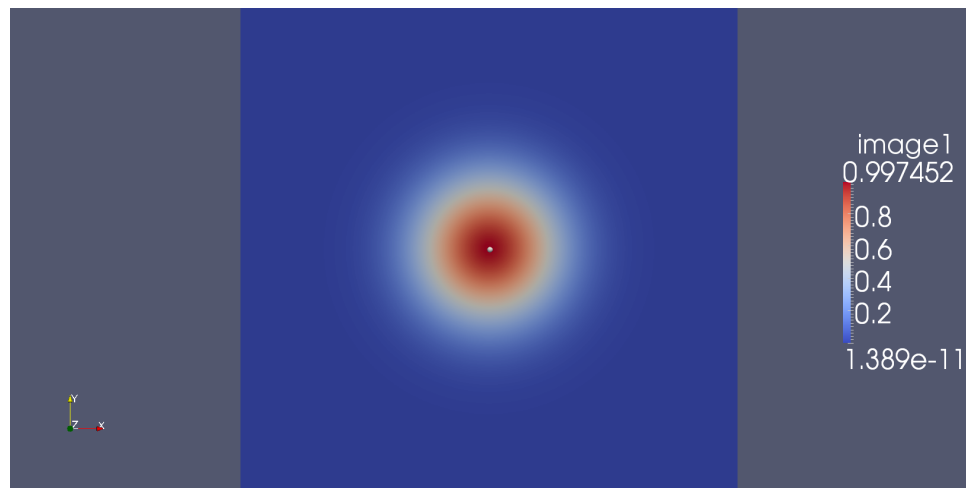


Figure 2.9: The given intial image.The central dot represents the point(0.5,0.5).

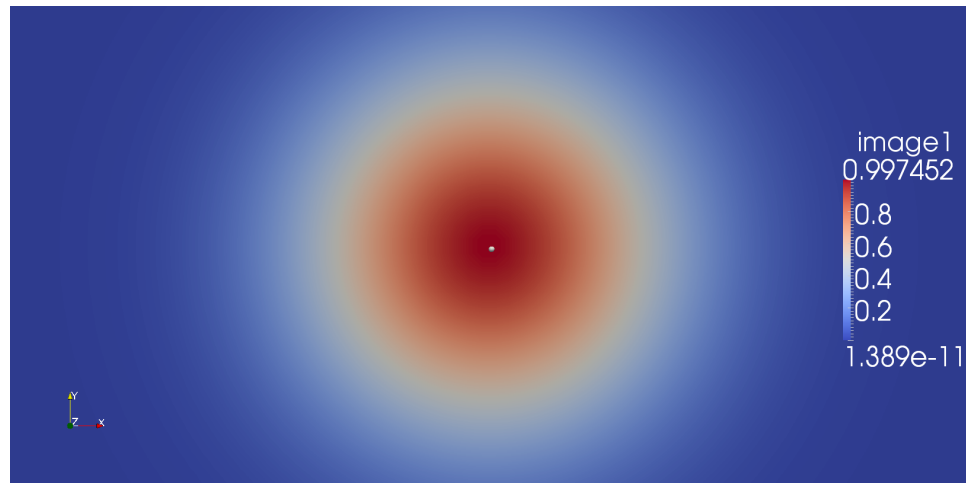


Figure 2.10: The magnified figure of the given initial image.

2.16.1 With discrete image derivatives

First we use images at two consecutive times 0 and Δt to calculate the derivatives of E . We obtain the following results:-

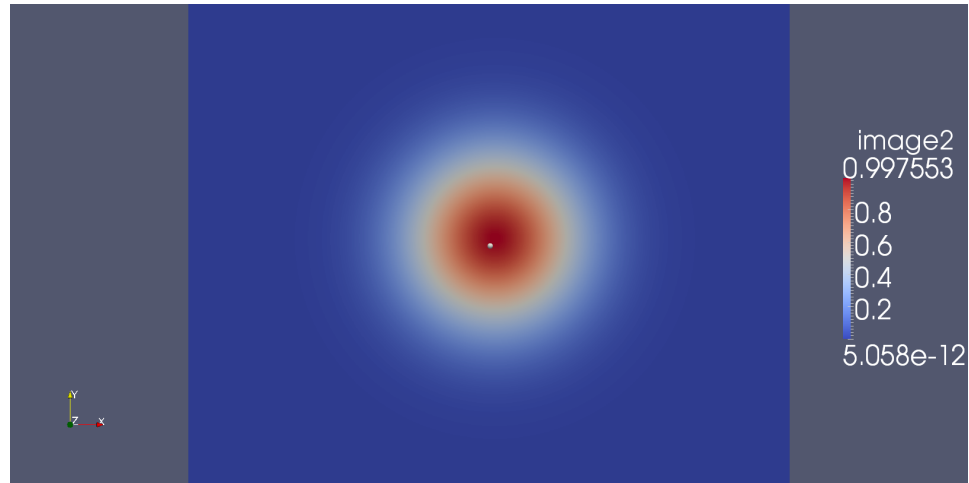


Figure 2.11: The image at time Δt . Notice how the image has moved w.r.t to the central dot.

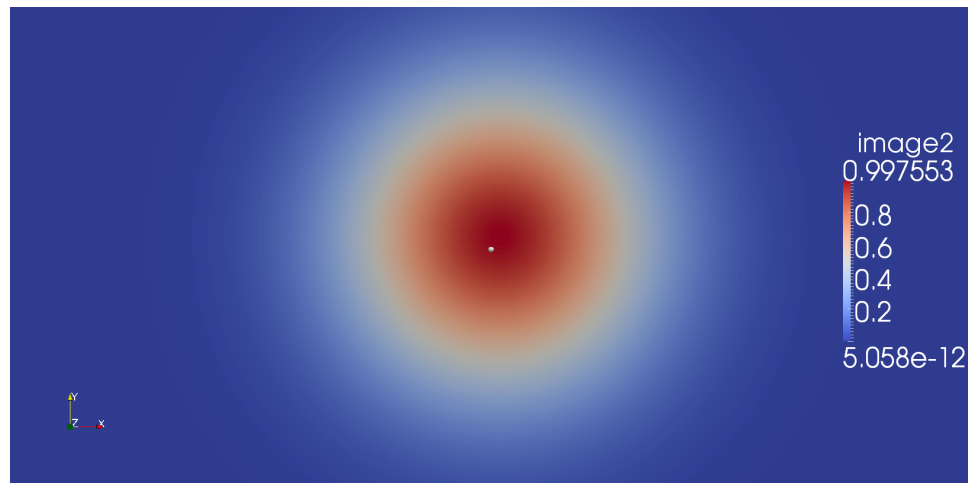


Figure 2.12: The magnified figure of the image at time Δt .

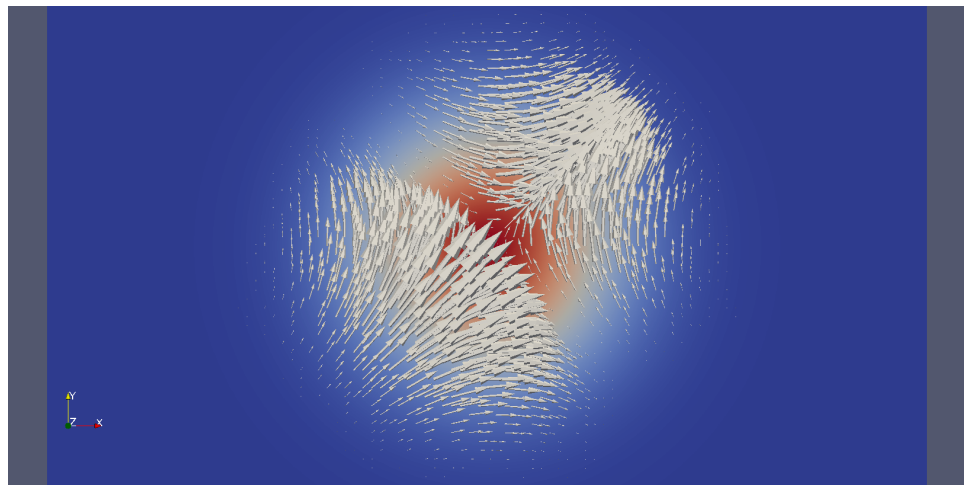


Figure 2.13: The velocities obtained at time Δt . The length of the arrows represent magnitude of velocity at that point and the direction of the arrows represent the velocity vector direction.

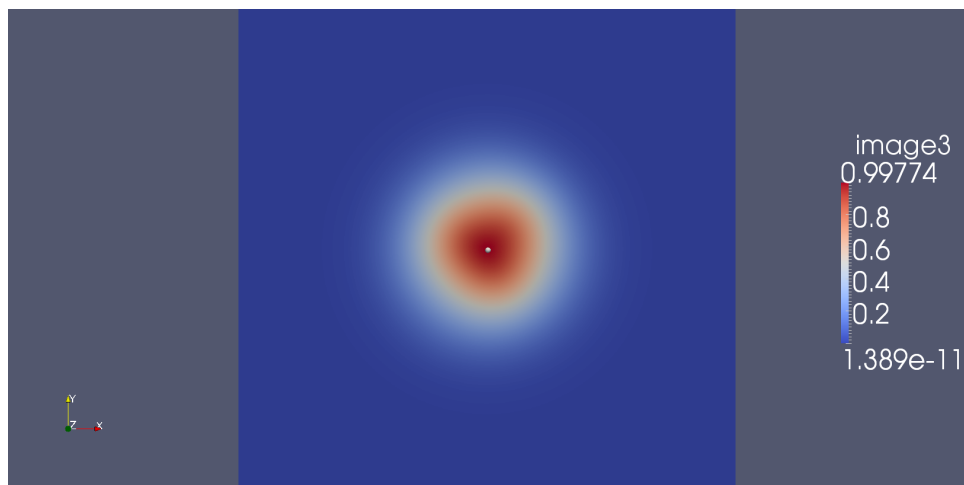


Figure 2.14: The image obtained at time Δt by moving the initial image with the obtained velocities

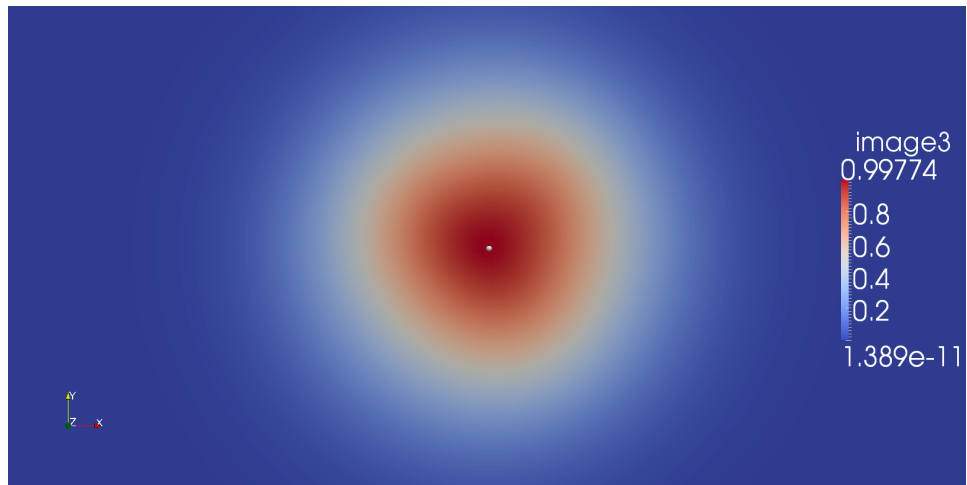


Figure 2.15: Magnification of the image obtained by moving the initial image with the obtained velocities

2.16.2 With continuous image derivatives

Since the image we have entered is C^∞ so we pass on the actual derivatives of the image at time $\frac{\Delta t}{2}$ in the program.

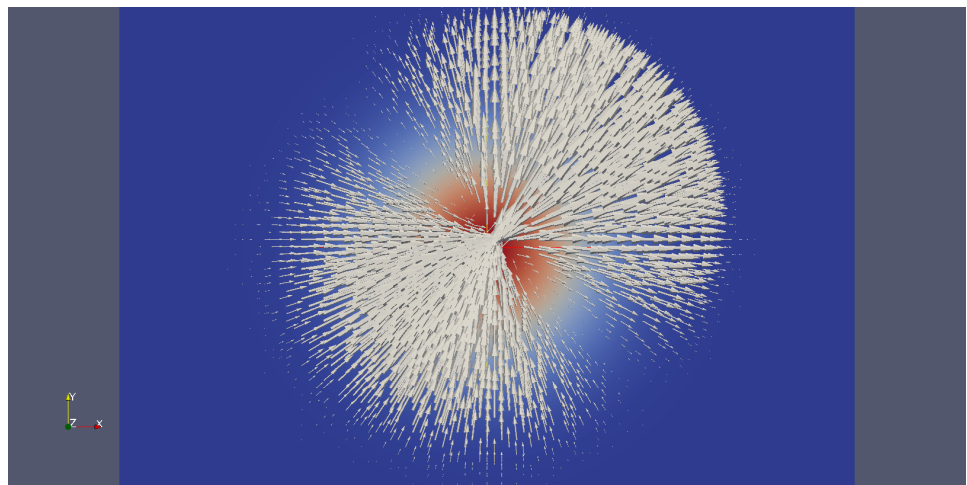


Figure 2.16: The velocities obtained at time $\frac{\Delta t}{2}$.

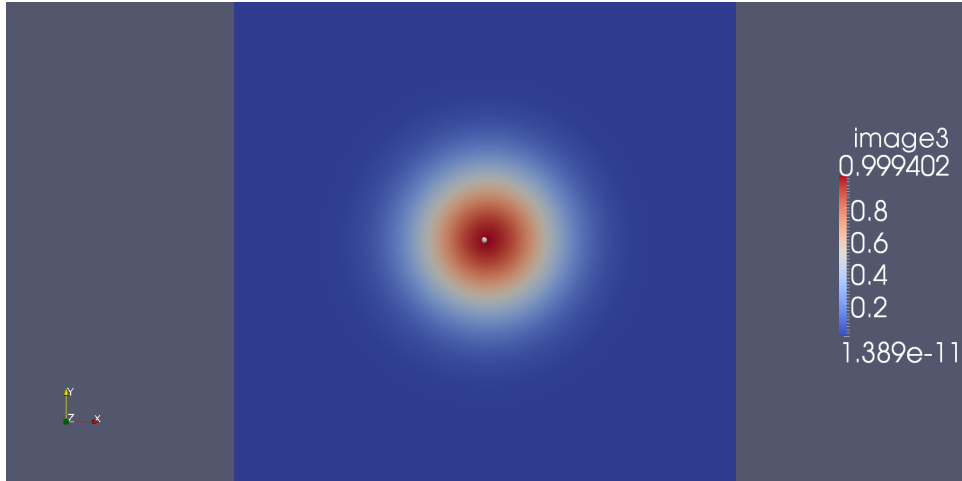


Figure 2.17: Image obtained at time $\frac{\Delta t}{2}$ by moving the initial image with the obtained velocities.

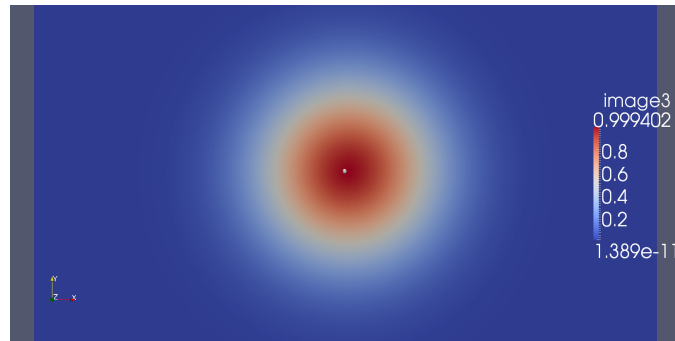


Figure 2.18: Magnification of the image obtained by moving the initial image with the obtained velocities.

2.17 Conclusions

The pictures shows the results obtained. We have used Neumann Boundary conditions in our program for the way \bar{u} and \bar{v} are calculated at the point i, j, k they use the surrounding 8 neighbours and u and v are updated using \bar{u} and \bar{v} . When i, j, k represents the position adjacent to the boundary then we assume that the value of u on the boundary equals $u(i, j, k)$. In this way there is no change of flux across the boundary and hence we have Neumann Boundary condition. (Fig 2.9) and (Fig 2.10) represents the given image at time 0. For the first case we use the discrete formulation of the derivatives using the initial given image and the image at time Δt and then we implement the program. The results are shown from (Fig 2.11) to (Fig

2.15). The velocity vectors obtained are proper in a neighbourhood of the line $(y - 0.5) = (x - 0.5)$ but in other regions we see that velocities are not proper as we had expected constant velocities $u = 1.0, v = 1.0$. That is why the middle portion of the image has moved in the proper direction as we expect to but the other parts of the image move in other directions. We already know the exact velocity with which we have moved the initial image and so we calculate the relative L^2 error in the obtained velocities w.r.t the exact ones. The **relative L^2 error in the velocity** was found out to be 1.025654 which is of order 1.

So in an attempt to decrease the order of L^2 error we have approximated the image derivatives as well as the laplacians of the velocities using finite differences. We cannot do without the approximations of the laplacians but what we can do is to have the correct image derivatives. Since our image is C^∞ , so we can calculate its derivatives w.r.t x, y, t and use them in the program. We pass the image derivatives at time $\frac{\Delta t}{2}$ and then calculate the velocities. The results are shown from (Fig 2.16) to (Fig 2.18). Using those velocities we move the initial image and find the image formed at time $\frac{\Delta t}{2}$. We again find the same results as before. The **L^2 error in the velocity** was found out to be 1.025178 which has **decreased** but is still of order 1.

We also tried changing the smoothing parameter α and the following results are obtained

α	L^2 error	
	Approximate Image Derivatives	Exact Image Derivatives
0.2	1.025654	1.01615
0.4	1.025654	1.022831
0.6	1.025654	1.024355
0.8	1.025654	1.024915
1	1.025654	1.025178
1.2	1.025654	1.025324
1.4	1.025654	1.025412
1.6	1.025654	1.025470
1.8	1.025654	1.025509
2	1.025654	1.025537

Table 2.1: Variation of relative L^2 error with the smoothing parameter α

The above given data suggests that the relative L^2 error is of order 1 and it is not to improve irrespective of different values of α . So the problem could be for the approximation of the laplacians of the velocities by finite differences. In an attempt to reduce the order of the relative error we could try the finite element method as it approximates the space and not the solution. So with this idea we proceed onto implementing the finite element method to calculate the optical flow velocities. But before doing that we

would want to establish the existence and uniqueness of the solution of the optical flow problem and also derive some estimates on the solution.

Chapter 3

Existence Of Minimizer

3.1 Introduction

So far what we have seen is just a numerical implementation of minimisation of optical flow functional (2.2) in using finite difference method. But we found that the results were not that accurate. So our idea was to implement the finite element method. But before doing that we will try and show that a minimizer exists for the optical flow functional under some given conditions and also we will derive some estimates on the solution.

3.2 Formulation Of The Problem

We set Ω to be the unit square $[0,1] \times [0,1]$ as Ω . We are to minimize the functional $J(U)$ over the field of optical flow velocities U in Ω where $J(U)$ is given by (2.2).

We assume our image $E \in W^{1,\infty}(\Omega)$ and hence in $L^2(\Omega)$ as Ω is bounded because

$$\begin{aligned}\int_{\Omega} E^2 dx dy &\leq \|E\|_{L^\infty}^2 \int_{\Omega} dx dy \\ &\leq \|E\|_{L^\infty}^2 \\ &< \infty\end{aligned}$$

as $|\Omega| = \int_{\Omega} dx dy = 1$.

Theorem 3.2.1. *The functional given in (2.2) is convex with respect to U .*

Proof. Let

$$U_1 = \begin{pmatrix} u_1 \\ v_1 \end{pmatrix} \text{ and } U_2 = \begin{pmatrix} u_2 \\ v_2 \end{pmatrix}$$

and let (\cdot) denote the usual inner product in \mathbb{R}^2 . Then for $0 \leq \alpha \leq 1$ we have,

$$\begin{aligned}
& J(\alpha U_1 + (1 - \alpha)U_2) \\
&= \frac{1}{2} \int_{\Omega} (\nabla E \cdot (\alpha U_1 + (1 - \alpha)U_2)) + E_t)^2 dx dy + \\
&\quad \frac{K}{2} \int_{\Omega} \|\nabla(\alpha u_1 + (1 - \alpha)u_2)\|^2 + \|\nabla(\alpha v_1 + (1 - \alpha)v_2)\|^2 dx dy \\
&\leq \frac{1}{2} \int_{\Omega} (\nabla E \cdot (\alpha U_1 + (1 - \alpha)U_2))^2 + (\alpha + 1 - \alpha)E_t^2 + 2E_t(\nabla E \cdot (\alpha U_1 + (1 - \alpha)U_2)) dx dy + \\
&\quad \frac{K}{2} \int_{\Omega} \|\nabla(\alpha u_1 + (1 - \alpha)u_2)\|^2 + \|\nabla(\alpha v_1 + (1 - \alpha)v_2)\|^2 dx dy \\
&= \frac{1}{2} \int_{\Omega} (\nabla E \cdot (\alpha U_1 + (1 - \alpha)U_2))^2 + (\alpha + 1 - \alpha)E_t^2 + 2E_t(\nabla E \cdot (\alpha U_1 + (1 - \alpha)U_2)) dx dy + \\
&\quad \frac{K}{2} \int_{\Omega} \|(\alpha \nabla u_1 + (1 - \alpha) \nabla u_2)\|^2 + \|(\alpha \nabla v_1 + (1 - \alpha) \nabla v_2)\|^2 dx dy
\end{aligned}$$

Now,

$$\begin{aligned}
& \int_{\Omega} E_t(\nabla E \cdot (\alpha U_1 + (1 - \alpha)U_2)) dx dy \\
&= \alpha \int_{\Omega} E_t(\nabla E \cdot U_1) dx dy + (1 - \alpha) \int_{\Omega} E_t(\nabla E \cdot U_2) dx dy
\end{aligned}$$

Let $a, b \in \mathbb{R}$ and $A, B \in V$, an inner product space with inner product $(\cdot)_V$ and norm $\|\cdot\|$

We have,

$$\begin{aligned}
(\alpha a + (1 - \alpha)b)^2 &= \alpha^2 a^2 + (1 - \alpha)^2 b^2 + \alpha(1 - \alpha)2ab \\
&\leq \alpha^2 a^2 + (1 - \alpha)^2 b^2 + \alpha(1 - \alpha)(a^2 + b^2) \\
&= \alpha a^2 + (1 - \alpha)b^2, \text{ where } 0 \leq \alpha \leq 1.
\end{aligned}$$

and

$$\begin{aligned}
\|(\alpha A + (1 - \alpha)B)\|^2 &= \alpha^2 \|A\|^2 + (1 - \alpha)^2 \|B\|^2 + \alpha(1 - \alpha)2(A \cdot B)_V \\
&\leq \alpha^2 \|A\|^2 + (1 - \alpha)^2 \|B\|^2 + \alpha(1 - \alpha)(\|A\|^2 + \|B\|^2) \\
&= \alpha \|A\|^2 + (1 - \alpha) \|B\|^2, \text{ where } 0 \leq \alpha \leq 1.
\end{aligned}$$

Therefore,

$$\begin{aligned} & \frac{K}{2} \int_{\Omega} \|(\alpha \nabla u_1 + (1 - \alpha) \nabla u_2)\|^2 + \|(\alpha \nabla v_1 + (1 - \alpha) \nabla v_2)\|^2 dx dy \\ & \leq \frac{K}{2} \left\{ \alpha \int_{\Omega} \|\nabla u_1\|^2 + \|\nabla u_2\|^2 dx dy + (1 - \alpha) \int_{\Omega} \|\nabla v_1\|^2 + \|\nabla v_2\|^2 dx dy \right\} \end{aligned}$$

Again,

$$\begin{aligned} \int_{\Omega} (\nabla E \cdot (\alpha U_1 + (1 - \alpha) U_2))^2 &= \int_{\Omega} (\alpha (\nabla E \cdot U_1) + (1 - \alpha) (\nabla E \cdot U_2))^2 dx dy \\ &\leq \alpha \int_{\Omega} (\nabla E \cdot U_1)^2 dx dy + (1 - \alpha) \int_{\Omega} (\nabla E \cdot U_1)^2 dx dy \end{aligned}$$

This gives,

$$J(\alpha U_1 + (1 - \alpha) U_2) \leq \alpha J(U_1) + (1 - \alpha) J(U_2) \quad \forall \quad 0 \leq \alpha \leq 1 \quad (3.1)$$

So J is a convex functional w.r.t U . \square

Theorem 3.2.2. *The unique minimizer of J will be given by the unique solution of $J'(U) = 0$, where ' denotes the Gateaux Derivative.*

Proof. See Appendix B \square

In the following we determine the unique solution of $J'(U) = 0$.

Now J is the functional as given in (2.2). So,

$$J(U + \epsilon \bar{U}) = \frac{1}{2} \int_{\Omega} (\nabla E \cdot (U + \epsilon \bar{U})) + E_t^2 dx dy + \frac{K}{2} \int_{\Omega} \|\nabla(u + \epsilon \bar{u})\|^2 + \|\nabla(v + \epsilon \bar{v})\|^2 dx dy$$

$$\text{where } \bar{U} = \begin{pmatrix} \bar{u} \\ \bar{v} \end{pmatrix} \in Z = (H^1(\Omega))^2.$$

$$\begin{aligned} &= \frac{1}{2} \int_{\Omega} E_t^2 + 2E_t(\nabla E \cdot (U + \epsilon \bar{U})) + (\nabla E \cdot U)^2 + \epsilon^2 (\nabla E \cdot \bar{U})^2 + 2\epsilon(\nabla E \cdot U)(\nabla E \cdot \bar{U}) \\ &+ \frac{K}{2} \int_{\Omega} \|\nabla u\|^2 + \epsilon^2 \|\nabla \bar{u}\|^2 + 2\epsilon(\nabla u \cdot \nabla \bar{u}) + \|\nabla v\|^2 + \epsilon^2 \|\nabla \bar{v}\|^2 + 2\epsilon(\nabla v \cdot \nabla \bar{v}) \end{aligned}$$

This implies,

$$J(U + \epsilon \bar{U}) - J(U) = \frac{1}{2} \int_{\Omega} 2\epsilon E_t(\nabla E \cdot \bar{U}) + \epsilon^2 (\nabla E \cdot \bar{U})^2 + 2\epsilon(\nabla E \cdot U)(\nabla E \cdot \bar{U})$$

$$+ \frac{K}{2} \int_{\Omega} 2\epsilon(\nabla u \cdot \nabla \bar{u}) + 2\epsilon(\nabla v \cdot \nabla \bar{v}) + \epsilon^2 \|\nabla \bar{u}\|^2 + \epsilon^2 \|\nabla \bar{v}\|^2$$

So we have,

$$\lim_{\epsilon \rightarrow 0} \frac{J(U + \epsilon \bar{U}) - J(U)}{\epsilon} = \int_{\Omega} (E_t + (\nabla E \cdot U))(\nabla E \cdot \bar{U}) + K \int_{\Omega} (\nabla u \cdot \nabla \bar{u}) + (\nabla v \cdot \nabla \bar{v}) \quad (3.2)$$

Now applying integration by parts we get,

$$\begin{aligned} \int_{\Omega} (\nabla u \cdot \nabla \bar{u}) &= - \int_{\Omega} (\bar{u} \Delta u) + \int_{\partial\Omega} \left(\frac{\partial u}{\partial \nu} \cdot \bar{u} \right), \\ \int_{\Omega} (\nabla v \cdot \nabla \bar{v}) &= - \int_{\Omega} (\bar{v} \Delta v) + \int_{\partial\Omega} \left(\frac{\partial v}{\partial \nu} \cdot \bar{v} \right) \end{aligned}$$

If we assume zero Dirichlet or Neumann boundary conditions on the flow velocity U we have,

$$\int_{\partial\Omega} \left(\frac{\partial u}{\partial \nu} \cdot \bar{u} \right) = 0 = \int_{\partial\Omega} \left(\frac{\partial v}{\partial \nu} \cdot \bar{v} \right)$$

This gives,

$$\lim_{\epsilon \rightarrow 0} \frac{J(U + \epsilon \bar{U}) - J(U)}{\epsilon} = \int_{\Omega} (E_t + (\nabla E \cdot U))(\nabla E \cdot \bar{U}) - K \int_{\Omega} (\Delta U \cdot \bar{U})$$

Since \bar{U} is arbitrary, so $J'(U)(\bar{U}) = 0$ gives the optimality conditions

$$\begin{cases} (E_t + \nabla E \cdot U)E_x - K\Delta u = 0 \\ (E_t + \nabla E \cdot U)E_y - K\Delta v = 0 \end{cases} \quad (3.3)$$

which are the required Euler-Lagrange equations for finding the minimum of the functional J .

Equations (3.3) can be written as,

$$\begin{aligned} -\Delta u + \frac{E_x^2}{K}u + \frac{E_x E_y}{K}v &= -\frac{E_x E_t}{K} \\ -\Delta v + \frac{E_x E_y}{K}u + \frac{E_y^2}{K}v &= -\frac{E_y E_t}{K} \end{aligned}$$

In matrix notation we have,

$$LU + BU = F, \quad (3.4)$$

where $U = \begin{pmatrix} u \\ v \end{pmatrix}$, $L = \begin{pmatrix} -\Delta & 0 \\ 0 & -\Delta \end{pmatrix}$, $B = \frac{1}{K} \begin{pmatrix} E_x^2 & E_x E_y \\ E_x E_y & E_y^2 \end{pmatrix}$,
 $F = \frac{1}{K} \begin{pmatrix} -E_x E_t \\ -E_y E_t \end{pmatrix}$.

3.3 Existence and Uniqueness Of Solution Of $J'(U) = 0$

We take $H = (L^2(\Omega))^2$ with the corresponding norm $\|\cdot\|_H$ and $Z = (H^1(\Omega))^2$ with the corresponding norm $\|\cdot\|_Z$ and $\|\cdot\|_{L^2}$ represents the usual norm $L^2(\Omega)$.

3.3.1 Zero Dirichlet boundary condition for velocity

In this case $U \in (H_0^1(\Omega))^2$.

Theorem 3.3.1. *There exists an unique solution for $J'(U) = 0$ in H where J is the functional as in (2.2) and it is assumed that the velocity of the optical flow satisfies zero Dirichlet boundary condition.*

Proof. By (3.4) we have,

$$LU + BU = F$$

This gives us,,

$$\begin{aligned} U &= -L^{-1}BU + L^{-1}F \\ &= G(U) \end{aligned}$$

We form the following iteration

$$U_{n+1} = G(U_n) \quad (3.5)$$

So if we can show that $G : H \rightarrow H$ is a contraction mapping, then there will exist a fixed point U_0 of (3.5) which is also unique.

$$\|G(U_1) - G(U_2)\|_H = \|L^{-1}B(U_1 - U_2)\|_H$$

$$= \left\| \begin{pmatrix} (-\Delta)^{-1}E_x^2(u_1 - u_2) \\ (-\Delta)^{-1}E_x^2(u_1 - u_2) \end{pmatrix} \right\|_H$$

As we have assumed that the space where U lies is $(H_0^1(\Omega))^2$, so we have

$$\|(-\Delta)^{-1}F\|_H \leq C_1 \|F\|_H$$

where C_1 is a constant depending on F and Ω . Therefore,

$$\begin{aligned} \|G(U_1) - G(U_2)\|_H &\leq \frac{C_1}{K} \left\{ \|E_x^2(u_1 - u_2)\|_{L^2} + \|E_y^2(v_1 - v_2)\|_{L^2} \right\} \\ &\leq \frac{C_1}{K} \left\{ \|E_x\|_{L^\infty}^2 \|(u_1 - u_2)\|_{L^2} + \|E_y\|_{L^\infty}^2 \|(v_1 - v_2)\|_{L^2} \right\} \\ &\leq \frac{C}{K} \left\{ \|(u_1 - u_2)\|_{L^2} + \|(v_1 - v_2)\|_{L^2} \right\}, \text{ where } C = \max \left\{ \|E_x\|_{L^\infty}^2, \|E_y\|_{L^\infty}^2, C_1 \right\} \\ &< \|U\|_H, \quad \text{if } K > C \end{aligned}$$

which can be done as K is a smoothing parameter to be chosen by us.

So $G : H \rightarrow H$ is a contraction mapping.

Hence, $J'(U) = 0$ has an unique solution in H . \square

We will show later in Section 3.4 that the unique solution obtained above belongs to Z .

3.3.2 Zero Neumann boundary condition for velocity

Next we assume that we have Neumann boundary condition for the optical flow velocity.

In general, we might not be able to show existence and uniqueness of solution for (3.4). But under certain hypothesis we will show that problem (3.4) has an unique solution.

We write $J'(U)[V] = 0 \quad \forall V \in Z$ as $A(U, V) = F(V)$ where $A(U, V)$ is a symmetric bilinear form on $Z \times Z$ associated to the functional (2.2) and $F(V)$ is a linear form on Z

So we have

$$A(U, V) = \int_{\Omega} (\nabla E \cdot U)(\nabla E \cdot V) + K \int_{\Omega} \nabla u_1 \cdot \nabla v_1 + \nabla u_2 \cdot \nabla v_2 \quad (3.6)$$

and

$$F(V) = - \int_{\Omega} E_t \cdot (\nabla E \cdot V) \quad (3.7)$$

$$\text{where } U = \begin{pmatrix} u_1 \\ u_2 \end{pmatrix} \quad V = \begin{pmatrix} v_1 \\ v_2 \end{pmatrix}.$$

Theorem 3.3.2. *The Bilinear form $A(U, V)$ as given in (3.6) is continuous $\forall U, V \in Z$.*

Proof.

$$\begin{aligned} |A(U, V)| &= \left| \int_{\Omega} (\nabla E \cdot U)(\nabla E \cdot V) + K \int_{\Omega} (\nabla u_1 \cdot \nabla v_1 + \nabla u_2 \cdot \nabla v_2) \right| \\ &\leq \|\nabla E \cdot U\|_{L^2} \|\nabla E \cdot V\|_{L^2} + K(\|\nabla u_1\|_H \|\nabla v_1\|_H + \|\nabla u_2\|_H \|\nabla v_2\|_H) \end{aligned}$$

By the inequality, $(a+b)^2 \leq (a+b)^2 + (a-b)^2 = 2(a^2 + b^2)$, we have,

$$\begin{aligned} \|\nabla E \cdot U\|_{L^2} &\leq \left[2\|E_x\|_{L^\infty}^2 \int_{\Omega} u_1^2 + 2\|E_y\|_{L^\infty}^2 \int_{\Omega} u_2^2 \right]^{\frac{1}{2}} \\ &\leq \left[2 \max \left\{ \|E_x\|_{L^\infty}^2, \|E_y\|_{L^\infty}^2 \right\} \right]^{\frac{1}{2}} \|U\|_H \end{aligned}$$

and we obtain

$$|A(U, V)| \leq C_1 (\|U\|_H \|V\|_H + \|\nabla u_1\|_H \|\nabla v_1\|_H + \|\nabla u_2\|_H \|\nabla v_2\|_H)$$

$$\leq C_1 [\|U\|_H^2 + \|\nabla u_1\|_H^2 + \|\nabla u_2\|_H^2]^{\frac{1}{2}} \cdot [\|V\|_H^2 + \|\nabla v_1\|_H^2 + \|\nabla v_2\|_H^2]^{\frac{1}{2}}$$

$$= C_1 \|U\|_Z \cdot \|V\|_Z$$

where,

$$C_1 = 2 \max \left\{ 2\|E_x\|_{L^\infty}^2, 2\|E_y\|_{L^\infty}^2, \frac{K}{2} \right\}.$$

Hence $A(U, V)$ is continuous $\forall U, V \in Z$ \square

Theorem 3.3.3. *The linear form $F(V)$ as in (3.7) is continuous $\forall V \in Z$.*

Proof.

$$\begin{aligned} |F(V)| &= \left| - \int_{\Omega} E_t (\nabla E \cdot V) \right| \\ &\leq \|E_t \nabla E\|_H \|V\|_H \\ &\leq \|E_t \nabla E\|_H \|V\|_Z \\ &\leq \|E_t\|_H \|\nabla E\|_H \|V\|_Z \\ &= C_2 \|V\|_Z \end{aligned}$$

where $C_2 = \min\{\|E_t\|_H, \|\nabla E\|_H\}$

Hence $F(V)$ is continuous $\forall V \in Z$ \square

Before trying to determine whether an unique solution of $J'(U) = 0$ exists or not, we first state the famous Lax-Milgram theorem which wil be used in the forthcoming stages.

Theorem 3.3.4 (Lax-Milgram). *Let V be a hilbert space , $a(.,.) : V \times V \rightarrow \mathbb{R}$ a continuous and coercive bilinear form, $F(\cdot) : V \rightarrow \mathbb{R}$ a linear and continuous functional. Then there exists an unique solution to the problem find $u \in V$:*

$$a(u, v) = F(v) \quad \forall v \in V$$

Theorem 3.3.5. *If $A(.,.)$ as in (3.6) is coercive then $A(U, V) = F(V)$ has an unique solution $\forall V \in Z$ and hence $J'(U)[V] = 0 \quad \forall V \in Z$ has an unique solution U_0 which is an unique minimizer of the functional $J(U)$ as in (2.2).*

Proof. Using Lax-Milgram's Theorem in Z we get the first part of the theorem. The second part follows from the fact that $A(U, V) = F(V)$ is equivalent to the fact that $J'(U)[V] = 0 \quad \forall V \in Z$. \square

Now we will show that the bilinear form $A(U, V)$ is Z -coercive under some given conditions.

Case 1:

First we assume that on a part Ω_1 of the boundary Ω , U vanishes, where $\mu(\Omega_1) > 0$.

Theorem 3.3.6. *Under the above hypothesis, the bilinear form $A(U, V)$ as in (3.6) is Z -coercive.*

Proof. We have,

$$\begin{aligned} A(U, U) &= \int_{\Omega} (\nabla E \cdot U)^2 + K \int_{\Omega} (\nabla u_1)^2 + (\nabla u_2)^2 \\ &\geq K \int_{\Omega} (\nabla u_1)^2 + (\nabla u_2)^2 \\ &\geq K \|U\|_Z. \text{ (By Poincare's Inequality, see [KES])} \end{aligned}$$

So the Bilinear Form $A(U, V)$ is coercive and so $A(U, V) = F(V)$ has an unique solution $\forall V \in J(\Omega)$ and hence $J'(U)=0$ has an unique solution U_0 which is an unique minimizer of the functional $J(U)$ as in (2.2). \square

Case 2:

In this case we do not assume any condition on the flow velocity across the boundary of Ω . But we assume something on the image E i.e we assume that E_x and E_y are linearly independent and they are in $H(\Omega)$. We then show the bilinear form is coercive.

Theorem 3.3.7. *Under the above hypothesis, the bilinear form $A(U, V)$ as in (3.6) is Z -coercive.*

Proof. The following derivations are based on the work of Horn and Schunck, Nagel and can be found in [SC91].

We we use the Poincare-Wirtinger's Inequality:-

$$\int_{\Omega} (U - T)^2 dx dy \leq D \int_{\Omega} |\nabla U|^2 dx dy \quad (3.8)$$

where

$$T = \frac{1}{|\Omega|} \int_{\Omega} U dx dy, |\Omega| = \int_{\Omega} dx dy = 1 \quad (3.9)$$

and D is a constant depending on Ω .

Suppose $A(., .)$ is not coercive. Then \nexists any constant $M > 0$ s.t.

$$A(U, U) \geq M \|U\|_Z^2$$

So for any $M > 0 \exists U \in Z$ s.t.

$$A(U, U) < M \|U\|_Z^2$$

We choose $M = \frac{1}{n}$ and get a sequence of M_n 's and correspondingly we will get U_n . Without loss of generality we can take $\|U_n\|_Z$ as 1. If not , we can take $V_n = \frac{U_n}{\|U_n\|_Z}$ and replace U_n with V_n .

So we get a sequence $\{U_n\}_{n \in \mathbb{N}}$ in Z with $\|U_n\|_Z = 1$ and $A(U_n, U_n) \rightarrow 0$ as $n \rightarrow \infty$.

From (3.8) using the bilinear form A we have,

$$\int_{\Omega} (u_n - T1_n)^2 dx dy \rightarrow 0 \quad (3.10)$$

and

$$\int_{\Omega} (v_n - T2_n)^2 dx dy \rightarrow 0 \quad \text{for } n \rightarrow \infty. \quad (3.11)$$

where

$$T1_n = \frac{1}{|\Omega|} \int_{\Omega} u_n dx dy, T2_n = \frac{1}{|\Omega|} \int_{\Omega} v_n dx dy$$

As,

$$\int_{\Omega} (E_x u + E_y v)^2 dx dy \leq 2|E_x^2|_{\infty} \int_{\Omega} u^2 dx dy + 2|E_y^2|_{\infty} \int_{\Omega} v^2 dx dy$$

we have,

$$\int_{\Omega} [E_x(u_n - T1_n) + E_y(v_n - T2_n)]^2 dx dy \rightarrow 0 \quad \text{for } n \rightarrow \infty. \quad (3.12)$$

$$\begin{aligned} & \text{Now } E_t(\nabla E.V) \left[\int_{\Omega} (E_x T1_n + E_y T2_n)^2 dx dy \right]^{\frac{1}{2}} \\ &= \left[\int_{\Omega} (E_x u_n + E_y v_n + E_x(T1_n - u_n) + E_y(T2_n - v_n))^2 dx dy \right]^{\frac{1}{2}} \\ &\leq \left[\int_{\Omega} (E_x u_n + E_y v_n)^2 dx dy \right]^{\frac{1}{2}} + \left[\int_{\Omega} (E_x(T1_n - u_n) + E_y(T2_n - v_n))^2 dx dy \right]^{\frac{1}{2}} \\ &\leq [A(U_n, U_n)]^{\frac{1}{2}} + \left[\int_{\Omega} (E_x(T1_n - u_n) + E_y(T2_n - v_n))^2 dx dy \right]^{\frac{1}{2}} \\ &\rightarrow 0 \text{ for } n \rightarrow \infty \quad (\text{Using 3.12}) \end{aligned}$$

We have

$$\begin{aligned} \|p + q\|_H^2 &= \|p\|_H^2 + \|q\|_H^2 + 2(p, q) \\ &\geq \|p\|_H^2 + \|q\|_H^2 - 2\|p\|_H\|q\|_H \frac{|(p, q)|}{\|p\|_H\|q\|_H} \\ &\geq \|p\|_H^2 + \|q\|_H^2 - (\|p\|_H^2 + \|q\|_H^2) \frac{|(p, q)|}{\|p\|_H\|q\|_H} \\ &= (\|p\|_H^2 + \|q\|_H^2) \left\{ 1 - \frac{|(p, q)|}{\|p\|_H\|q\|_H} \right\} \end{aligned}$$

We take $p = E_x T1_n, q = E_y T2_n$

So we get

$$\int_{\Omega} (E_x T1_n + E_y T2_n)^2 dx dy \geq \left[\|E_x\|_H^2 (T1_n)^2 + \|E_y\|_H^2 (T2_n)^2 \right] \left\{ 1 - \frac{|(E_x, E_y)|}{\|E_x\|_H\|E_y\|_H} \right\}$$

As L.H.S $\rightarrow 0$ as $n \rightarrow \infty$ as shown above and by linear independency of E_x and E_y $1 - \frac{|(p, q)|}{\|p\|_H\|q\|_H} > 0$ and $\|E_x\|_H$ and $\|E_y\|_H$ are not identically 0.

we have

$$T1_n \rightarrow 0 \text{ and } T2_n \rightarrow 0 \text{ as } n \rightarrow \infty \quad (3.13)$$

But this gives a contradiction as,

$$\begin{aligned}
\|U_n\|_Z &= 1 \\
&= \|(U_n - T_n) + T_n\|_Z \\
&\leq \|(U_n - T_n)\|_Z + \|T_n\|_Z \\
&\rightarrow 0 \text{ as } n \rightarrow \infty \text{ By (3.10), (3.11), (3.13).}
\end{aligned}$$

So $A(.,.)$ is coercive.

Hence $J'(U) = 0$ has an unique solution $U = U_0$ in $J(\Omega)$

□

In the Dirichlet case, an unique minimizer of the functional $J(U)$ exists in $H(\Omega)$ and in the Neumann case, an unique minimizer of the functional $J(U)$ exists in $J(\Omega)$, provided E_x and E_y are linearly independent or in some part of $\partial\Omega$ there is no velocity flux.

But we will now show that if the minimizer of the functional J , as in (2.2), belongs to H , then it is also in Z . So in both the cases we have an unique minimizer in Z .

3.4 Estimates For The Minimizer

Now we will derive some estimates for the unique minimizer obtained in the above cases.

3.4.1 Dirichlet Case

Theorem 3.4.1. *The unique minimizer of $J(U)$, $U = U_0$ obtained in Theorem 3.3.1 for the Dirichlet case exists in Z .*

Proof. We have seen that U_0 satisfies (3.4). Then we have,

$$(LU_0, U_0) + (BU_0, U_0) = (F, U_0) \text{ (Taking inner product of (3.4) with } U_0)$$

This gives,

$$\|\nabla U_0\|_H^2 + (BU_0, U_0) = (F, U_0)$$

since

$$(LU_0, U_0) = -(\Delta U_0, U_0)$$

Using integration by parts and dirichlet boundary conditions we get,

$$\begin{aligned}(LU_0, U_0) &= (\nabla U_0, \nabla U_0) \\ &= \|\nabla U_0\|_H^2\end{aligned}$$

Adding $\|U_0\|_H^2$ on both sides we get,

$$\|U_0\|_H^2 + \|\nabla U_0\|_H^2 + (BU_0, U_0) = (F, U_0) + \|U_0\|_H^2 \quad (3.14)$$

Now

$$\sup_{\|U_0\|_H \neq 0} \frac{|(BU_0, U_0)|}{\|U_0\|_H^2} = \|B\|$$

This implies,

$$-(BU_0, U_0) \leq \|B\| \|U_0\|_H^2 \quad (3.15)$$

Therefore equation (3.14) gives

$$\begin{aligned}\|U_0\|_Z^2 &= (F, U_0) - (BU_0, U_0) + \|U_0\|_H^2 \\ &\leq \|F\|_H \|U_0\|_H + (1 + \|B\|) \|U_0\|_H^2 \quad (\text{Using (3.15)}) \\ &< \infty \text{ as } U_0 \in H(\Omega).\end{aligned} \quad (3.16)$$

Hence $U_0 \in Z$. □

So we see that for the Dirichlet case also, the unique minimizer $U_0 \in Z$. Now we will prove an estimate for U_0 in terms of the image derivatives.

Theorem 3.4.2. U_0 obtained in Theorem 3.3.1 satisfies

$$\|U_0\|_Z \leq C \|E_t \nabla E\|_H$$

where constant C depends on Ω and the smoothing parameter K .

Proof. By (3.14) we have $(LU_0, U_0) + (BU_0, U_0) = (F, U_0)$

$$\text{where } F = \begin{pmatrix} -\frac{E_x E_t}{K} \\ -\frac{E_y E_t}{K} \end{pmatrix}.$$

But $(LU_0, U_0) = \|\nabla U_0\|_H^2$

and

$$\begin{aligned}
(BU_0, U_0) &= \left(\begin{pmatrix} \frac{E_x^2}{K} & \frac{E_x E_y}{K} \\ \frac{E_x E_y}{K} & \frac{E_y^2}{K} \end{pmatrix} \begin{pmatrix} u_0 \\ v_0 \end{pmatrix}, \begin{pmatrix} u_0 \\ v_0 \end{pmatrix} \right) \\
&= \frac{1}{K} \begin{pmatrix} E_x^2 u_0 + E_x E_y v_0 \\ E_x E_y u_0 + E_y^2 v_0 \end{pmatrix} \begin{pmatrix} u_0 \\ v_0 \end{pmatrix} \\
&= \frac{1}{K} (u_0 E_x + v_0 E_y)^2 \geq 0.
\end{aligned}$$

So we have, $\|\nabla U_0\|_H^2 \leq (LU_0, U_0) \leq (F, U_0)$

But $\|\nabla U_0\|_H^2 \geq C(\Omega) \|U_0\|_Z^2$ (By Poincare's Inequality where $C(\Omega) > 0$ is a constant depending on Ω)

So,

$$\begin{aligned}
\|U_0\|_Z^2 &\leq \frac{1}{C(\Omega)} (F, U_0) \\
&\leq \frac{1}{C(\Omega)} \|F\|_H \|U_0\|_H \text{ (By Holder's Inequality).} \\
&\leq \frac{1}{C(\Omega)} \|F\|_H \|U_0\|_Z \\
&= \frac{1}{K \cdot C(\Omega)} \|E_t \nabla E\|_H \|U_0\|_Z
\end{aligned}$$

Suppose $U_0 \neq 0$ identically. Then we have the following estimate,

$$\|U_0\|_Z \leq \frac{1}{E(\Omega, K)} \|E_t \nabla E\|_H \quad (3.17)$$

where $E(\Omega, K) = K \cdot C(\Omega)$. □

3.4.2 Neumann Case

Theorem 3.4.3. U_0 obtained in Theorem 3.3.6 and Thoerem 3.3.7 satisfies

$$\|U_0\|_Z \leq C \|E_t \nabla E\|_H$$

where constant C depends on Ω and the smoothing parameter K .

Proof. For the Neumann Case we have seen from Theorem 3.3.6 and Thoerem 3.3.7 that the Bilinear form $A(U, V)$ is coercive in $J(\Omega)$.

So \exists a constant $D = D(\Omega, K)$ s.t.

$$F(U_0) = A(U_0, U_0) \geq D(\Omega, K) \|U_0\|_Z^2 \quad (3.18)$$

where $F(U_0) = E_t(\nabla E \cdot U_0)$

Therefore,

$$\begin{aligned} \|U_0\|_Z^2 &\leq \frac{1}{D(\Omega, K)} F(U_0) \\ &\leq \frac{1}{D(\Omega, K)} \|E_t \nabla E\|_H \|U_0\|_H \\ &\leq \frac{1}{D(\Omega, K)} \|E_t \nabla E\|_H \|U_0\|_Z \end{aligned}$$

So the following estimate for the neumann case holds:-

$$\|U_0\|_Z \leq \frac{1}{D(\Omega, K)} \|E_t \nabla E\|_H \quad (3.19)$$

□

Comparing the expressions of (3.17) and (3.19), we find that both the estimates are the same except for the constants $E(\Omega)$ and $D(\Omega, K)$. Even the constants depend on the domain Ω and K . So the two estimates for the Dirichlet and the Neumann case are compatible with each other.

Hence we see that U_0 depends continuously on the given data i.e the image derivatives.

Chapter 4

Finite Element Method for the optical flow problem

4.1 Introduction

We saw in the first chapter that using the finite difference iterative scheme for finding the optical flow given a sequence of images, the relative L^2 errors in the optical flow velocity was a huge one. It meant that the iterative method did not capture properly the motion of the images. One of the reasons could be because of the fact that finite difference approximations to the laplacians are used which is based on the approximation of the Laplacians of the velocity by an weighted average of the velocities at the neighbouring eight points. So it does not capture the velocities in every direction. So to improve on the way of approximations of the Laplacians we will try for some other suitable method. One of them could be the finite element method whose main concept is based on the approximation of the space rather than approximation of the solution.

In this chapter we will discuss about finite element methods and how we can use it to determine the optical flow velocity pattern of a given sequence of images.

4.2 Approximation via the Galerkin method

The weak formulation of a pde set on a domain Ω can be written in the following way

find $u \in V$:

$$a(u, v) = F(v) \quad \forall v \in V \tag{4.1}$$

where V is an appropriate Hilbert space, $a(., .)$ is a continuous bilinear form from $V \times V$ in \mathbb{R} , $F(\cdot)$ is a continuous linear functional from V in \mathbb{R} . Suppose the bilinear form $a(., .)$ is coercive. Then under the above hypotheses

the Lax-Milgram theorem(Th.3.3.4) ensures existence and uniqueness of the solution.

Let V_h be a family of Hilbert spaces that depends on a positive parameter h , s.t.

$$V_h \subseteq V, \dim V_h = N_h < \infty \quad \forall h > 0$$

The approximate problem takes the form

find $u_h \in V_h$:

$$a(u_h, v_h) = F(v_h) \quad \forall v_h \in V_h \quad (4.2)$$

Such type of approximate problem is called the *Galerkin problem*. Let us denote with $\{\phi_j, j = 1, 2, \dots, N_h\}$ a basis of V_h . Then it is sufficient that (4.1) be verified for each function of the basis, as all the functions in V_h can be written as a linear combination of the ϕ_j . Then we have,

$$a(u_h, \phi_i) = F(\phi_i), i = 1, 2, \dots, N_h \quad (4.3)$$

As $U_h \in V_h$,

$$u_h(x) = \sum_{j=1}^{N_h} u_j \phi_j(x), x \in \Omega$$

where the $u_j, j = 1, \dots, N_h$ are the unknown coefficients. The equations (4.3) then become

$$\sum_{j=1}^{N_h} u_j a(\phi_j, \phi_i) = F(\phi_i), \quad i = 1, 2, \dots, N_h \quad (4.4)$$

We denote A by the matrix(called *stiffness matrix*) with elements

$$A_{ij} = a(\phi_j, \phi_i)$$

and by f the vector with components $f_i = F(\phi_i)$. If we denote by u the vector having as components the unknown coefficients ,(4.4) is equivalent to the linear system

$$Au = f \quad (4.5)$$

We will now show some properties of the matrix A under some given conditions which will enable us to check for the existence of an unique solution of (4.1).

Theorem 4.2.1. *If the bilinear form $a(., .)$ is coercive then the matrix A associated to the discretization of (4.1) with the Galerkin method is positive definite.*

Proof. A matrix $B \in \mathbb{R}^{n \times n}$ is said to be positive definite if

$$v^T B v \geq 0 \quad v \in \mathbb{R}^n \text{ and } v^T B v = 0 \text{ iff } v = 0 \quad (4.6)$$

Let $v = (v_i) \in \mathbb{R}^{N_h}$. We have by the bilinearity and coercivity of the form $a(., .)$,

$$\begin{aligned}
v^T A v &= \sum_{j=1}^{N_h} \sum_{i=1}^{N_h} v_i A_{ij} v_j \\
&= \sum_{j=1}^{N_h} \sum_{i=1}^{N_h} v_i a(\phi_j, \phi_i) v_j \\
&= \sum_{j=1}^{N_h} \sum_{i=1}^{N_h} a(v_j \phi_j, v_i \phi_i) \\
&= a\left(\sum_{j=1}^{N_h} v_j \phi_j, \sum_{i=1}^{N_h} v_i \phi_i\right) \\
&= a(v_h, v_h) \\
&\geq \alpha \|v_h\|_V^2 \geq 0.
\end{aligned}$$

where $v_h(x) = \sum_{j=1}^{N_h} v_j \phi_j(x) \in V_h$. Moreover, if $v^T A v = 0$ then by what we have just obtained,

$$\begin{aligned}
\|v_h\|_V^2 &= 0 \\
\Rightarrow v_h &= 0 \\
\Rightarrow v &= 0
\end{aligned}$$

□

Property 4.2.1. *The matrix A is symmetric if and only if the bilinear form $a(., .)$ is symmetric.*

Proof. $A_{ij} = a(\phi_i, \phi_j) = a(\phi_j, \phi_i) = A_{ji}$. Hence A is symmetric if and only if the bilinear form $a(., .)$ is symmetric. □

4.3 Analysis of the Galerkin method

In this section we will briefly discuss about three of the fundamental properties of Galerkin method:

1. Existence and uniqueness of the discrete solution u_h .
2. Stability of the discrete solution u_h .
3. Convergence of u_h to the exact solution u of problem (4.1) for $h \rightarrow 0$.

4.3.1 Existence and uniqueness

The Lax-Milgram theorem (theorem 3.3.4) holds for any Hilbert space ,hence, in particular for the space V_h . Furthermore the bilinear form $a(.,.)$ and the functional $F(.)$ are the same as in the variational problem (4.1). Thus the hypotheses required by the Lax-Milgram theorem are fulfilled. The following result can be then derived:

Corollary 4.3.1. *If the bilinear form $a(.,.)$ is coercive then the solution of the Galerkin problem (4.2) exists and is unique.*

4.3.2 Stability

Corollary 4.3.1 helps us to prove the following stability result.

Corollary 4.3.2. *Under the hypotheses of Corollary 4.3.1, the Galerkin method is stable, uniformly with respect to h , as the following upper bound holds for the solution*

$$\|u_h\|_V \leq \frac{1}{\alpha} \|F\|_{V'}$$

where α is the coercivity constant for the bilinear form $a(.,.)$, and $\|F\|_{V'}$ is the norm of the functional F defined as

$$\|F\|_{V'} = \sup_{v \in V \setminus \{0\}} \frac{|F(v)|}{\|v\|_V}$$

Proof. If u_h is almost everywhere equal to zero we are done, else we have by the coercivity of the bilinear form $a(.,.)$

$$\alpha \|u_h\|_V^2 \leq a(u_h, u_h) = F(u_h) \leq |F(u_h)|$$

Again as F is linear and continuous, we have

$$|F(u_h)| \leq \|F\|_{V'} \|u_h\|_V$$

Hence the result. □

The stability of the method guarantees that the norm $\|u_h\|_V$ of the discrete solution remains bounded for h tending to zero, uniformly with respect to h .

4.3.3 Convergence

We now want to prove that the weak solution of the (4.2) converges to the solution of the problem (4.1) when h tends to zero. Consequently, by taking a sufficiently small h , it will be possible to approximate the exact solution u as accurately as desired by the Galerkin solution u_h . We first prove the following consistency property

Lemma 4.3.1 (Céa). *The Galerkin method is strongly consistent, that is*

$$a(u - u_h, v_h) = 0 \quad \forall v_h \in V_h \quad (4.7)$$

Proof. Since $V_h \subseteq V$, the exact solution u satisfies the weak problem (4.1) for each element $v = v_h \in V_h$, hence we have

$$a(u, u_h) = F(v_h) \quad \forall v_h \in V_h. \quad (4.8)$$

By subtracting side to side (4.2) from (4.8), we obtain

$$a(u, v_h) - a(u_h, v_h) = 0 \quad \forall v_h \in V_h.$$

from which, thanks to the bilinearity of the form $a(., .)$, (4.7) follows. \square

Next we prove a theorem regarding the error committed when the approximate solution u_h is taken instead of the exact solution u .

Theorem 4.3.1. *If u and u_h denote the solutions of (4.1) and (4.2) respectively, then we have*

$$\|u - u_h\|_V \leq \frac{M}{\alpha} \inf_{v_h \in V_h} \|u - v_h\|_V \quad (4.9)$$

where M and α are the constants of continuity and coercivity respectively for the bilinear form $a(., .)$.

Proof. If v_h is an arbitrary element of V_h we obtain

$$a(u - u_h, u - u_h) = a(u - u_h, u - v_h) + a(u - u_h, v_h - u_h).$$

The last term is null thanks to (4.7), as $v_h - u_h \in V_h$. Moreover

$$|a(u - u_h, u - v_h)| \leq M \|u - u_h\|_V \|u - v_h\|_V$$

by exploiting the continuity of the bilinear form. On the other hand, by the coercivity of $a(., .)$ it follows

$$a(u - u_h, u - u_h) \geq \alpha \|u - u_h\|_V^2$$

hence we have

$$\|u - u_h\|_V \leq \frac{M}{\alpha} \|u - v_h\|_V \quad \forall v_h \in V_h$$

Such inequality holds for all functions $v_h \in V_h$ and therefore we find

$$\|u - u_h\|_V \leq \frac{M}{\alpha} \inf_{v_h \in V_h} \|u - v_h\|_V \quad (4.10)$$

\square

It is then evident that in order for the method to converge, it will be sufficient to require that, for h tending to zero, the space V_h tends to "fill" the entire space V . Precisely it must turn out that

$$\lim_{h \rightarrow 0} \inf_{v_h \in V_h} \|v - v_h\|_V = 0 \quad \forall v \in V \quad (4.11)$$

The above property is also known as the **density property**. In that case, the Galerkin method is convergent and it can be written that

$$\lim_{h \rightarrow 0} \|u - u_h\|_V = 0$$

The space V_h must therefore be carefully chosen in order to guarantee the density property (4.11). Once this requirement is satisfied, convergence will be verified in any case, independently of how u is made; conversely it will be seen later that the speed with which the discrete solution converges to the exact solution will depend, in general, on both the choice of V_h and the regularity of u . In the following section we will try to achieve specifically the above objective.

4.4 The finite element method

Let Ω be a bounded domain in \mathbb{R}^n . The goal of this section is to create approximations of the space $H^1(\Omega)$ that depend on a parameter h .

Definition 4.4.1. A finite element is a triple (K, \sum, P) such that

1. $K \subseteq \Omega$ with a Lipschitz continuous boundary ∂K and interior of K is non-empty.
2. \sum is a finite set of linear forms over $C^\infty(K)$. The set \sum is said to be the set of degrees of freedom of the finite element.
3. P is a finite dimensional space of real-valued functions over K such that \sum is P -unisolvent i.e if $\sum = \{\phi_i\}_{i=1}^N$ and $\alpha_i, 1 \leq i \leq N$ are any scalars, then there exists an unique function $p \in P$ such that

$$\phi_i(p) = \alpha_i \quad 1 \leq i \leq N \quad (4.12)$$

(4.12) of Definition (4.4.1) is equivalent to the conditions that $\dim P = N = \text{cardinality of } \sum$ and that there exists a set of functions $\{p_j\}_{j=1}^N$ with $\phi_i(p_j) = \delta_{ij}$ ($1 \leq i, j \leq N$) which forms a basis of P over \mathbb{R} . Given any $p \in P$ we may write

$$p = \sum_{i=1}^N \phi_i(p) p_i \quad (4.13)$$

4.4.1 Examples of finite elements

We will now give some examples of finite elements which will be used in the optical flow problem. But before that we define the following

Definition 4.4.2. An n -simplex is the convex hull in \mathbb{R}^n of $(n + 1)$ points $\{a_j\}_{j=1}^{n+1}$ such that if $a_j = \{a_{kj}\}_{k=1}^n$ and A is the matrix

$$A = \begin{pmatrix} a_{11} & a_{12} & \cdots & a_{1,n+1} \\ a_{21} & a_{22} & \cdots & a_{2,n+1} \\ \vdots & \vdots & \ddots & \vdots \\ a_{n1} & a_{n2} & \cdots & a_{n,n+1} \\ 1 & 1 & 1 & 1 \end{pmatrix}$$

then $\det(A) \neq 0$

Definition 4.4.3. Let $k \geq 0$ be an integer. Then, P_K is the space of all polynomials of degree $\leq k$ in x_1, x_2, \dots, x_n

i.e.

$$P_K = \{p(x_1, x_2, \dots, x_n) = \sum_{i_1, i_2, \dots, i_n \geq 0, i_1 + i_2 + \dots + i_n \leq k} a_{i_1 i_2 \dots i_n} x_{i_1}^{i_1} x_{i_2}^{i_2} \dots x_{i_n}^{i_n} \text{ with } a_{i_1 i_2 \dots i_n} \in \mathbb{R}\}$$

Example 4.4.1 (The n -simplex of Type 1). Let K be an n -simplex. Let $P_K = P_1$. We define a set $\sum = \{p(a_i); 1 \leq i \leq n + 1\}$ of degrees of freedom for $p \in P_K$, where $\{a_i\}_{i=1}^{n+1}$ are the vertices of K . The set \sum determines every polynomial $p \in P_K$ uniquely. Hence (K, \sum, P_K) is a finite element of Type 1.

Example 4.4.2 (The n -simplex of Type 2). Let K be an n -simplex with vertices $\{a_i\}_{i=1}^{n+1}$. Let $a_{ij}(i < j)$ be the mid-points of the line joining a_i and a_j i.e. $a_{ij} = \frac{1}{2}(a_i + a_j)$. Let $P_K = P_2$. We define for $p \in P_2$, the set $\sum = \{p(a_i), 1 \leq i \leq n + 1; p(a_{ij}), 1 \leq i < j \leq n + 1\}$ (See Fig 4.1). Then \sum determines $p \in P_2$ completely. Hence (K, \sum, P_K) is a finite element of Type 2

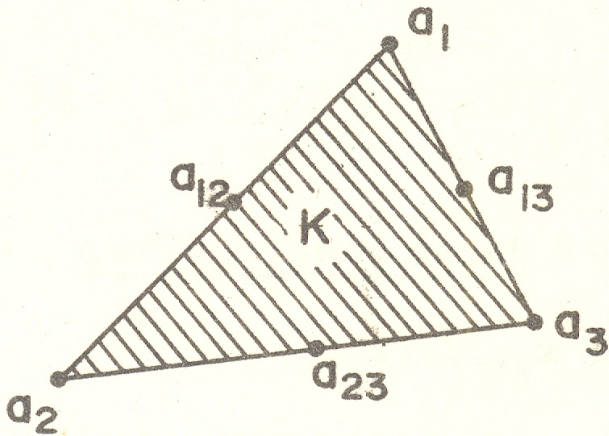


Figure 4.1: n -simplex of Type 2

Similarly we could use n -simplices of Type r to get other forms of finite elements using P_r . Again we consider another space of polynomials.

Definition 4.4.4. Let $k \geq 1$ be an integer. Then

$$Q_k = \{p : p(x) = \sum_{0 \leq i_j \leq k, 1 \leq j \leq n} a_{i_1 \dots i_n} x_1^{i_1} \dots x_n^{i_n}\}$$

We have the inclusions $P_k \subset Q_k \subset P_{nk}$

Example 4.4.3 (The Rectangle of Type 1). Let K be an unit square in \mathbb{R}^2 i.e. $K = [0, 1]^2$. Let $P_K = Q_1$. We define a set $\Sigma = \{p(a_i); 1 \leq i \leq 4\}$ of degrees of freedom for $p \in P_K$, where $\{a_i\}_{i=1}^4$ are the vertices of K (See Fig 4.2). Then Σ determines $p \in Q_1$ completely. Hence (K, Σ, P_K) is a finite element.

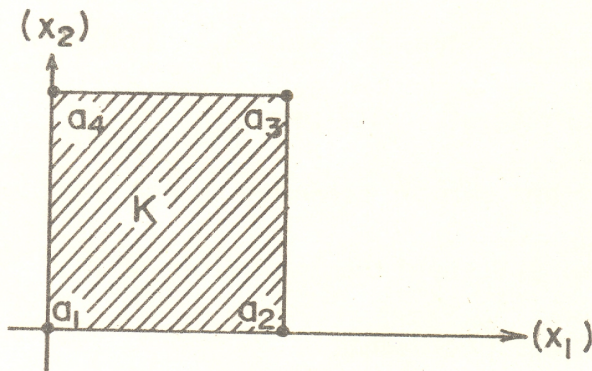


Figure 4.2: Rectangle of Type 1

Example 4.4.4 (The Rectangle of Type 2). Let K be an unit square in \mathbb{R}^2 i.e. $K = [0, 1]^2$. Let $P_K = Q_2$. We define a set $\Sigma = \{p(a_i); 1 \leq i \leq 9\}$ of degrees of freedom for $p \in P_K$, where $\{a_i\}_{i=1}^9$ are union of the vertices, mid-points of the sides and the centre of the square K (See Fig 4.3). Then Σ determines $p \in Q_2$ completely. Hence (K, Σ, P_K) is a finite element.

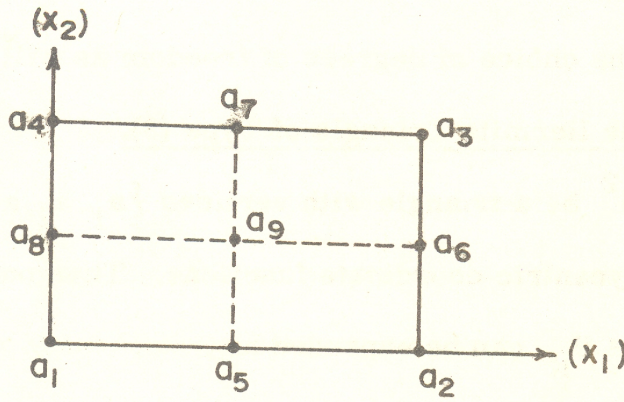


Figure 4.3: Rectangle of Type 2

Similarly we can construct finite elements of type k using Q_K .

We saw in the above examples that the set of degrees of freedom for a finite element K (which could be a triangle in 2-d or cube in 3-d) has the following types:

Type 1: ϕ_i^0 given by $p \mapsto p(a_i^0)$. The points $\{a_i^0\}$ were the vertices, the midpoints of sides, etc.....

Type 2: $\phi_{i,k}^1$ given by $p \mapsto Dp(a_i^1)(\xi_{i,k}^1)$ where $\{a_i^1\}$ are the vertices of the finite element K and $Dp(a_i^1)$ is the total derivative of p at the point (a_i^1) .

Type 3: $\phi_{i,kl}^2$ given $p \mapsto D^2p(a_i^2)(\xi_{i,k}^2, \xi_{i,l}^2)$ where $\{a_i^2\}$ are the vertices of the finite element K and $D^2p(a_i^2)$ is the second derivative of p at the point (a_i^1) .

In all the above cases $\{a_i^s\}$ for $s = 0, 1, 2$ are points of K and are called the **nodes of the finite element**.

Definition 4.4.5. A finite element is called a Lagrange finite element if its degrees of freedom are only of Type 1. Otherwise it is called a Hermite finite element.

As said before that our aim was to create approximations of the space $H^1(\Omega), V_h$ which depend on a parameter h . We will use the finite elements in

the above given examples to create the approximate spaces V_h . But before that we need simple inclusions such as $V_h \subset H^1(\Omega)$ or $H_0^1(\Omega)$. We will establish a simple criterion to realise this.

Theorem 4.4.1. *Let ζ_h be a finite triangulation of Ω such that $\bar{\Omega} = \bigcup_{K \in \zeta_h} K$ where the sets K are the finite elements. If for every $K \in \zeta_h$, $P_K \subset H^1(K)$ and $V_h \subset C^0(\bar{\Omega})$, then $V_h \subset H^1(\Omega)$. If in addition $v = 0$ on $\partial\Omega$ for all $v \in V_h$, then $V_h \subset H_0^1(\Omega)$.*

Proof. Let $v \in V_h$. Since $v|K \in L^2(K)$ for every $K \in \zeta_h$ it follows that $v \in L^2(\Omega)$. Hence to complete the proof it only remains to show that for $1 \leq i \leq n$, there exist $v_i \in L^2(\Omega)$ such that for each $\phi \in D(\Omega)$ we have,

$$\int_{\Omega} \phi v_i dx = - \int_{\Omega} \frac{\partial \phi}{\partial x_i} v dx \quad (4.14)$$

Then it will follow that $\frac{\partial v}{\partial x_i} = v_i$ and hence $v \in H^1(\Omega)$.

However, $v|_K \in P_K \subset H^1(K)$ implies that $\frac{\partial v|_K}{\partial x_i} \in L^2(K), 1 \leq i \leq n$. Let $\phi \in D(\Omega)$. Since the boundary ∂K of any K of the triangulation is Lipschitz continuous, we apply integration by parts to get

$$\int_K \frac{\partial v|_K}{\partial x_i} \phi dx = - \int_K (v|_K) \frac{\partial \phi}{\partial x_i} dx + \int_{\partial K} (v|_K) \phi \nu_{i,K} d\nu_K$$

where $d\nu_K$ is the measure on ∂K and $\bar{\nu} = (\nu_{1,K}, \dots, \nu_{n,K})$ is the outer normal on ∂K . Summing over all the finite elements K , we get

$$\begin{aligned} \int_{\Omega} \phi v_i dx &= \sum_{K \in \zeta_h} \int_K \phi \frac{\partial v|_K}{\partial x_i} dx \\ &= - \int_{\Omega} \frac{\partial \phi}{\partial x_i} v dx + \sum_{K \in \zeta_h} \int_{\partial K} (v|_K) \phi \nu_{i,K} d\nu_K \end{aligned}$$

where v_i is the function whose restriction to each K is $\frac{\partial v|_K}{\partial x_i}$.

The summation on the right-hand side of the above equation is zero for the following reasons:

On the boundary $\partial\Omega$, since $\phi \in D(\Omega)$, the integral corresponding to $\partial K \cap \partial\Omega$ is zero. So the problem, if any, is only on the other portion of the boundary of each K . However, these always occur as common boundaries of adjacent finite elements. The value of $v|_K$ on the common boundary of two adjacent finite elements is the same ($V_h \subset C^0(\bar{\Omega})$). But the outer normals are equal and opposite from orientation considerations. (See Fig 4.4).

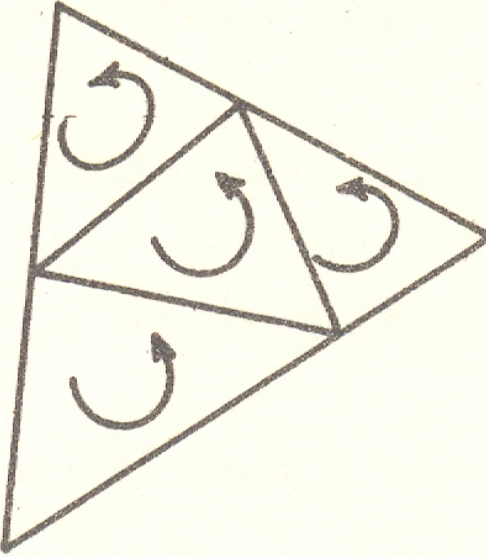


Figure 4.4: The orientations of the normals in adjacent finite elements

Hence the contributions from each K along the common boundaries cancel one another. Thus the summation yields only zero. Hence v_i satisfies (4.14) for $1 \leq i \leq n$, and clearly $v_i \in L^2(\Omega)$. The last part of the theorem follows from the characterisation of $H_0^1(\Omega)$ spaces. \square

4.4.2 Finite element spaces

Now that we have obtained the above inclusions we now proceed to give examples of some finite element spaces which approximate the space $H^1(\Omega)$ or $H_0^1(\Omega)$. Before that we consider some assumptions on the triangulation ζ_h of the domain Ω . The h parameter is related to the spacing of the triangulation. We set $h_K = \text{diam}(K)$ for each $K \in \zeta_h$, where $\text{diam}(K) = \max_{x,y \in K} |x-y|$ is the diameter of the element K . Now we define $h = \max_{K \in \zeta_h} h_K$. Moreover, we will impose the triangulation satisfy the following regularity condition. Let ρ_K be the diameter of the circle inscribed in the triangle K (also called the sphericity of K); a family of triangulations $\{\zeta_h, h > 0\}$ is said to be regular if, for a suitable $\delta > 0$, the condition

$$\frac{h_K}{\rho_K} \leq \delta \quad \forall K \in \zeta_h \quad (4.15)$$

is verified. This condition instantly excludes very deformed triangles. Henceforth we will be using such regular grids.

Now we consider the following family of spaces

$$X_h^r = \{v_h \in C^0(\bar{\Omega}) : v_h|_K \in P_r \quad \forall K \in \zeta_h\}, \quad r = 1, 2, \dots \quad (4.16)$$

having denoted by P_r the space of polynomials with degree lower than or equal to r in all the variables. The spaces X_h^r are all subspaces of $H^1(\Omega)$ as they are constituted by differentiable functions except for at most a finite number of points (the vertices x_i of the triangulation ζ_h). They represent possible choices for the space V_h , provided that the boundary conditions are properly incorporated. The fact that the functions of X_h^r are locally(elementwise) polynomials will make the stiffness matrix A in (4.5) easy to compute.

To make the stiffness matrix a sparse matrix, we usually choose a basis $\{\phi_i\}$ for the X_h^r space such that the support of each $\{\phi_i\}$ have non-empty intersection only with that of a negligible number of other functions in the basis. It is also convenient that the basis be Lagrangian: in that case, the coefficients of the expansion of a generic function $v_h \in X_h^r$ on the basis itself will be the values taken by v_h in carefully chosen points, which we call nodes and which might form a superset of the vertices of ζ_h .

We can also define another kind of finite element spaces for rectangular finite elements of type r as described in Section 4.4

$$\overline{X}_h^r = \{v_h \in C^0(\bar{\Omega}) : v_h|_K \in Q_r \quad \forall K \in \zeta_h\}, \quad r = 1, 2, \dots \quad (4.17)$$

having denoted by Q_r the space of polynomials with degree lower than or equal to r in each variable. The spaces \overline{X}_h^r are also subspaces of $H^1(\Omega)$ as they are constituted by differentiable functions except for at most a finite number of points (the vertices of the rectangulation ζ_h). We again choose a Lagrangian basis for the space so that our stiffness matrix is a sparse matrix.

4.5 Interpolation Theory

In the previous section we have outlined the internal approximation method for $H^1(\Omega)$. We are naturally interested in the convergence of the solution $u_h \in V_h$ to the global solution $u \in H^1(\Omega)$. As a key step in this analysis we obtained the error estimate (4.10)

$$\|u - u_h\|_{H^1} \leq \frac{M}{\alpha} \inf_{v_h \in V_h} \|u - v_h\|_{H^1}$$

Let $v \in C^0(\bar{\Omega})$. We now define interpolant of v in the space of X_h^1 determined by the triangulation ζ_h as the function $\Pi_h^1 v$ such that $\Pi_h^1 v(N_i) = v(N_i)$ for each node N_i of ζ_h for $i = 1, 2, \dots, N_h$. If $\{\phi_i\}$ is the Lagrangian basis of the space X_h^1 , then

$$\Pi_h^1 v(x) = \sum_{i=1}^{N_h} v(N_i) \phi_i(x)$$

The operator $\Pi_h^1 : C^0(\bar{\Omega}) \rightarrow X_h^1$, associating a continuous function v to its interpolant $\Pi_h^1 v$ is called interpolation operator.

Analogously we can define an operator $\Pi_h^r : C^0(\bar{\Omega}) \rightarrow X_h^r$, for each integer $r \geq 1$. Having denoted by Π_K^r , the local interpolation operator associated to a continuous function v the polynomial $\Pi_K^r v \in P_r(K)$, interpolating v in the degrees of freedom of the element $K \in \zeta_h$, we define

$$\Pi_h^r v \in X_h^r : \quad \Pi_h^r|_K = \Pi_K^r(v|_K) \quad \forall K \in \zeta_h$$

From (4.10) we get

$$\begin{aligned} \|u - u_h\|_{H^1(\Omega)} &\leq \frac{M}{\alpha} \inf_{v_h \in V_h} \|u - v_h\|_{H^1(\Omega)} \\ &= \frac{M}{\alpha} \left[\sum_{K \in \zeta_h} \|u - \Pi_h^r\|_{H^1(K)}^2 \right]^{\frac{1}{2}} \\ &= \frac{M}{\alpha} \left[\sum_{K \in \zeta_h} \|u - \Pi_K^r\|_{H^1(K)}^2 \right]^{\frac{1}{2}} \end{aligned} \quad (4.18)$$

Thus the problem of estimating $\|u - u_h\|_{H^1(\Omega)}$ is reduced to the problem of estimating $\|u - \Pi_K^r\|_{H^1(K)}$. We will now state the the interpolation error estimates and an estimate for the error $\|u - u_h\|_{H^1(\Omega)}$. The proofs can be found in AQ. To prove these estimates, regularity of the triangulation is used as well as affine and invertible transformation $F_K : \hat{K} \rightarrow K$ between the reference triangle \hat{K} and the generic triangle K (see Fig 4.5) is used. Such a map is defined by $F_K(\hat{x}) = B_K \hat{x} + b_K$, $B_K \in \mathbb{R}^{2 \times 2}$, $b_K \in \mathbb{R}^2$, and it satisfies the relation $F_K(\hat{K}) = K$.

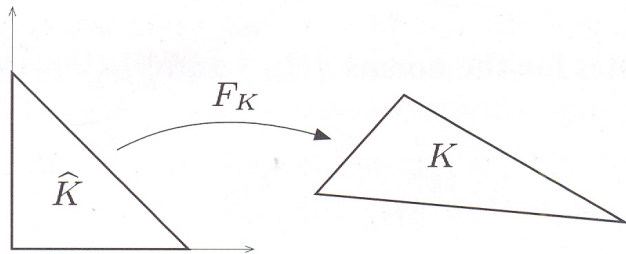


Figure 4.5: The map F_K between the reference triangle \hat{K} and the generic triangle K

Theorem 4.5.1 (Global estimate for the interpolation error). *Let $\{\tau_h\}_{h>0}$ be a family of regular grids*

of the domain Ω and let $m = 0, 1$ and $r \geq 0$. Then there exists a constant $C = C(r, m, \bar{K}) > 0$ such that

$$|v - \Pi_h^r v|_{H^m(\Omega)} \leq C \left(\sum_{K \in \tau_h} h_K^{2(r+1-m)} |v|_{H^{r+1}(K)}^2 \right)^{\frac{1}{2}} \quad \forall v \in H^{r+1}(\Omega)$$

In particular we obtain

$$|v - \Pi_h^r v|_{H^m(\Omega)} \leq Ch^{r+1-m} |v|_{H^{r+1}(\Omega)} \quad \forall v \in H^{r+1}(\Omega)$$

Theorem 4.5.2 (Error estimate for the finite element solution). *Let $u \in V$ be the exact solution of the variational problem (1) and u_h be its approximate solution using the finite element method of degree r . If $u \in H^{r+1}(\Omega)$, then the following a priori error estimate hold:-*

$$\|u - u_h\|_{H^1(\Omega)} \leq \frac{M}{\alpha} C \left(\sum_{K \in \tau_h} h_K^{2r} |u|_{H^{r+1}(K)}^2 \right)^{\frac{1}{2}}$$

$$\|u - u_h\|_{H^1(\Omega)} \leq \frac{M}{\alpha} Ch^r |u|_{H^{r+1}(\Omega)}$$

C is a constant independent of h and u .

4.6 Finite element method for the Optical flow problem (2.2)

Now that we have the required prerequisites, we will solve the optical flow problem (2.2) using the finite element method. We will first formulate the problem in the finite element setup.

We are to minimize the functional J as given in (2.2). We showed in Theorem 3.2.2 that minimizing the functional J is equivalent to finding a solution of $J'(U) = 0$. We also showed in Section 3.3.2 that we can write $J'(U)[V] = 0 \quad \forall V \in Z$ as $A(U, V) = F(V)$ where $A(U, V)$ is a symmetric bilinear form on $Z \times Z$ associated to the functional J given by (3.6) and $F(V)$ is a linear form on Z given by (3.7). The approximate problem can be written as

find $U_h \in Z_h$:

$$A(U_h, V_h) = F(V_h) \quad \forall V_h \in Z_h$$

where Z_h is a suitable approximation of the space Z depending on a parameter h . So in the finite element setup, the optical flow problem reduces to find $U_h \in Z_h$:

$$\int_{\Omega} (\nabla E \cdot U_h) (\nabla E \cdot V_h) + K \int_{\Omega} (\nabla U_h \cdot \nabla V_h) = - \int_{\Omega} E_t (\nabla E \cdot V_h) \quad \forall V_h \in Z_h$$

We take the approximation of the space Z as the space $Z_h = (\bar{X}_h^1)^2$. So we are considering Type 1 rectangular finite elements. The characteristic Lagrangian basis functions are characterized by the following property $\Phi_i \in Z_h$ such that $\Phi_i(x_j) = \delta_{ij}$, $i, j = 0, 1, \dots, N_h$ where N_h are the number of nodes and δ_{ij} being the Kronecker delta. The function Φ_i is therefore piecewise linear in each coordinate, as we have rectangular finite elements, and equal to one at each x_i and zero at the remaining nodes of the triangulation.

4.6.1 Data

Our domain Ω is the unit square in \mathbb{R}^2 i.e. $[0, 1] \times [0, 1]$. We have taken our image at time t_0 to be E_0 defined as:-

$$E_0(x, y) = E(x, y, 0) = e^{[-50 * \{(x - 0.5)^2 + (y - 0.5)^2\}]}$$

and for testing the accuracy of the method we move the image with a pre-defined constant velocity of $(u, v) = (1, 1)$.

So at time t , the image will be given by,

$$E(x, y, t) = E_0(x - ut, y - vt) = E(x - ut, y - vt, 0)$$

using the characteristic method. We use the Neumann boundary conditions which are natural boundary conditions.

4.6.2 Programming procedure

We use deal.II libraries in C++ programming language to solve the problem. We refine the domain Ω uniformly three times i.e in the first step we divide Ω into four equal cells. In the second step we divide each of the four cells into equal four cells and so on upto three times. So the total number of active cells will be 64. Then the degrees of freedom in the refined grid are calculated and we now form the stiffness matrix A and the right hand side f as in (4.5) and hence the linear equation

$$AU = f, U \in T. \quad (4.19)$$

It will be a sparse matrix. It is invertible under the conditions for Neumann boundary conditions in Chapter 3 as the associated bilinear form is coercive (Theorem 4.2.1). Then the linear system in (4.19) is solved using the conjugate gradient method (See Appendix C). A preconditioner is also used to improve on the condition number of the matrix \bar{A} so that after inversion of the matrix the results are proper.

4.6.3 Results

With Neumann boundary conditions, we obtained the following velocity vector diagram for $K = 0.9$

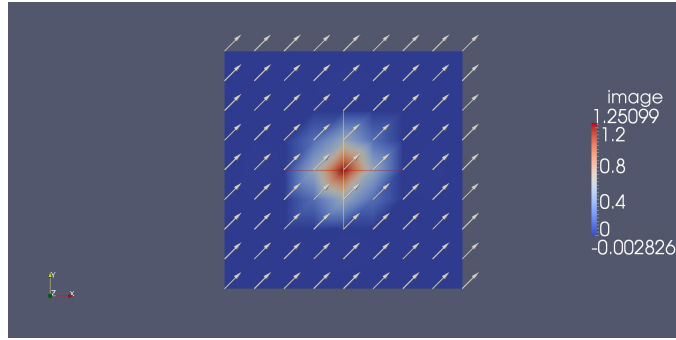


Figure 4.6: Image along with the velocity vectors for $K = 0.9$.

We also obtained the following velocity vector diagram for $K = 1.1$

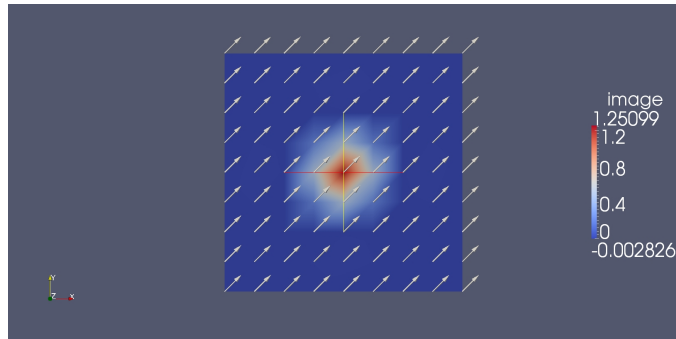


Figure 4.7: Image along with the velocity vectors for $K = 1.5$.

From Fig 4.6 and Fig 4.7 we can see that the velocity vectors have the same direction and almost the same magnitude as indicated by the L^2 error from Table 4.1. We changed the smoothing parameter K and calculated the L^2 error in the velocity and the error in the advection term $\int_{\Omega} E_t + \nabla E.U$. The results are shown below:

4.6.4 Conclusion

The order of the advection error is 10^{-28} and the order of the L^2 error is 10^{-13} which suggests that the optical flow velocities obtained using the finite element method satisfy the advection equation and are very close to the actual velocity since we already know the actual velocity in this case. We have also plotted a graph of L^2 error versus K to see for which values of K is the L^2 error very small. The graph is displayed below.

K	Relative L^2 Error	Advection Error
0.1	5.5502 e-13	9.57645 e-26
0.2	1.35063 e-13	6.84743 e-27
0.3	2.2402 e-13	3.27 e-26
0.4	6.30311e-13	2.49359 e-27
0.5	8.06069 e-13	4.05669 e-27
0.6	9.68666 e-13	5.98357 e-27
0.7	1.11661 e-13	7.80902 e-27
0.8	1.24088 e-13	9.44175 e-27
0.9	1.59248 e-13	1.62616 e-27
1	2.21603 e-13	3.56386 e-28
1.1	2.22272 e-13	3.58421 e-28
1.2	2.65804 e-13	5.19862 e-28
1.3	2.48961 e-13	2.70607 e-28
1.4	2.71351 e-13	3.36132 e-28
1.5	2.99787 e-13	6.08894 e-28
1.6	3.31377 e-13	6.62004 e-28
1.7	3.3914 e-13	4.17334 e-28
1.8	3.47395 e-13	4.95675 e-28
1.9	3.67301e-13	6.14862 e-28
2	4.06641 e-13	8.57827 e-28

Table 4.1: Variation of relative L^2 error and Advection error with the smoothing parameter K

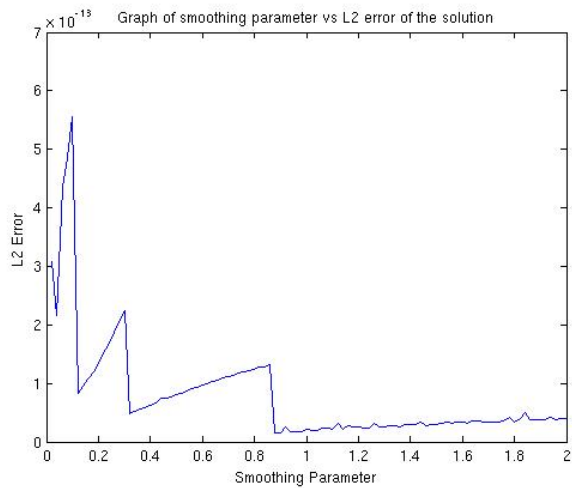


Figure 4.8: Graph of L^2 error vs K .

We find that the L^2 error is oscillating for different values of K from 0

to 2 but when $K > 1$ it gives less error (In fact near $K = 1$ it has the least error and near $K = 0$ it gives the greatest error). But the error is of order 10^{-13} which is very small and so optimal K cannot be determined. This suggests us to take higher values of K . We again plot a graph of L^2 error versus K when K ranges from 2 to 90.

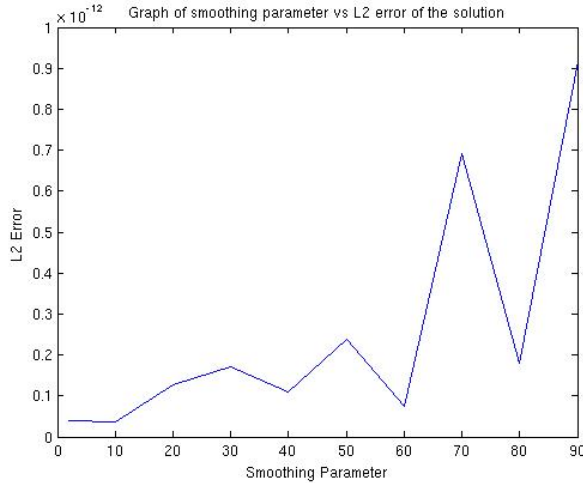


Figure 4.9: Graph of L^2 error vs K .

Again the order of the error is 10^{-13} which suggests that we can take any non-zero K and solve the problem. There does not exist any optimal K . But we have to be carefull not to choose K very close to 0 otherwise the matrix A may not be invertible.

So we see that the finite element method is better than the finite difference method as the error decreases by order of 10^{-13} . So we now proceed to the next chapter to solve the cloud motion problem emulating the optical flow techniques that has been tested upto now. We would like to capture the velocity of the fluid whose motion determines the motion of the clouds. We will assume that the fluid flow is potential and incompressible. We will solve it numerically using the finite element method as we found out that the method is more accurate than the finite difference method. We assume that the velocity potential satisfies the Laplace's equation and we will try and minimize the advection error with respect to suitable values of the normal flux of the velocity at the boundary.

Chapter 5

Finite Element method for the Potential flow problem

5.1 Introduction

With all the study of optical flow methods done in the previous chapters we now move on to the field of cloud motion. We are interested in the advection of clouds in some fluid due to the fluid flow. We will try to recover the underlying fluid flow. We assume that the fluid flow is potential and incompressible.

5.2 Constraints

Let E be a brightness pattern. We will again assume that brightness of a particular point in the pattern is constant, so

$$\frac{dE}{dt} = 0$$

This implies E satisfies

$$E_x u + E_y v + E_t = 0 \quad (5.1)$$

Let $U = (u, v)$ be the optical flow velocity. Then by our assumption on the flow

$$\begin{aligned} U &= \nabla \Phi \\ \Delta \Phi &= 0 \end{aligned} \quad (5.2)$$

Now to solve for Φ we have to give a boundary condition on it and so the natural choice would be to specify the normal rate of change of flux on the boundary. The condition can be written as

$$\nabla \Phi \cdot n = g \quad (5.3)$$

where g is some arbitrary function and n is the unit normal on the boundary of Ω . If U belongs to $Z = (H^1(\Omega))^2$ then g belongs to $H^{\frac{1}{2}}(\partial\Omega)$. Our aim is to determine a suitable g so that U satisfies (5.1), (5.2) and (5.3). Now to solve for Φ from (5.2) and (5.3) we have another constraint to be satisfied i.e

$$\int_{\partial\Omega} g = 0 \quad (5.4)$$

We will now modify the HS functional (2.2) and try to solve the problem incorporating the above constraints.

5.3 Problem Statement

Let $E : \Omega \times \mathbb{R}^+ \rightarrow \mathbb{R}$, be an image sequence, where $\Omega \subseteq \mathbb{R}^2$ is a bounded domain of the spatial coordinates and \mathbb{R}^+ is the domain of the time coordinate. We estimate the optical flow, the field $U \in H^1(\Omega)$ of optical velocities over Ω , by minimising the functional,

$$J(U) = \frac{1}{2} \int_{\Omega} (E_t + \nabla E \cdot U)^2 + \frac{K}{2} \int_{\partial\Omega} g^2 \quad (5.5)$$

over $g \in H^{\frac{1}{2}}(\partial\Omega)$, subject to the above given constraints, where K is a positive constant.

There are two terms in the functional. The first term comes as a result of the fact that brightness of a particular point in the image pattern is constant. The second term is added to have a control over the normal rate of change of optical flow flux on the boundary.

5.4 Minimization equations

We consider the auxillary functional

$$\begin{aligned} \tilde{J}(U, \psi, \lambda) &= \frac{1}{2} \int_{\Omega} (E_t + \nabla E \cdot U)^2 dx dy + \frac{K}{2} \int_{\partial\Omega} g^2 d\nu + \int_{\partial\Omega} g\psi d\nu - \\ &\quad \int_{\Omega} \nabla\Phi \cdot \nabla\psi dx dy + \lambda \int_{\partial\Omega} g \\ &= \frac{1}{2} \int_{\Omega} (E_t + \nabla E \cdot \nabla\Phi)^2 dx dy + \frac{K}{2} \int_{\partial\Omega} g^2 d\nu + \int_{\partial\Omega} g\psi d\nu - \\ &\quad \int_{\Omega} \nabla\Phi \cdot \nabla\psi dx dy + \lambda \int_{\partial\Omega} g, \end{aligned} \quad (5.6)$$

where $\psi \in H^1(\Omega)$ is the Lagrange multiplier for constraint on Φ and $\lambda \in \mathbb{R}$ is the Lagrange multiplier for the constraint $\int_{\partial\Omega} g = 0$.

5.4.1 Equation for Φ given from $\frac{\partial \tilde{J}}{\partial \psi} = 0$

We consider

$$\lim_{\epsilon \rightarrow 0} \frac{\tilde{J}(\psi + \epsilon \tilde{\psi}) - \tilde{J}(\psi)}{\epsilon} = 0, \quad \tilde{\psi} \in H^1(\Omega)$$

This gives

$$\int_{\partial\Omega} g \tilde{\psi} d\nu - \int_{\Omega} \nabla \Phi \cdot \nabla \tilde{\psi} dx dy, \quad \tilde{\psi} \in H^1(\Omega) \quad (5.7)$$

5.4.2 Equation for ψ given from $\frac{\partial \tilde{J}}{\partial \Phi} = 0$

We consider

$$\lim_{\epsilon \rightarrow 0} \frac{\tilde{J}(\Phi + \epsilon \tilde{\Phi}) - \tilde{J}(\Phi)}{\epsilon} = 0, \quad \forall \tilde{\Phi} \in H^1(\Omega)$$

This gives

$$-\int_{\Omega} \nabla \psi \cdot \nabla \tilde{\Phi} + \lim_{\epsilon \rightarrow 0} \frac{\frac{1}{2} \int_{\Omega} (E_t + \nabla E \cdot \nabla (\Phi + \epsilon \tilde{\Phi}))^2 - (E_t + \nabla E \cdot \nabla \Phi)^2}{\epsilon} = 0$$

which reduces to

$$-\int_{\Omega} \nabla \psi \cdot \nabla \tilde{\Phi} + \int_{\Omega} (E_t + \nabla E \cdot \nabla \Phi) (\nabla E \cdot \nabla \tilde{\Phi}) = 0, \quad \forall \tilde{\Phi} \in H^1(\Omega) \quad (5.8)$$

5.4.3 Equation for g given from $\frac{\partial \tilde{J}}{\partial \lambda} = 0$

We consider $\frac{\partial \tilde{J}}{\partial \lambda} = 0$ to get

$$\int_{\partial\Omega} g = 0 \quad (5.9)$$

5.4.4 Minimization equation obtained from $\frac{\partial \tilde{J}}{\partial g} = 0$

We consider

$$\lim_{\epsilon \rightarrow 0} \frac{\tilde{J}(g + \epsilon \tilde{g}) - \tilde{J}(g)}{\epsilon} = 0, \quad \tilde{g} \in H^{\frac{1}{2}}(\partial\Omega)$$

Then we get

$$\int_{\partial\Omega} (Kg + \psi + \lambda) \tilde{g} = 0, \quad \forall \tilde{g} \in H^{\frac{1}{2}}(\partial\Omega) \quad (5.10)$$

(5.10) gives us

$$Kg + \psi + \lambda = 0 \quad (5.11)$$

on $\partial\Omega$. This gives

$$\int_{\partial\Omega} (Kg + \psi + \lambda) d\nu = 0$$

Using (5.9) we get

$$\lambda \int_{\partial\Omega} d\nu = - \int_{\partial\Omega} \psi d\nu$$

This gives

$$\lambda = - \frac{\int_{\partial\Omega} \psi d\nu}{\int_{\partial\Omega} d\nu}$$

Therefore (5.11) implies

$$g = \frac{1}{K} \left(-\psi + \frac{\int_{\partial\Omega} \psi d\nu}{\int_{\partial\Omega} d\nu} \right) \quad (5.12)$$

on $\partial\Omega$.

5.5 Solving the problem

Now that we have got the equations (5.7), (5.8), (5.9), (5.10), (5.12), we will solve them using finite element method to recover the optical flow velocity for a given image pattern. We use Freefem++ software to achieve this objective. But first we will write down the original space Z where we are trying to find the solution, the approximate space Z_h depending on parameter h and the weak formulations for Φ , ψ in the space Z_h .

Our domain Ω is the unit square in \mathbb{R}^2 . We take $Z = (H^1(\Omega))^2$ and the approximation of the space Z as the space $Z_h = (X_h^1)^2$ where X_h^1 is the space defined in (4.16).

The weak formulation for ψ is

$$-\int_{\Omega} \nabla \psi \cdot \nabla \psi_h + \int_{\Omega} (E_t + \nabla E \cdot \nabla \Phi) (\nabla E \cdot \nabla \psi_h) = 0, \quad \forall \psi_h \in X_h^1(\Omega) \quad (5.13)$$

The weak formulation for Φ is

$$\int_{\partial\Omega} g \Phi_h - \int_{\Omega} \nabla \Phi \cdot \nabla \Phi_h, \quad \forall \Phi_h \in X_h^1(\Omega) \quad (5.14)$$

5.6 Data for constant flow

We have taken our image at time t_0 to be E_0 defined as:-

$$E_0(x, y) = E(x, y, 0) = e^{[-50 * \{(x-0.5)^2 + (y-0.5)^2\}]}$$

and for testing the accuracy of the method we move the image with a pre-defined constant velocity of $u = 1.0$ and $v = 1.0$.

So at time t , the image will be given by,

$$E(x, y, t) = E_0(x - ut, y - vt) = E(x - ut, y - vt, 0)$$

using the characteristic method.

5.7 Programming procedure

As we have said earlier that we will solve the above problem using Freefem++ software. The steps for solving the problem are enumerated below

1. We divide Ω into triangular finite elements. Freefem++ helps us to do so (In the previous chapter, the deal.II software was dividing Ω into rectangular finite elements).
2. We then give an arbitrary starting value of g and solve for Φ using its weak formulation. We note while solving for Φ we are using Neumann boundary conditions and so the solution is unique upto a constant. To remove ambiguity arising from the constants we modify the weak formulation for Φ as

$$\int_{\partial\Omega} g\Phi_h - \int_{\Omega} \nabla\Phi \cdot \nabla\Phi_h - \epsilon \int_{\Omega} \Phi\Phi_h, \quad \forall \Phi_h \in X_h^1(\Omega)$$

where $\epsilon = 10^{-10}$. So unless Φ is of order $\frac{1}{\epsilon}$ we satisfy (5.9) and also the solution obtained is unique and it is almost equal to the solution obtained from (5.14).

3. After we get Φ , we substitute it in (5.13) and solve for ψ .
4. We then modify g using (5.12).
5. Now we check the L^2 error of the difference of the modified g and the previous value of g . If the difference is less than a given value of tolerance, then we have obtained the solution Φ and hence the flow velocity $U = (\partial_x(\Phi), \partial_y(\Phi))$ else we use the modified value of g to again solve for Φ, ψ and then repeat the procedure.

5.8 Results

The results obtained by taking our image E as above are given below.
 Ω is divided into triangles as seen in Fig 5.1

Mesh

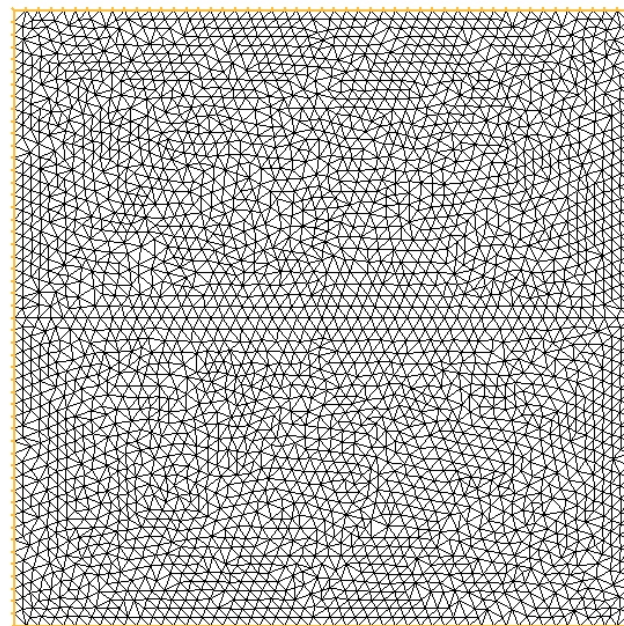


Figure 5.1: Ω divided into triangles

The image E is plotted as given in Fig 5.2

Image

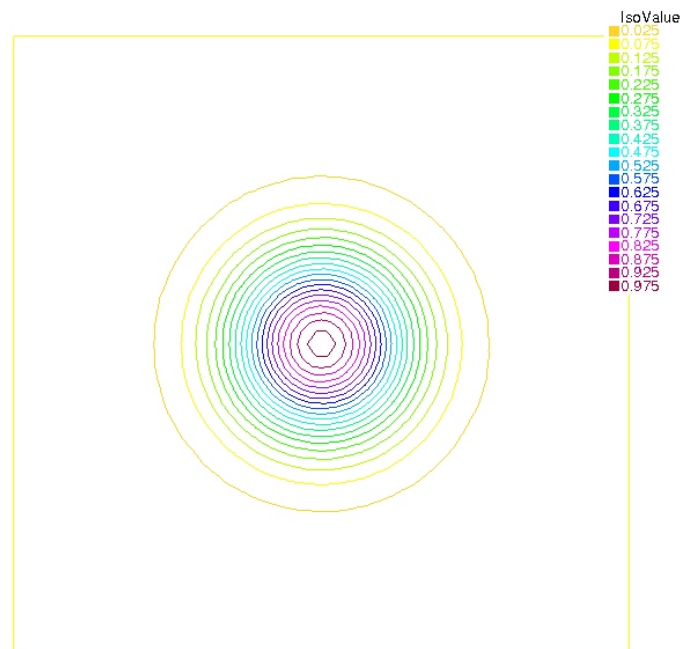


Figure 5.2: Image E

The velocity vectors for different values for K are shown below:

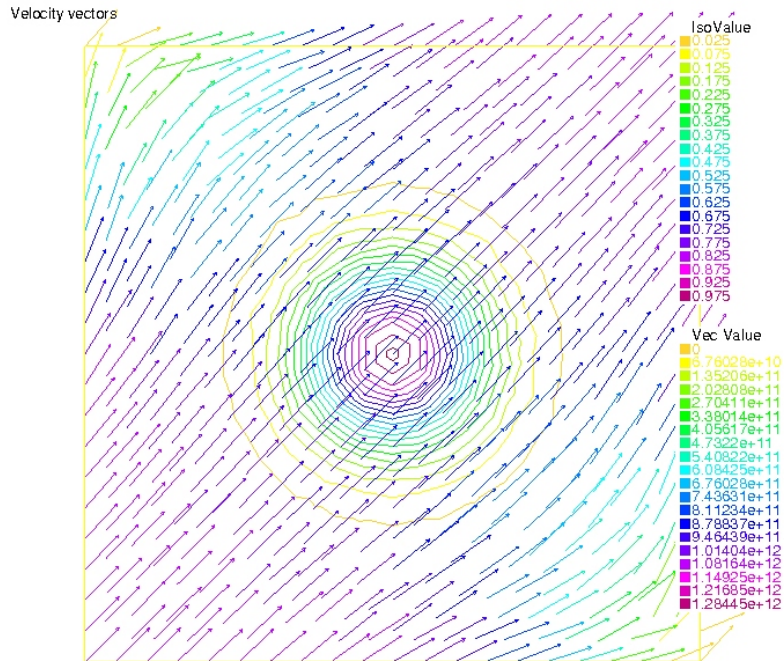


Figure 5.3: $K = 1$

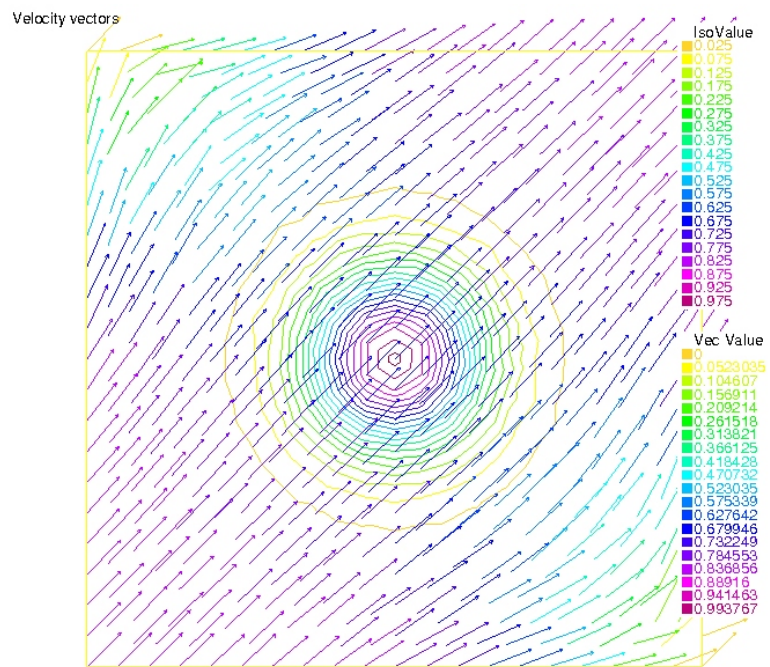


Figure 5.4: $K = 1.1$

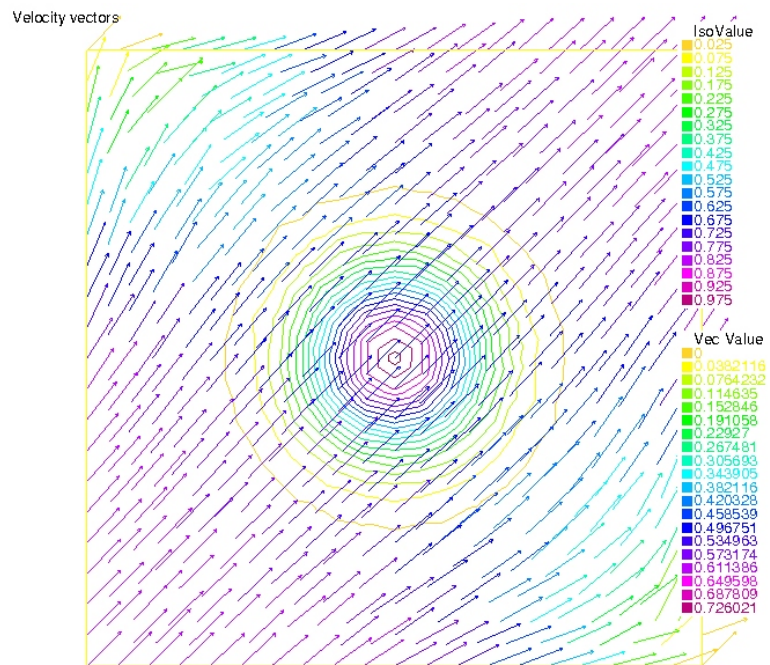


Figure 5.5: $K = 1.5$

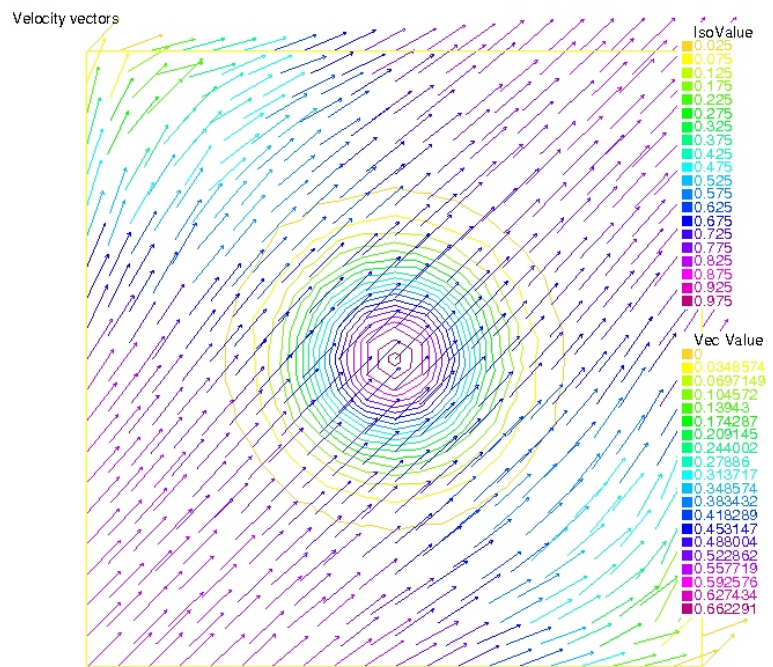


Figure 5.6: $K = 1.75$

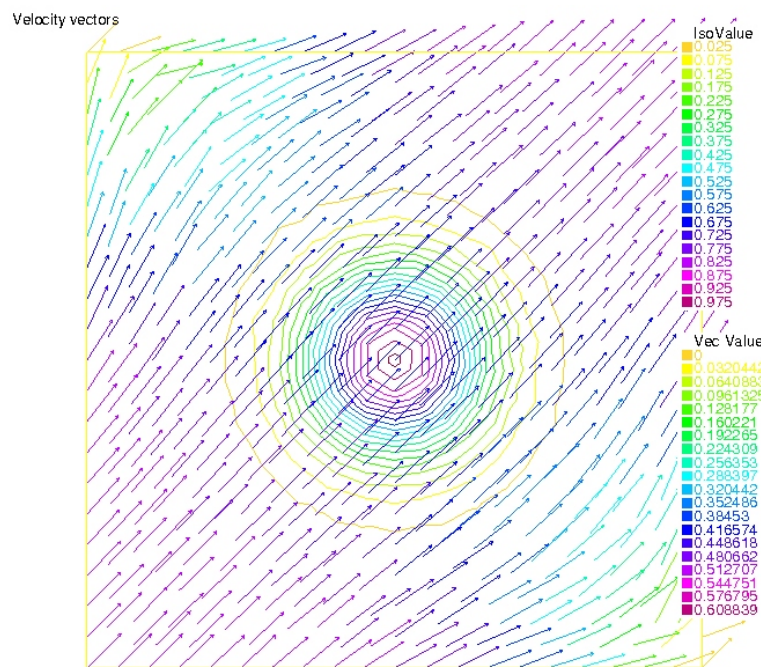


Figure 5.7: $K = 2$

From the above figures, we note that for $K = 1$ the magnitude of the velocity vectors are too high which suggests that $K = 1$ is not a good choice. But For $K = 1.1, 1.5, 1.75, 2$ we see that the average magnitude is near to 0.5 and it decreases as we increase K . We now draw a table for comparing the relative L^2 errors and the advection errors($\int_{\Omega} (E_t + \nabla E \cdot U)$) for different values of K .

K	Time taken/ Number of steps	Relative L^2 error	Advection error	Method Convergence Status
0.8	315 steps	-	-	No
1	315 steps	-	-	No
1.01	315 steps	-	-	No
1.06	315 steps	-	-	No
1.08	315 steps	-	-	No
1.09	315 steps	-	-	No
1.1	850.45 sec	0.530761	8.53735 e-5	Yes
1.2	47.375 sec	0.550122	8.16886 e-5	Yes
1.5	13.24 sec	0.599979	7.23131 e-5	Yes
1.75	9.23 sec	0.633987	6.599943 e-5	Yes
2	7.31 sec	0.662754	6.06881 e-5	Yes
3	4.33 sec	0.743681	4.59114 e-5	Yes

Table 5.1: Variation of relative L^2 error and advection error with the smoothing parameter K

Our tolerance level is set at 10^{-10} . We can see from above table that if $K \leq 1$ then the method does not converge at all. But even if we increase K then the method converges but as we increase K the relative L^2 error increases, not rapidly. But the advection error decreases as $K \geq 1.1$ even though the order of the error is 10^{-5} . Also time taken to compile is proportional to K . So to have a balance between the control of L^2 error and the advection error we would want to choose K such that the L^2 error is the minimum as the order of the L^2 error is much greater than the advection error. The results suggest that the optical flow velocity could be sensitive to K . Smaller values of K cannot be taken. Too higher values of K might over-regularize the flow velocity. So there exists an optimal value of K for which the relative L^2 error is the minimum. We plot a graph to see the same.

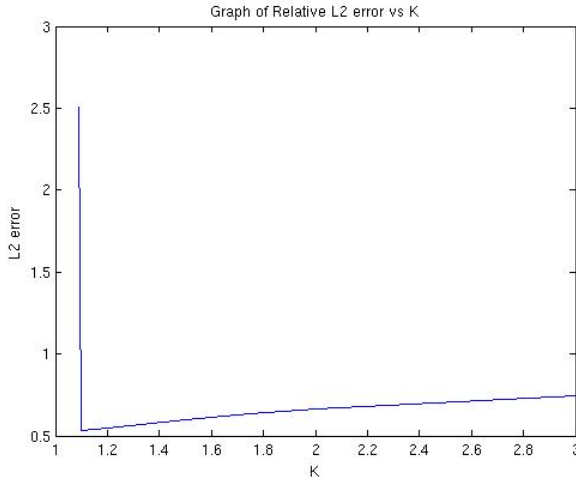


Figure 5.8: Graph of Relative L2 error vs K showing existence of an optimal K

From the above results we have an intuitive feeling that the optical flow velocity might depend on K . So we try for another example where the above given image E is subject to a point vortex.

5.9 Flow due to point vortex

We consider the same domain and the same image E . We now introduce a point vortex of strength $\kappa = 100.0$, whose singularity lies at the point $(-1, -1)$ i.e. outside the domain. The velocity components are given as

$$\begin{aligned} u &= -\frac{\kappa(y+1)}{2\pi[(x+1)^2 + (y+1)^2]} \\ v &= \frac{\kappa(x+1)}{2\pi[(x+1)^2 + (y+1)^2]} \end{aligned} \quad (5.15)$$

To test the method, we move the image E with the velocity $U = (u, v)$ according to the advection equation $E_t + \nabla E \cdot U = 0$ and then we will recover the velocity U . The results obtained are shown below:

5.10 Results

The mesh is the same as for the previous case. The image E is also the same. The velocity vectors are plotted for different values of K .

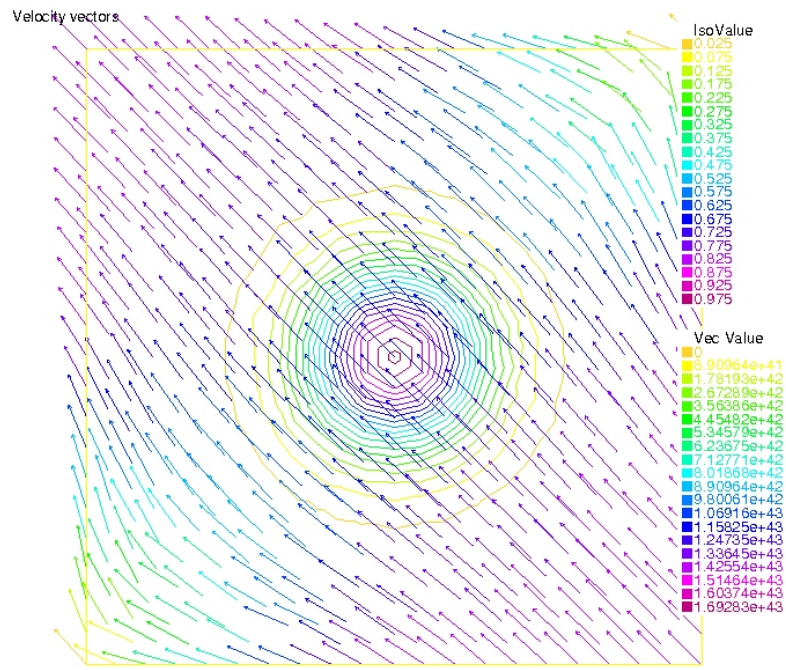


Figure 5.9: $K = 0.8$

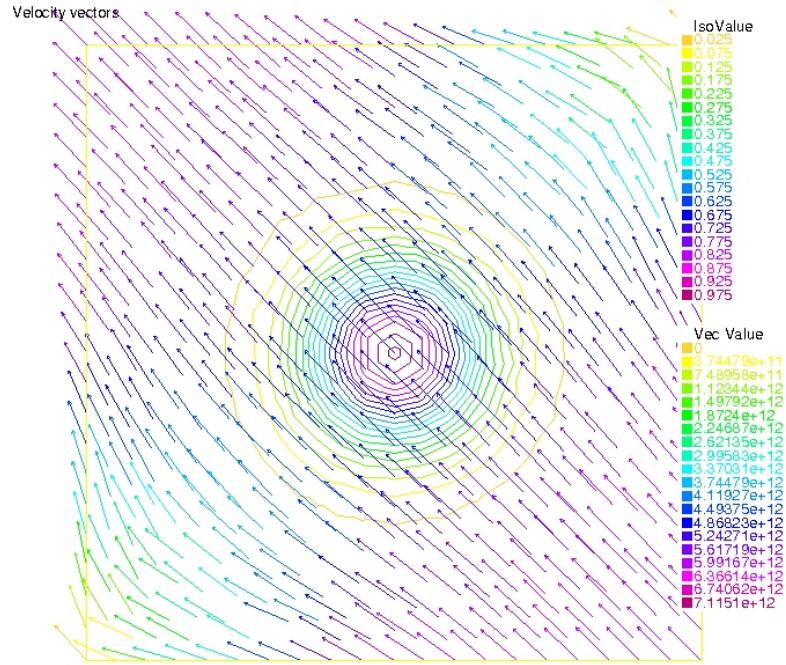


Figure 5.10: $K = 1$

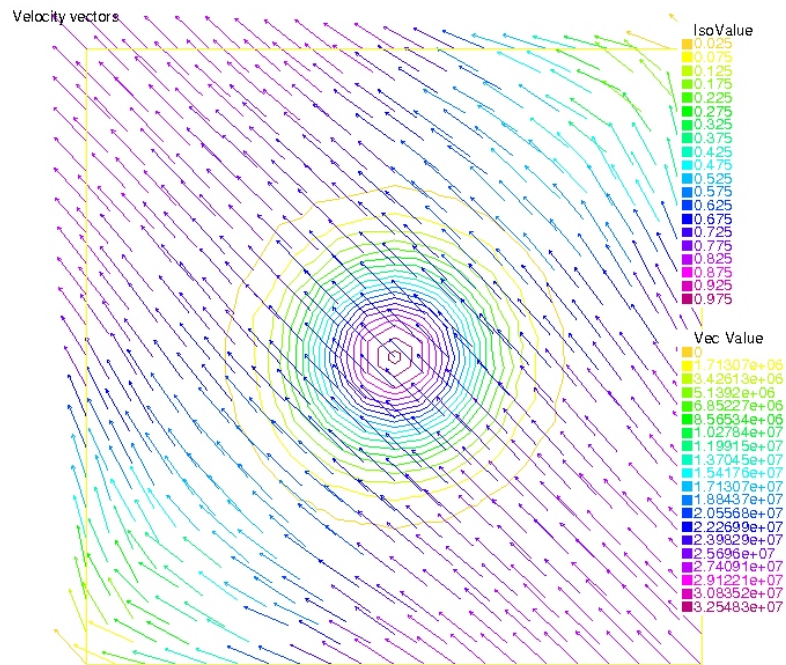


Figure 5.11: $K = 1.04$

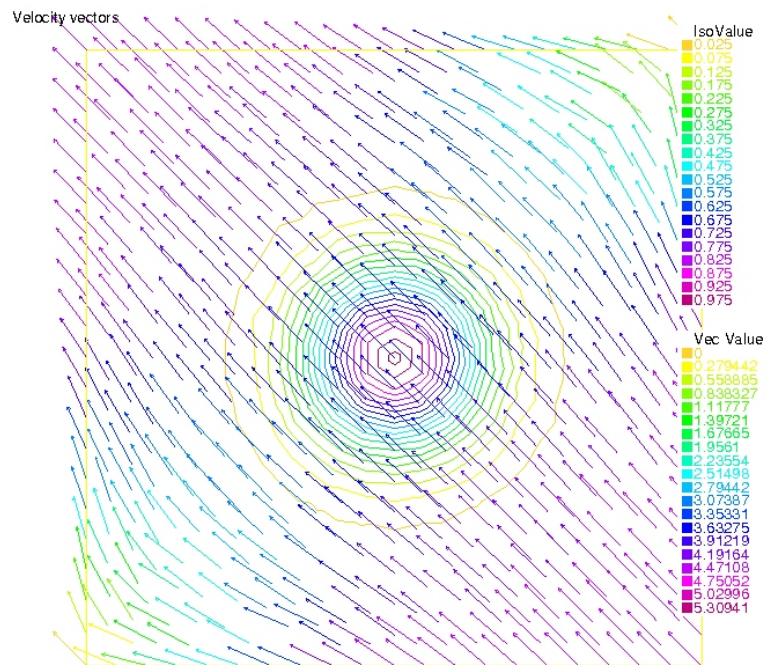


Figure 5.12: $K = 1.1$

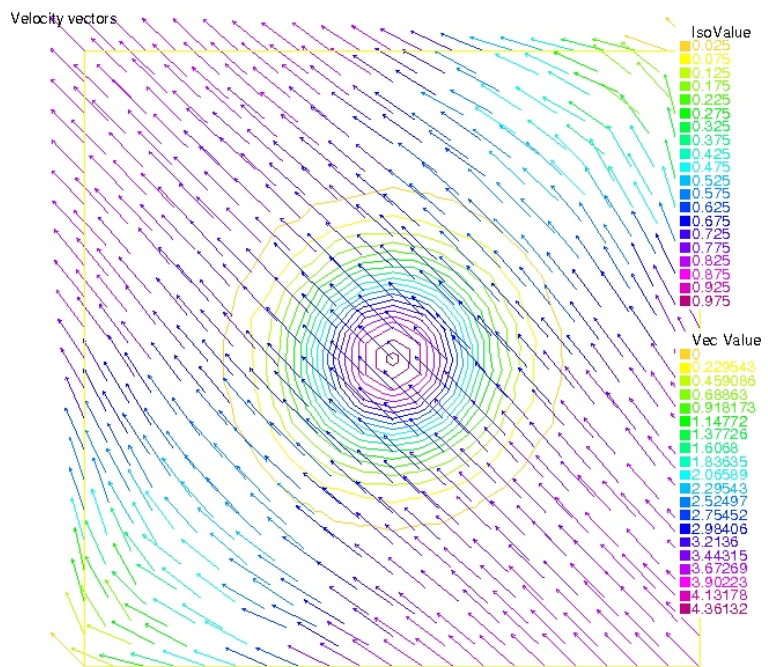


Figure 5.13: $K = 1.2$

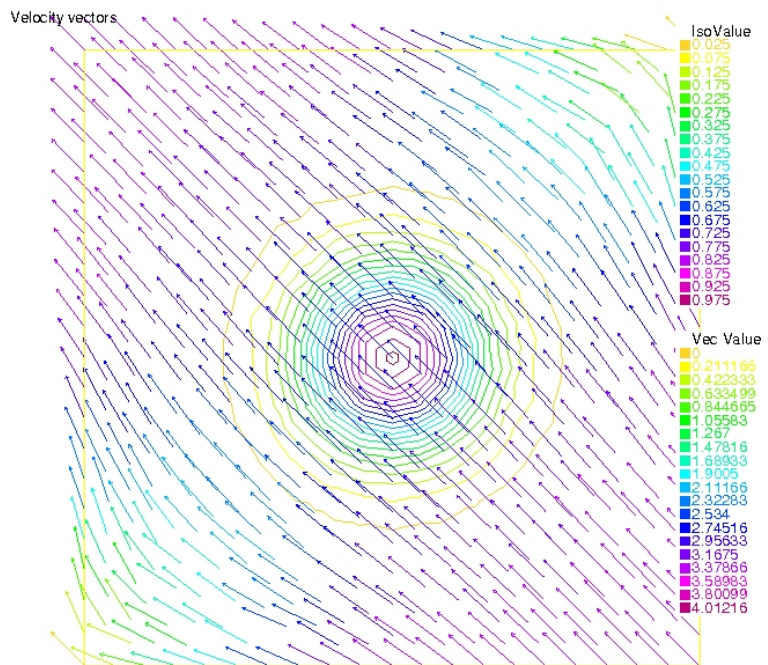


Figure 5.14: $K = 1.4$

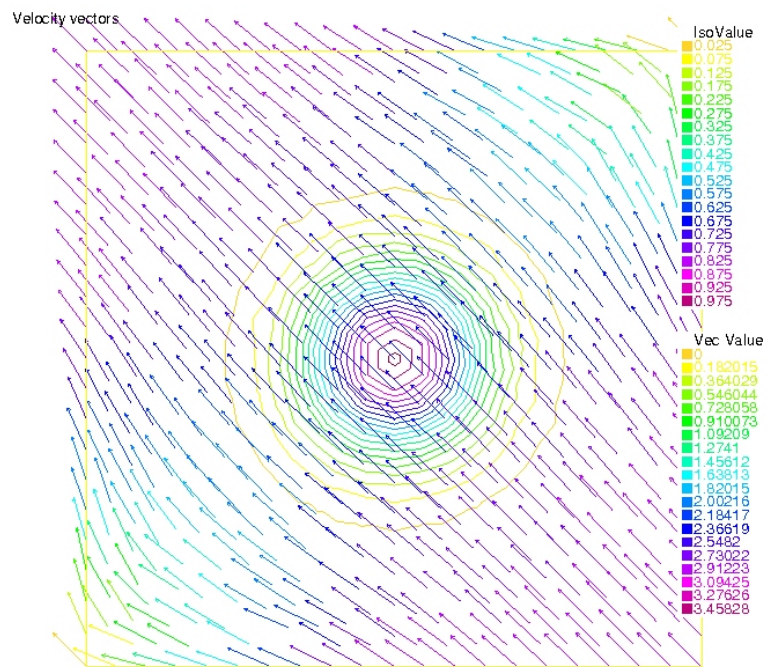


Figure 5.15: $K = 1.8$

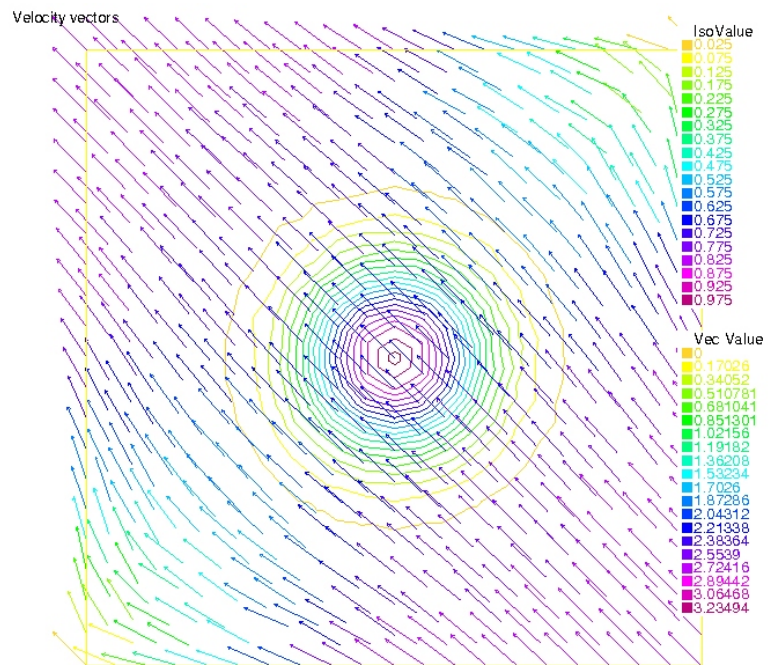


Figure 5.16: $K = 2$

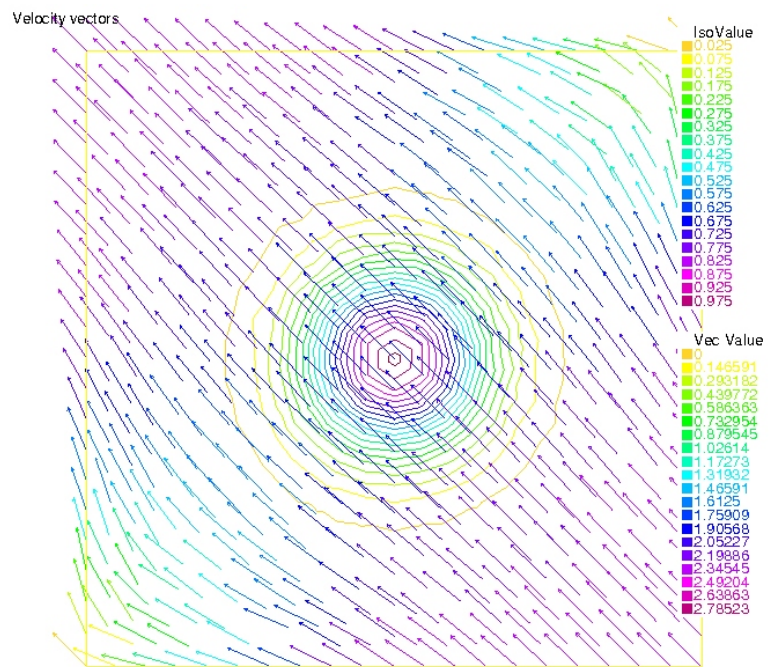


Figure 5.17: $K = 2.5$

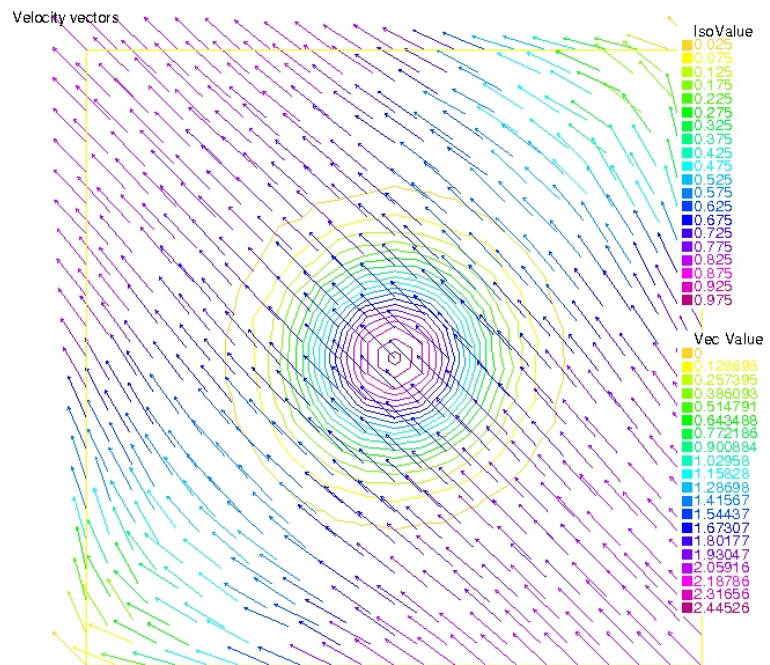


Figure 5.18: $K = 3$

5.11 Conclusions

From the above figures, we see a similar trend as we had got for the previous example. We note that for $K = 1$ the magnitude of the velocity vectors are too high which suggests that $K = 1$ is not a good choice. But For $K = 1.1, 1.2, 1.4, 1.8, 2, 2.5, 3$ we see that the average magnitude is near to 1 and it decreases as we increase K . We now draw a table for comparing the relative L^2 errors for different values of K .

K	Time taken/ Number of steps	Relative L^2 error	Advection Error	Method Convergence Status
0.8	315 steps	-	-	No
1	315 steps	-	-	No
1.04	315 steps	-	-	No
1.08	315 steps	-	-	No
1.1	869.78 sec	0.562607		Yes
1.2	42.79 sec	0.580036	4.81059 e-4	Yes
1.4	16.3 sec	0.611268	4.36944 e-4	Yes
1.8	8.3 sec	0.662055	3.70100 e-4	Yes
2	6.87 sec	0.682904	3.44042 e-4	Yes
2.5	5.06 sec	0.725437	2.92845 e-4	Yes
3	4.28 sec	0.75802	2.55113 e-4	Yes

Table 5.2: Variation of relative L^2 error with the smoothing parameter K for vortex flow.

Our tolerance level in this case is set at 10^{-7} . We can see from above table that if $K \leq 1$ then the method does not converge at all. But even if we increase K then the method converges but as we increase K the relative L^2 error increases, not rapidly. Again the time taken to compile is proportional to K . So we would want to choose K such that the L^2 error is the minimum. As in both the cases of constant flow and point vortex flow, we saw the same behaviour of the flow velocity with K we can now predict that for this method we have an universal optimal K which would minimize the L^2 error in the flow velocity. We again plot a graph to see which could be the optimal K .

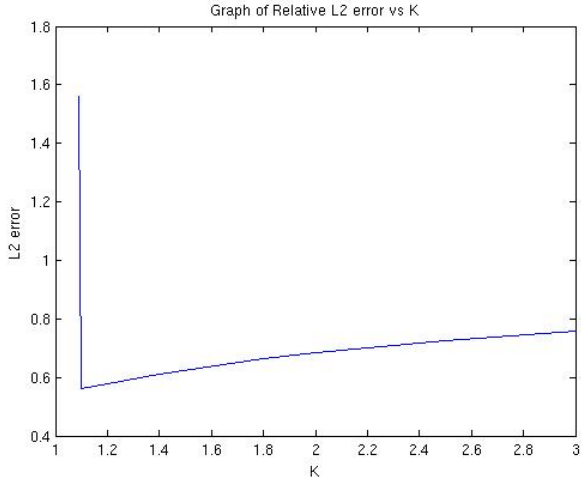


Figure 5.19: Graph of Relative L2 error vs K showing existence of an optimal K for vortex flow.

We compare the two graphs Graph 5.8 and Graph 5.19 and we find that the optimal K lies between 1.1 and 1.2 and for both the cases values are almost equal.

So our further work will be to develop a mathematical theory for the convergence of the method with respect to K and trying to find out which could be the optimal K . But as the L^2 error in the velocity is of the order 0.5, it suggests that the above method is not that accurate. We would like to reduce the error significantly. So we might have to modify the method. One way of doing so could be to introduce time dynamics into the method. Until now we have only considered image data given at a particular point of time. But as it is not working accurately, we could try providing image data at various instants of time and then try to recover the flow velocity. Also until now we have only entered images which are given by a mathematical formula. Henceforth we will consider images E given in form of pixels i.e totally discrete data and then try to capture the velocity. We could then see what sort of information is required to capture the velocity accurately.

Chapter 6

Conclusion

The main aim of the thesis was to build a method to determine the two dimensional velocities of a fluid by capturing the movement of the objects in the fluid. If such a method could be developed, then we could try to apply it to determine the motion of clouds using data from the geo-stationary satellites. This information could be useful for farmers, meteorologists, etc. This chapter will summarize the main contributions of the thesis and will also hint at future work to be done.

6.1 Contributions

6.1.1 Methodology

1. In the second chapter, we determined fluid flow velocities by minimising the Horn-Schunck functional along with the two constraints: the data conservation constraint and the smoothness constraint. We pointed out with illustrations why they were needed. Then we used a finite difference iterative scheme to solve the problem in case of a simple example whose domain of definition is the unit square and we already know the exact velocity of the fluid.
2. In the third chapter, we proved that there exists a unique minimiser of the Horn-Schuck functional subject to some conditions and we also showed the regularity of the minimizer and some estimates on it in terms of the given image data which suggested that the velocity field obtained depends continuously on the image derivatives, the domain of definition and the smoothing parameter.
3. In the fourth chapter, we determined fluid flow velocities of the same example as in the first chapter by minimising the Horn-Schunck functional and implemented it using the finite element method with the help of deal.II software in C++. Then the results of the finite differ-

ence method from the first chapter and the finite element method in this chapter were compared.

4. In the fifth chapter, we took up the cloud motion problem and assumed that the underlying fluid flow is compressible and a potential flow. Then we modified the Horn Schunck functional, as we wanted to relax the conditions required for solving the fluid flow problem using the original functional, and found out the minimising equations. We then solved two problems using the finite element method using the Freefem++ software: the first one being the same example as tested in chapter one and the second one being a flow due to point vortex with source of the vortex outside the domain of definition.

6.1.2 Results

1. After the comparing the finite difference and the finite element method implemented in the second and fourth chapters we found out that the finite element method was comparatively far more better than the finite difference method. With this idea we went about solving the cloud motion problem using the finite element method.
2. As we had to change our assumptions on the flow we modified the Horn-Schunck functional and solved the cloud motion problem using the finite element method. We had two test cases and for testing the accuracy of the results we had moved the fluid with a pre-defined velocity and tried to recover the same. But we found that the results were not that accurate in the sense that the relative L^2 error was of order 0.5-1.0. Different values of the smoothing parameter K was tried out but the error order remained the same. This suggested a problem with the method.

6.1.3 Inference

The results obtained in chapter five suggested that the method used had some problems. One of the problems could be because of the lack of information. We had always considered image data at a fixed time. We never considered image sequences at different instants of time. This suggests the future work which could be done.

6.2 Future work

We could try and modify our method so that we can incorporate images at various instants of time. We would then have sufficient information about the fluid flow which could help us calculate the flow field accurately. Furthermore we have calculated the flow field with continuous information of a

moving object in the fluid. In future we will try calculating the flow field when have information of the image in form of pixels. We would like to create a good method finally so that we provide the best information about cloud motion to the farmers, meterologists who work hard for the sake of the benefit of the world to make it a better and safer place to live in.

Appendix A

Rate of change of image brightness

Consider a patch of brightness pattern that is displaced a distance δx in the x -direction and δy in the y -direction in time δt . The brightness of the patch is assumed to remain constant so that

$$E(x, y, t) = E(x + \delta x, y + \delta y, t + \delta t)$$

Expanding the right hand side about the point (x, y, t) we get,

$$E(x, y, t) = E(x, y, t) + \delta x \frac{\partial E}{\partial x} + \delta y \frac{\partial E}{\partial y} + \delta t \frac{\partial E}{\partial t} + \epsilon$$

where ϵ contains second and higher order terms in $\delta x, \delta y$ and δt . After subtracting $E(x, y, t)$ from both sides and dividing through by δt we have

$$\frac{\delta x}{\delta t} \frac{\partial E}{\partial x} + \frac{\delta y}{\delta t} \frac{\partial E}{\partial y} + \frac{\partial E}{\partial t} + O(\delta t) = 0$$

where $O(\delta t)$ is a term of order δt , and we assume that δx and δy vary as δt . In the limit as $\delta t \rightarrow 0$ this becomes

$$\frac{\partial E}{\partial x} \frac{dx}{dt} + \frac{\partial E}{\partial y} \frac{dy}{dt} + \frac{\partial E}{\partial t} = 0$$

which is same as

$$E_t + \nabla E \cdot U = 0$$

where $U = (u, v)$ and $u = \frac{dx}{dt}$, $v = \frac{dy}{dt}$.

Appendix B

Existence Of An Unique Global Minimizer

First we will show that the functional $J(U)$, as given in (2.2), is continuous on $J(\Omega)$. We use the following results (See [RV])

Let X be an open set in a normed linear space L with norm $\|.\|$.

Theorem B.0.1. *Let J be a convex functional on X . If J is bounded from above in a neighbourhood of a point $U_0 \in X$ then it is locally bounded i.e each $U \in X$ has a neighbourhood on which J is bounded.*

Proof. :- We first show that if J is bounded above in an ϵ -neighbourhood of some point, it is bounded below in the same neighbourhood. Taking the point 0 for convinience, suppose $|J(U)| \leq B \quad \forall U \in N_\epsilon(0)$ where $N_\epsilon(0)$ is a neighbourhood of the origin given by

$$N_\epsilon(0) = \{U \in X : \|U\| < \epsilon\}$$

Since

$$0 = \frac{1}{2}U + \frac{1}{2}(-U)$$

By convexity of J we get,

$$J(0) \leq \frac{1}{2}J(U) + \frac{1}{2}J(-U)$$

This gives,

$$J(U) \geq 2J(0) - J(-U)$$

Now, $\|U\| < \epsilon$ implies $\|-U\| < \epsilon$.

Therefore

$$-J(-U) \geq -B, J(U) \geq 2J(0) - B$$

This means J is bounded from below.

Now for proving the theorem, we take J to be bounded from above by B on an ϵ -neighbourhood N of the origin. We will show J to be bounded in a neighbourhood of $U \in X, U \neq 0$. We choose $\rho > 1$ so that $V = \rho U \in X$ and let $\lambda = \frac{1}{\rho}$. Then

$$M = \{W \in L : W = (1 - \lambda)Y + \lambda V, Y \in N\}$$

is a neighbourhood of $\lambda V = U$ with radius $(1 - \lambda)\epsilon$. Moreover

$$J(W) \leq (1 - \lambda)J(Y) + \lambda J(V) \leq B + J(V).$$

So J is bounded above on M and by the first part of this proof J is bounded below on M . \square

Definition B.0.1. A functional J defined on an open set X is said to be **locally Lipschitz** if at each $U \in X \exists$ a neighbourhood $N_\epsilon(U)$ and a constant $K(U)$ s.t. if $V, W \in N$, then,

$$|J(V) - J(W)| \leq K\|V - W\|$$

If this inequality holds throughout a set $Y \subseteq X$ with K independent of U then we say that J is **Lipschitz** on Y .

Theorem B.0.2. Let J be convex on an open set $X \subseteq L$. If J is bounded from above in a neighbourhood of one point of X , then J is locally Lipschitz in X .

Proof. By Theorem B.0.1, J is locally bounded. So given U_0 we may find a neighbourhood $N_{2\epsilon}(U_0) \subseteq X$ on which J is bounded, say by M . Then J satisfies the stated Lipschitz condition on $N_\epsilon(U_0)$, for if it does not, we may choose $U_1, U_2 \in N_\epsilon(U_0)$ s.t.

$$\frac{|J(U_2) - J(U_1)|}{\|U_2 - U_1\|} > \frac{2M}{\epsilon}$$

Then we may choose $\alpha > 0$ s.t. $U_3 = U_2 + \alpha(U_2 - U_1)$ is in $N_{2\epsilon}(U_0)$ and $\|U_3 - U_2\| = \epsilon$. Because J is convex on the line through U_1, U_2, U_3 , we may use the following inequality,

$$\frac{|J(U_3) - J(U_2)|}{\|U_3 - U_2\|} \geq \frac{|J(U_2) - J(U_1)|}{\|U_2 - U_1\|} > \frac{2M}{\epsilon}$$

This gives us $|J(U_3) - J(U_2)| > 2M$, contradicting the fact that $|J| \leq M$.

Hence J is locally Lipschitz. \square

Theorem B.0.3. *Let J be convex on X . If J is bounded from above in an neighbourhood of one point of X , then J is continuous on X .*

Proof. Theorem B.0.2 implies J is locally Lipschitz, from which continuity follows immediately. \square

Theorem B.0.4. *The functional J as given in (2.2) is continuous*

Proof. We will use the Theorem B.0.3 to prove our statement. In our case $X = L = J(\Omega)$. Now $0 \in X$ and $J(0) = \frac{1}{2} \int_{\Omega} E_t^2 dx dy$

We have assumed our image E and its derivative E_x, E_y, E_t are bounded by M . Let $U \in J(\Omega)$ s.t. $\|U\|_Z < 1$. So

$$\begin{aligned} |J(U)| &= \left| \frac{1}{2} \int_{\Omega} ((\nabla E \cdot U)) + E_t)^2 + \frac{K}{2} \int_{\Omega} \|\nabla u\|^2 + \|\nabla v\|^2 \right| \\ &\leq \frac{1}{2} \int_{\Omega} ((\nabla E \cdot U)) + E_t)^2 + \frac{K}{2} \|U\|_Z^2 \\ &\leq \frac{1}{2} \int_{\Omega} (E_t^2 + (\nabla E \cdot U)^2 + 2 \cdot E_t \cdot (\nabla E \cdot U)) + \frac{K}{2} \|U\|_Z^2 \\ &= \frac{1}{2} \int_{\Omega} (E_t^2 + (E_x u + E_y v)^2 + 2 \cdot E_t \cdot (E_x u + E_y v)) + \frac{K}{2} \|U\|_Z^2, [U = (u, v)] \\ &\leq \frac{1}{2} \int_{\Omega} [M^2 + M^2(u + v)^2 + 2 \cdot M \cdot \left(\int_{\Omega} (\nabla E)^2 \right)^{\frac{1}{2}} \left(\int_{\Omega} U^2 \right)^{\frac{1}{2}}] + \frac{K}{2} \|U\|_Z^2 \text{ (Holder's Inequality)} \\ &\leq M^2 \cdot \frac{1}{2} \int_{\Omega} (1 + 2(u^2 + v^2)) + M \cdot \left(\int_{\Omega} M^2 \right)^{\frac{1}{2}} \|U\|_Z + \frac{K}{2} \|U\|_Z^2 \\ &\leq M^2 \cdot \frac{1}{2} \left(\int_{\Omega} \right) + M^2 \cdot \|U\|_Z^2 + M^2 \cdot \left(\int_{\Omega} \right) + \frac{K}{2} \\ &\leq \frac{3}{2} \cdot M \cdot \mu(\Omega) + M^2 + \frac{K}{2} \\ &< \infty. \end{aligned}$$

where $\mu(\Omega)$ is the measure of our bounded domain Ω . So in an $\epsilon (= 1)$ neighbourhood of 0, $J(U)$ is bounded above. Also J is convex (By (3.1)). So using the above Theorem B.0.3 we have J is continuous for all $U \in J(\Omega)$. \square

Now we show the existence of the derivative of (2.2).

B.1 Existence Of Gateaux Derivative Of J

Theorem B.1.1. *The Gateaux Derivative of (2.2) exists.*

Proof. The Gateaux Derivative of J at the point U acting on V is defined as

$$\lim_{\epsilon \rightarrow 0} \frac{J(U + \epsilon V) - J(U)}{\epsilon}$$

if it exists and is denoted by $J'(U, V)$

By (3.2), the Gateaux Derivative of J is

$$J'(U; V) = \int_{\Omega} (E_t + (\nabla E \cdot U))(\nabla E \cdot V) + K \int_{\Omega} (\nabla u_1 \cdot \nabla v_1) + (\nabla u_2 \cdot \nabla v_2)$$

where

$$U = (u_1, u_2), V = (v_1, v_2).$$

We will show it is well defined.

Now,

$$\begin{aligned} |J'(U; V)| &\leq \left| \int_{\Omega} (E_t + (\nabla E \cdot U))(\nabla E \cdot V) \right| + K \left| \int_{\Omega} (\nabla u_1 \cdot \nabla v_1) + (\nabla u_2 \cdot \nabla v_2) \right| \\ &\leq \left| \int_{\Omega} E_t(\nabla E \cdot V) \right| + \left| \int_{\Omega} (\nabla E \cdot U)(\nabla E \cdot V) \right| + K \left| \int_{\Omega} (\nabla u_1 \cdot \nabla v_1) + (\nabla u_2 \cdot \nabla v_2) \right| \\ &\leq \|E_t\|_H \|\nabla E \cdot U\|_H \|\nabla E \cdot V\|_H + K(\|\nabla u_1\|_H \|\nabla v_1\|_H + \|\nabla u_2\|_H \|\nabla v_2\|_H) \end{aligned}$$

By the inequality, $(a + b)^2 \leq (a + b)^2 + (a - b)^2 = 2(a^2 + b^2)$, we have,

$$\begin{aligned} \|\nabla E \cdot U\|_H &\leq \left[2\|E_x\|_{L^\infty}^2 \int_{\Omega} u_1^2 + 2\|E_y\|_{L^\infty}^2 \int_{\Omega} u_2^2 \right]^{\frac{1}{2}} \\ &\leq \left[2 \max \left\{ \|E_x\|_{L^\infty}^2, \|E_y\|_{L^\infty}^2 \right\} \right]^{\frac{1}{2}} \|U\|_H \end{aligned}$$

Hence we obtain

$$\begin{aligned} |J'(U, V)| &\leq C_1(\|U\|_H + \|U\|_H \|V\|_H + \|\nabla u_1\|_H \|\nabla v_1\|_H + \|\nabla u_2\|_H \|\nabla v_2\|_H) \\ &\leq C_1\|U\|_H + C_1[\|U\|_H^2 + \|\nabla u_1\|_H^2 + \|\nabla u_2\|_H^2]^{\frac{1}{2}} \cdot [\|V\|_H^2 + \|\nabla v_1\|_H^2 + \|\nabla v_2\|_H^2]^{\frac{1}{2}} \\ &= C_1(\|U\|_H + \|U\|_Z \cdot \|V\|_Z) < \infty. \end{aligned}$$

where,

$$C_1 = 2 \max \left\{ \|E_x\|_{L^\infty}^2, \|E_y\|_{L^\infty}^2, \frac{\|E_t^2\|_H \cdot \|E_x\|_{L^\infty}^2}{2}, \frac{\|E_t^2\|_H \cdot \|E_y\|_{L^\infty}^2}{2}, \frac{K}{2} \right\}.$$

So $J'(U, V)$ exists and is well defined. \square

B.2 Equivalence of $J'(U)=0$ and existence of a minimizer for J

Theorem B.2.1. *If the Gateaux derivative vanishes at a point $U = U_0$ then it is a minimizer of (2.2).*

Proof. We have,

$$\begin{aligned} J(U_0 + \epsilon(V - U_0)) &= J((1 - \epsilon)U_0 + \epsilon V) \\ &\leq (1 - \epsilon)J(U_0) + \epsilon J(V) \quad (\text{By Convexity of } J) \end{aligned}$$

for any $V \in J(\Omega)$. Let $V - U_0 = H$. Then,

$$J(U_0 + \epsilon H) - J(U_0) = \epsilon(J(V) - J(U_0))$$

This gives,

$$\frac{J(U_0 + \epsilon H) - J(U_0)}{\epsilon} = J(V) - J(U_0)$$

Taking limit on both sides as $\epsilon \rightarrow 0$, the left hand side goes to $J'(U_0)$ and the right hand side remains constant as it is independent of ϵ . But $J'(U_0) = 0$. So $J(V) - J(U_0) \geq 0 \quad \forall V \in J(\Omega)$.

Hence $J(V) \geq J(U_0) \quad \forall V \in J(\Omega)$. So U_0 minimizes J globally. \square

Theorem B.2.2. *If there is a global minimizer of (2.2) at $U = U_0$ then Gateaux Derivative of J at U_0 vanishes.*

Proof. Suppose not. Then,

$$\lim_{\epsilon \rightarrow 0} \frac{J(U_0 + \epsilon H) - J(U_0)}{\epsilon} = K$$

If $K > 0$ then,

$$\frac{J(U_0 + \epsilon H) - J(U_0)}{\epsilon} > \frac{K}{2} \quad (\text{for sufficiently small } \epsilon).$$

If $K < 0$ then,

$$J(U_0 + \epsilon H) - J(U_0) < \epsilon \frac{K}{2}$$

and hence,

$$J(U_0 + \epsilon H) < J(U_0) + \epsilon \frac{K}{2} < J(U_0)$$

which contradicts the fact that U_0 is a global minimizer of J as $U_0 + \epsilon H \in J(\Omega)$ when $H \in J(\Omega)$.

If $K < 0$ then,

$$\frac{J(U_0 + \epsilon H) - J(U_0)}{\epsilon} < 2K \text{ (for sufficiently small } \epsilon).$$

If $\epsilon > 0$ then,

$$J(U_0 + \epsilon H) - J(U_0) < \epsilon 2K.$$

and hence,

$$J(U_0 + \epsilon H) < J(U_0) + \epsilon 2K < J(U_0)$$

which again contradicts the fact that U_0 is a global minimizer of J as $U_0 + \epsilon H \in J(\Omega)$ when $H \in J(\Omega)$.

So the Gateaux derivative of J at the global minimum point U_0 is 0. \square

So it follows from above that if there is an unique solution of $J'(U) = 0$ then that unique solution is the global minimizer for J , where J is convex.

Appendix C

Conjugate Gradient method

C.1 Introduction

The solution of the approximate problem: find $u_h \in V_h$:

$$a(u_h, v_h) = F(v_h) \quad \forall v_h \in V_h \quad (\text{C.1})$$

can be found using iterative methods. One such method is the conjugate gradient method. We will discuss about theory of the method in this chapter. Let $\{\phi_i\}_{i=1}^{N_h}$ be a basis of V_h . Let A be the stiffness matrix given by $A = (a(\phi_i, \phi_j))$ and $f = (F(\phi_i))$. If $a(., .)$ is symmetric, then (C.1) is equivalent to the minimization problem

$$J(u_h) = \min_{v_h \in V_h} J(v_h) \quad (\text{C.2})$$

where

$$J(v) = \frac{1}{2}v^T A v - v^T f, v \in \mathbb{R}^{N_h}. \quad (\text{C.3})$$

So u_h is a solution of (C.2) iff $Au_h = f$.

C.2 Conjugate gradient

Definition C.2.1. *The directions $w_1, w_2 \in \mathbb{R}^N$ are said to be conjugate with respect to the matrix A if*

$$w_1^T A w_2 = 0$$

In the conjugate gradient method, we construct conjugate directions using the gradient of the functional. Then the functional is minimised by proceeding along the conjugate direction. We have the following theorem

Theorem C.2.1. *Let w_1, w_2, \dots, w_N be n mutually conjugate directions. Let*

$$x_{k+1} = x_k - \lambda_k w_k$$

where λ_k minimizes

$$\phi(\lambda) = J(x_k - \lambda w_k), \lambda \in \mathbb{R}$$

J is given in (C.3). When $x_1 \in \mathbb{R}^N$ is given, we have

$$x^{N+1} = x^*$$

where

$$Ax^* = f$$

Proof. Let

$$r_n = -J'(x_n) = f - Ax_n$$

Since λ_k minimizes $\phi(\lambda)$, we have

$$\phi'(\lambda_k) = (J'(x_k - \lambda_k w_k), -w_k) = 0$$

This gives

$$\lambda_k = \frac{(r_k)^T w_k}{(w_k)^T A w_k} \quad (\text{C.4})$$

Since w_1, w_2, \dots, w_N are mutually conjugate directions, they are linearly independent. Therefore there exist $\alpha_i, i \leq i \leq n$, such that

$$x_1 - x^* = \sum_{k=1}^n \alpha_k w_k$$

From this, using the fact that w_j are mutually conjugate, we obtain

$$(x_1 - x^*)^T A w_j = \alpha_j (w_j)^T A w_j$$

This gives

$$\alpha_j = \frac{(x_1 - x^*)^T A w_j}{(w_j)^T A w_j} \quad (\text{C.5})$$

Using induction we show that

$$\alpha_k = \lambda_k$$

Since $Ax^* = f$, we have

$$r_1 = f - Ax_1 = A(x_* - x_1)$$

This shows that

$$\alpha_1 = \lambda_1$$

Let $\alpha_i = \lambda_i$ for $1 \leq i \leq k$. From the definition of x_k we obtain,

$$x_k = x_1 - \sum_{i=1}^{k-1} \lambda_i w_i = x_1 - \sum_{i=1}^{k-1} \alpha_i w_i,$$

(by induction hypothesis). Since

$$(w_i)^T Aw_k = 0, 1 \leq i \leq k-1,$$

we get

$$(x_k - x_1)^T Aw_k = 0$$

This together with (C.4) and (C.5) shows that

$$\alpha_k = \lambda_k$$

Thus $\alpha_k = \lambda_k$ for $1 \leq k \leq n$. The definition of x_k implies

$$x_{N+1} = x_1 - \sum_{i=1}^n \lambda_i w_i = x_1 - \sum_{i=1}^n \alpha_i w_i = x^*$$

□

Now the final theorem in this Appendix is about the iterations to taken for implementing the conjugate gradient method and the convergence of the method to the actual solution of $Au = f$.

Theorem C.2.2. *Let $x_0 \in \mathbb{R}^N$. Define $w_1 = f - Ax_1$. Knowing x_n and w_{n-1} we define x_{n+1} and w_n by*

$$x_{n+1} = x_n + \alpha_n w_n$$

$$w_n = r_n + \beta_n w_{n-1}$$

where

$$r_n = f - Ax_n, \alpha_n = \frac{(r_n, w_n)}{(w_n, Aw_n)}, \beta_n = \frac{(r_n, r_n)}{(r_{n-1}, r_{n-1})}$$

Then w_n are mutually conjugate directions and x_{N+1} is the unique solution of $Ax = f$.

Proof. A proof of this theorem can be found in [DL69]. □

Remark C.2.1. *It can be shown that*

$$x_n - x_{N+1} \sim \left(\frac{1 - \sqrt{c}}{1 + \sqrt{c}} \right)^n$$

where $c = \frac{m}{M}$, $m = \inf_{x \neq 0} \frac{(Ax, x)}{\|x\|^2}$, $M = \sup_{x \neq 0} \frac{(Ax, x)}{\|x\|^2}$. The convergence rate for conjugate gradient method is faster than the steepest descent method, atleast for quadratic functionals. Also as Condition Number of $A \sim \frac{C}{h^2}$ when $V_h \subset H^1(\Omega)$, so conjugate gradient method is preferred over steepest descent method for finite elements.

Bibliography

- [B92a] M. J. Black. Combining intensity and motion for incremental segmentation and tracking over long image sequences. In G. Sandini, editor, *Proc. of Second European Conference on Computer Vision, ECCV-92*, volume 588 of LNCS-Series, pages 485–493. Springer-Verlag, May 1992.
- [BA90a] M. J. Black and P. Anandan. Constraints for the early detection of discontinuity from motion. In *Proc. National Conf. on Artificial Intelligence, AAAI-90*, pages 1060–1066, Boston, MA, 1990.
- [BA90b] M. J. Black and P. Anandan. A model for the detection of motion over time. In *Proc. Int. Conf. on Computer Vision, ICCV-90*, pages 33–37, Osaka, Japan, December 1990.
- [BR87] P. Bouthemy and J. S. Rivero. A hierarchical likelihood approach for region segmentation according to motion-based criteria. In *Proc. First Int. Conf. on Computer Vision, ICCV-87*, pages 463–467, London, England, June 1987.
- [DL69] D.G. Luenberger. Optimization by vector space methods. *John Wiley*, 1969.
- [ES91] E. Simoncelli, E. Adelson, and D. Heeger. Probability distributions of optical flow. In *Proc. CVPR*, 310–315, 1991.
- [GP87] E. Gamble and T. Poggio. Integration of intensity edges with stereo and motion. Technical Report Artificial Intelligence Lab Memo No. 970, MIT, 1987.
- [H86] B. K. P. Horn. *Robot Vision*. The MIT Press, Cambridge, Massachusetts, 1986.
- [HB90] F. Heitz and P. Bouthemy. Multimodal motion estimation and segmentation using Markov random fields. In *Proc. IEEE Int. Conf. on Pattern Recognition*, pages 378–383, June 1990.
- [HS81] B. K. P. Horn and B. G. Schunck. Determining optical flow. *Artificial Intelligence*, 17(1-3):185–203, 1981.

- [KES] Topics in Functional Analysis and Applications. *New Age International Publishers*, 2008.
- [LZ] L. Zhou, C. Kambhamettu, D. Goldgof, K. Palaniappan, and A. Hasler. Tracking nonrigid motion and structure from 2D satellite cloud images without correspondences. *IEEE Trans.PAMI*, 23(11):1330–1336.
- [MB87] D. W. Murray and B. F. Buxton. Scene segmentation from visual motion using global optimization. *IEEE Trans. on Pattern Analysis and Machine Intelligence*, PAMI-9(2):220–228, March 1987.
- [MM04] Amar Mitiche and Abdol-Reza Mansouri. On the convergence of the Horn and Schunck Optical-Flow Estimation Method. *IEEE Transactions on Image Processing*, Vol. 13 No. 6 June 2004.
- [PO80] J. L. Potter. Scene segmentation using motion information. *IEEE Trans. on Systems, Man and Cybernetics*, 5:390–394, 1980.
- [PR90] S. Peleg and H. Rom. Motion based segmentation. In *Proc. IEEE Int. Conf. on Pattern Recognition*, pages 109–113, June 1990.
- [RV] A. Wayne Roberts and Dale E. Varberg. Convex Functions, *Academic Press, New York and London*, 1973
- [SC89a] B. G. Schunck. Image flow segmentation and estimation by constraint line clustering. *IEEE Transactions on Pattern Analysis and Machine Intelligence*, 11(10):1010–1027, October 1989.
- [SC91] C.Schnörr. Determining Optical Flow for Irregular Domains by Minimizing Quadratic Functionals of a Certain Class. *International Journal of Computer Vision*, 6:1, 25-38 (1991).
- [MB92] Michael Julian Black. Robust Incremental Optical Flow YALEU/CSD/RR 923
- [SMS79] J. E. Stout, D. W. Martin, and D. N. Sikdar. Estimating GATE rainfall with geosynchronous satellite images. *Mon. Wea. Rev.*, 107:585–598, 1979.
- [SU87] A. Spoerri and S. Ullman. The early detection of motion boundaries. In *Proc. 1st ICCV*, pages 209–218, London, UK, June 1987.
- [TB91] M. J. Tarr and M. J. Black. A computational and evolutionary perspective on the role of representation in computer vision. Technical Report YALEU/DCS/RR-899, Yale University, October 1991.

- [TH82] W. B. Thompson, K. M. Mutch, and V. Berzins. Edge detection in optical flow fields. In *Proc. of the Second National Conference on Artificial Intelligence*, pages 26–29, August 1982.
- [TH85] W. B. Thompson, K. M. Mutch, and V. A. Berzins. Dynamic occlusion analysis in optical flow fields. *IEEE Transactions on Pattern Analysis and Machine Intelligence*, PAMI-7(4):374–383, July 1985.
- [TH80] W. B. Thompson. Combining motion and contrast for segmentation. *IEEE Transactions on Pattern Analysis and Machine Intelligence*, AMI-2:543–549, 1980.